INFORMATION TO USERS

This manuscript has been reproduced from the microfilm master. UMI films the text directly from the original or copy submitted. Thus, some thesis and dissertation copies are in typewriter face, while others may be from any type of computer printer.

The quality of this reproduction is dependent upon the quality of the copy submitted. Broken or indistinct print, colored or poor quality illustrations and photographs, print bleedthrough, substandard margins, and improper alignment can adversely affect reproduction.

In the unlikely event that the author did not send UMI a complete manuscript and there are missing pages, these will be noted. Also, if unauthorized copyright material had to be removed, a note will indicate the deletion.

Oversize materials (e.g., maps, drawings, charts) are reproduced by sectioning the original, beginning at the upper left-hand corner and continuing from left to right in equal sections with small overlaps. Each original is also photographed in one exposure and is included in reduced form at the back of the book.

Photographs included in the original manuscript have been reproduced xerographically in this copy. Higher quality 6" x 9" black and white photographic prints are available for any photographs or illustrations appearing in this copy for an additional charge. Contact UMI directly to order.

UMI

A Bell & Howell Information Company
300 North Zeeb Road, Ann Arbor MI 48106-1346 USA
313/761-4700 800/521-0600

NUCLEON-NUCLEON BREMSSTRAHLUNG CALCULATION: STUDIES OF THE OFF-SHELL PROTON ELECTROMAGNETIC VERTEX AND OF PSEUDOSCALAR VS PSEUDOVECTOR PION-NUCLEON COUPLINGS

by

YI LI

A dissertation submitted to the Graduate Faculty in Physics in partial fulfillment of the requirements for the degree of Doctor of Philosophy, The City University of New York

1998

This manuscript has been read and accepted for the Graduate Faculty in Physics in satisfaction of the dissertation requirement for the degree of Doctor of Philosophy.

9/11/98
Date

Professor Ming Kung Liou
Chair of Examining Committee

9/11/98
Date

Professor Louis S. Celenza
Executive Officer

Professor Louis S. Celenza

Doctor Benjamin F. Gibson

Professor Peter M. S. Lesser

Professor William M. Schreiber
Supervisory Committee

The City University of New York

Abstract

NUCLEON-NUCLEON BREMSSTRAHLUNG CALCULATION: STUDIES OF THE OFF-SHELL PROTON ELECTROMAGNETIC VERTEX AND OF PSEUDOSCALAR VS PSEUDOVECTOR PION-NUCLEON COUPLINGS

by

YI LI

Advisor: Professor Ming Kung Liou

The nucleon-nucleon bremsstrahlung processes ($pp\gamma$ and $np\gamma$) have been used as a tool to study the problems related to both the off-shell proton electromagnetic vertex and pseudoscalar (ps) vs pseudovector (pv) πN coupling. We have developed an approach which can be applied to investigate the two problems together. The following important results have been obtained: (i) The $pp\gamma$ analyzing powers calculated using the on-shell $p\gamma p$ vertex, with ps or pv coupling, yield very poor results for most of the cases with small proton scattering angles at 280 MeV. (ii) The calculations using the off-shell $p\gamma p$ vertex and ps coupling in most cases produce $pp\gamma$ cross sections which fail to fit the TRIUMF data at 200 and 280 MeV. (iii) The $pp\gamma$ data for both cross sections and analyzing powers in the energy region between 157 and 280 MeV can only be consistently described by the calculations using the off-shell $p\gamma p$ vertex and pv coupling. Thus our results indicate that the off-shell $p\gamma p$ vertex must be used in relativistic $pp\gamma$ calculations, and the pseudovector coupling is the best choice for the πN vertex. (iv) The on-shell nucleon electromagnetic vertex has been applied to calculate $np\gamma$ cross

sections. The cross sections calculated using the ps coupling are extremely close to that calculated using the pv coupling, implying that the $np\gamma$ results are not sensitive to the ps-pv question. (v) Exchange effects (the internal contribution) dominate the $np\gamma$ cross section. This important fact is exactly what has been found in potential-model calculations. (vi) Noncoplanarity effects are very significant in both $pp\gamma$ and $np\gamma$ processes, even though such effects are quite different in the two processes. Noncoplanarity effects may be responsible for some discrepancies between theory and experiment. (vii) More accurate $pp\gamma$ and $np\gamma$ data, both cross sections and analyzing powers, are needed for further investigation of the off-shell nucleon electromagnetic vertex and of ps vs pv πN couplings.

DEDICATION

To my wife, Jing

for her care, enthusiasm, and encouragement

ACKNOWLEDGMENTS

This work has been accomplished under the guidance of Professor Ming Kung Liou. I wish to express my gratitude for all the time and effort Professor Liou has devoted in teaching and training me; his encouragement and enthusiasm have been a continuous source of inspiration for me. I would also like to express my thanks to Professor William M. Schreiber for his great help in both my graduate study and teaching.

I wish to thank my thesis committee members, Professor Louis S. Celenza, Professor Peter M. S. Lesser, and Doctor Benjamin F. Gibson of Los Alamos National Laboratory, for their helpful advice.

TABLE OF CONTENTS

LIST OF TABLES

LIST OF FIGURES

Chapter I

INTRODUCTION

During the last three decades, various nuclear bremsstrahlung processes have been studied both experimentally and theoretically [1]. The best-known processes include nucleon-nucleon bremsstrahlung ($pp\gamma$ and $np\gamma$), proton-deuteron bremsstrahlung ($pd\gamma$), proton-helium bremsstrahlung ($p\alpha\gamma$), proton-carbon bremsstrahlung ($p\,^{12}C\,\gamma$), proton-oxygen bremsstrahlung ($p\,^{16}O\,\gamma$), and pion-proton bremsstrahlung ($\pi^{\pm}p\gamma$). In addition to the investigation of off-shell effects, there are other important motivations for investigating these bremsstrahlung processes. For example, bremsstrahlung processes in the vicinity of resonances have been used either to investigate the electromagnetic properties of resonances [2,3] or to extract the nuclear time delay which can be used to study the details of nuclear reactions [4]. Hadron-hadron bremsstrahlung processes, especially those processes containing significant resonance or exchange effects, have been useful in determining the range of validity of theoretical models and calculational approximations.

The $pp\gamma$ and $np\gamma$ processes have been extensively studied since 1963 to investigate the off-shell behavior of two-nucleon interactions [1]. Recently, these two processes have received new attention for the following reasons: (i) New $pp\gamma$ data, both cross sections and analyzing powers, measured with modern techniques have become available [5-9]. (ii) More sophisticated bremsstrahlung calculations, using either contemporary two-nucleon potentials or other approaches, have been performed [10-27]. (iii) Large discrepancies between TRIUMF's $pp\gamma$ cross section data [7] and theoretical

predictions have challenged experimentalists to perform more precise measurements [9] and theorists to improve their model calculations. (iv) The $np\gamma$ process appears to be the most likely source of energetic photons emitted from heavy-ion collisions [28], and it is probably an ideal process for studying meson exchange effects [29,11]. The discrepancies between theory and TRIUMF's experiment remain unresolved. Various theoretical attempts have been made to resolve these discrepancies. Since the $pp\gamma$ process involves two identical protons, the electric-dipole radiation is suppressed and, furthermore, no photon emission results from single-meson exchange between the two protons at the tree level. Therefore, most theorists have concentrated their attention on higher order effects and corrections. These higher order effects and corrections include rescattering terms, relativistic spin corrections, negative energy states, Δ-isobar admixtures, electromagnetic form factors, higher order exchange currents, and the difference between pseudoscalar and pseudovector πN couplings. Although the contributions from some of these effects and the corrections are significant, the magnitude of the overall correction has not resolved the existing discrepancies. Thus, further experimental and theoretical studies are certainly warranted. Most recently, the noncoplanarity effects on the $pp\gamma$ cross sections, a significant effect which had not been systematically studied, have also been investigated [30].

A variety of models and approximations has been proposed during the past three decades for bremsstrahlung calculations. In studying $pp\gamma$ and $np\gamma$ processes, most theoretical investigations have focused on nonrelativistic potential model calculations using various phenomenological potentials as input. A common goal of these potential model calculations is to distinguish different potentials by off-shell effects so that the

best one could be selected upon comparison with $pp\gamma$ and/or $np\gamma$ data. Another well-known approach, proposed four decades ago by Low [31], is the soft-photon approximation. This approximation is based upon a fundamental theorem called the soft-photon theorem or the low-energy theorem for photons. The theorem was first proved by Low [31] and it was extended and generalized later by many other authors [1,2,19,25,32-34]. Various soft-photon amplitudes, which are consistent with the theorem, have been constructed. Recently, these amplitudes have been thoroughly tested and the results can be summarized as follows: (i) Low's conventional amplitude, which has been applied to describe all kinds of bremsstrahlung processes during the last four decades, fails completely to describe bremsstrahlung processes with significant resonance effects or meson exchange effects. (ii) Evidence suggests that at least two distinct classes of soft-photon amplitudes are required to describe nuclear bremsstrahlung processes. The two-u-two-t special amplitudes (TuTts), which represent a class evaluated using the Mandelstan variables $(u_1, u_2, t_p, t_q$, defined in Ref.[1]), were found to be optimal for processes involving strong u-channel exchange effects [1,19,25]. The two-s-two-t special amplitudes (TsTts), which represent a class evaluated at (s_i, s_f, t_p, t_q), were found to be optimal for processes involving strong s-channel resonance effects [1,2,4,33,34]. Finally, a third approach is the one-boson-exchange (OBE) model. This is the approach used in this work [21,27]. All our $pp\gamma$ and $np\gamma$ calculations are based on a realistic OBE model proposed by Horowitz [35].

Both $pp\gamma$ and $np\gamma$ processes have been studied in this work. Using Horowitz's realistic OBE model as an input, we have calculated both coplanar and noncoplanar cross sections for these two processes, and we have also calculated the analyzing

powers for the $pp\gamma$ process. In these calculations, the pion-nucleon coupling ($p\pi^o p$, $n\pi^o n$ and $p\pi^+ n$ vertices) has been treated not only as a pseudoscalar (ps) but also as a pseudovector (pv). For the nucleon electromagnetic vertices, we have used the on-shell nucleon electromagnetic vertex (on-shell $p\gamma p$ and on-shell $n\gamma n$ vertices) in our $pp\gamma$ and $np\gamma$ calculations, and we have also used the off-shell proton electromagnetic vertex (off-shell $p\gamma p$ vertex) in the $pp\gamma$ calculations. The idea of using nucleon-nucleon bremsstrahlung as a tool for investigating ps and pv πN couplings is rather new. The possibility of using the $pp\gamma$ process to distinguish between models employing these two couplings has been discussed most recently by our group [21,27] and later by another group [23]. The ps-pv question and the on-shell vs off-shell $p\gamma p$ vertex problem are two major topics of our investigation.

In Chapters II and III, we focus on the $pp\gamma$ process. The contribution from the rescattering term, while omitted in Chapter II, has been investigated in Chapter III. In order to systematically investigate the ps-pv question and the on-shell vs off-shell $p\gamma p$ vertex problem together, we have performed the following calculations: (i) Using the on-shell $p\gamma p$ vertex, both $pp\gamma$ cross sections ($\sigma^{ps}_{pp\gamma}$ for ps coupling and $\sigma^{pv}_{pp\gamma}$ for pv coupling, both coplanar and noncoplanar cases) and analyzing powers (A_y^{ps} for ps coupling and A_y^{pv} for pv coupling) have been calculated. (ii) Using the off-shell $p\gamma p$ vertex, both $pp\gamma$ cross sections ($\bar{\sigma}^{ps}_{pp\gamma}$ for ps coupling and $\bar{\sigma}^{pv}_{pp\gamma}$ for pv coupling, both coplanar and noncoplanar cases) and analyzing powers ($\bar{A}_y^{ps}$ for ps coupling and $\bar{A}_y^{pv}$ for pv coupling) have been calculated. The calculations of $\sigma^{ps}_{pp\gamma}$, $\sigma^{pv}_{pp\gamma}$, A_y^{ps} and A_y^{pv} are straight forward since the on-shell $p\gamma p$ vertex is well defined. This is not the case, however, for the calculations of $\bar{\sigma}^{ps}_{pp\gamma}$, $\bar{\sigma}^{pv}_{pp\gamma}$, $\bar{A}_y^{ps}$ and $\bar{A}_y^{pv}$, mainly because the off-

shell $p\gamma p$ vertex involves an unknown form factor. As will be discussed in Section II.2, the off-shell $p\gamma p$ vertex depends on two real form factors, $F_2^+(\omega^2)$ and $F_2^-(\omega^2)$. $F_2^+(\omega^2)$ was studied by Nyman [36], and his formula for $F_2^+(\omega^2)$ has been used in this work. $F_2^-(\omega^2)$ is an unknown form factor. Based on the threshold dominance assumption, Nyman derived an approximate expression for $F_2^-(\omega^2)$. However, we have found that the threshold dominance approximation for $F_2^-(\omega^2)$ is insufficient. To improve this approximation, we have developed a new approach to study $F_2^-(\omega^2)$. Specifically, we have obtained an expansion of $F_2^-(\omega^2)$ in powers of $(\omega^2/m^2 - 1)$, where m is the proton mass. For an incident energy below 280 MeV, the expansion converges rapidly and an expression which includes the first three terms of the expansion gives a very good approximation for $F_2^-(\omega^2)$. Treating the three coefficients of the expansion as free parameters, they can be determined by fitting to TRIUMF's analyzing powers at 280 MeV [7]. In this way, we have constructed a complete expression (including both $F_2^+(\omega^2)$ and $F_2^-(\omega^2)$) for the off-shell $p\gamma p$ vertex.

Our calculated $pp\gamma$ cross sections are compared with the Harvard data at 157 MeV [37], the old TRIUMF data at 200 MeV [5], and the TRIUMF data at 280 MeV [7], while our calculated $pp\gamma$ analyzing powers are compared with TRIUMF's analyzing powers at 280 MeV [7]. Our ultimate goal is to find a theoretical calculation which can be used to consistently describe the combined $pp\gamma$ data, including cross sections and analyzing powers in the energy region from 157 to 280 MeV. We have demonstrated that the combined $pp\gamma$ data can only be consistently described by the calculations using the off-shell $p\gamma p$ vertex and pv-coupling [27]. In Chapter III, we

will prove that this conclusion remains unchanged even if the rescattering term is taken into consideration. Furthermore, our study shows that the form factor $F_2^-(\omega^2)$ is required in order to describe the measured analyzing powers.

In Chapter IV, we study the $np\gamma$ process. Again, all theoretical calculations are based on Horowitz's realistic OBE model. A unique feature of the OBE approach is that the constructed $np\gamma$ amplitude is both Lorentz invariant and gauge invariant, and it takes into account exchange effects explicitly. This feature makes our approach quite different from the nonrelativistic potential model approach.

Most of the nucleon-nucleon bremsstrahlung experiments performed during the last three decades were $pp\gamma$ experiments. Very few $np\gamma$ cross sections (only for large scattering angles), and no analyzing powers, have been measured. An ongoing experiment at Los Alamos Neutron Science Center will produce new $np\gamma$ data in the near future [38]. Generally speaking, the $np\gamma$ experiments are much more difficult to perform than the $pp\gamma$ experiments, partly because the neutron beams lack the high quality and/or intensity required for precise measurements. Since $np\gamma$ analyzing power data are not available, the unknown off-shell neutron electromagnetic form factor, $F_2^-(\omega^2)$, cannot be determined. Therefore we have used only the on-shell nucleon electromagnetic vertex to calculate all coplanar and noncoplanar $np\gamma$ cross sections ($\sigma_{np\gamma}^{ps}$ for ps coupling and $\sigma_{np\gamma}^{pv}$ for pv coupling). In order to investigate noncoplanarity effects, we have also calculated the integrated cross section, $d\sigma_{np\gamma}^{ps(pv)}/d\Omega_3\, d\Omega_4$, as a function of the noncoplanarity angle $\bar{\phi}$. Because the deviation between $\sigma_{np\gamma}^{ps}$ and $\sigma_{np\gamma}^{pv}$, $\Delta_{np\gamma} = \sigma_{np\gamma}^{ps} - \sigma_{np\gamma}^{pv}$, is extremely small for all cases investigated, the results of this calculation cannot be used to resolve the ps-pv problem.

We therefore focus our investigation on relativistic effects, noncoplanarity effects, and exchange current effects.

Chapter II

PROTON-PROTON BREMSSTRAHLUNG

Most of the essential formulas used in this work are discussed in this chapter. The chapter has been divided into six sections. In Section II.1, we define the pp elastic amplitude based on Horowitz's OBE model. Justifications for using Horowitz's model are also discussed. In Section II.2, we study the off-shell $p\gamma p$ vertex and its two real electromagnetic form factors, $F_2^+(\omega^2)$ and $F_2^-(\omega^2)$. We show how the unknown form factor $F_2^-(\omega^2)$ can be determined from the $pp\gamma$ analyzing power data. In Section II.3, we construct four bremsstrahlung amplitudes without including the rescattering term. Two amplitudes are obtained from the off-shell $p\gamma p$ vertex, i.e., one for the ps coupling $\bar{M}_\mu^{ps}$ and another for the pv coupling $\bar{M}_\mu^{pv}$. Two other amplitudes are derived from the on-shell $p\gamma p$ vertex for the ps coupling M_μ^{ps} and the pv coupling M_μ^{pv}. The amplitudes $\bar{M}_\mu^{pv}$, $\bar{M}_\mu^{ps}$, M_μ^{pv} and M_μ^{ps} are used to calculate the cross sections (analyzing powers) $\bar{\sigma}_{pp\gamma}^{pv}(\bar{A}_y^{pv})$, $\bar{\sigma}_{pp\gamma}^{ps}(\bar{A}_y^{ps})$, $\sigma_{pp\gamma}^{pv}(A_y^{pv})$, and $\sigma_{pp\gamma}^{ps}(A_y^{ps})$, respectively. In Section II.4, we give the formulas for calculating the cross sections (analyzing powers), $\bar{\sigma}_{pp\gamma}^{pv}(\bar{A}_y^{pv})$, $\bar{\sigma}_{pp\gamma}^{ps}(\bar{A}_y^{ps})$, $\sigma_{pp\gamma}^{pv}(A_y^{pv})$ and $\sigma_{pp\gamma}^{ps}(A_y^{ps})$. In Section II.5 we present our results, which include the calculated cross sections and analyzing powers and their comparison with the experimental data at 157, 200, and 280 MeV. In Section II.6, we discuss our results and their implications.

II.1 Elastic pp Amplitude

We consider photon emission accompanying the scattering of two protons.

$$p(p_1^\mu) + p(p_2^\mu) \rightarrow p(p_3^\mu) + p(p_4^\mu) + \gamma(K^\mu) \ . \tag{II-1}$$

Here, p_1^μ and p_2^μ are the four-momenta for the incident proton and the target proton, respectively, while p_3^μ and p_4^μ are the four-momenta for the two outgoing protons. The emitted photon has four-momentum K^μ and polarization vector ϵ^μ. These five four-momenta satisfy energy-momentum conservation,

$$p_1^\mu + p_2^\mu = p_3^\mu + p_4^\mu + K^\mu \ , \tag{II-2}$$

and they can be used to define the following Mandelstam variables

$$\begin{aligned} s_{12} &= (p_1 + p_2)^2 \ , & s_{34} &= (p_3 + p_4)^2 \ , \\ t_{13} &= (p_1 - p_3)^2 \ , & t_{24} &= (p_2 - p_4)^2 \ , \\ u_{23} &= (p_2 - p_3)^2 \ , & u_{14} &= (p_1 - p_4)^2 \ . \end{aligned} \tag{II-3}$$

In the limit when K approaches zero, the $pp\gamma$ process (II-1) reduces to the corresponding pp elastic scattering process,

$$p(p_1^\mu) + p(p_2^\mu) \rightarrow p(\bar{p}_3^\mu) + p(\bar{p}_4^\mu) \ , \tag{II-4a}$$

where

$$\begin{aligned} \bar{p}_3^\mu &= \lim_{K \rightarrow 0} p_3^\mu \ , \\ \bar{p}_4^\mu &= \lim_{K \rightarrow 0} p_4^\mu \ . \end{aligned} \tag{II-4b}$$

In this limit, Eqs. (II-2) and (II-3) become

$$p_1^\mu + p_2^\mu = \bar{p}_3^\mu + \bar{p}_4^\mu \ , \tag{II-5}$$

$$\begin{aligned} s &= (p_1 + p_2)^2 = (\bar{p}_3 + \bar{p}_4)^2 \ , \\ t &= (p_1 - \bar{p}_3)^2 \ , \quad u = (p_2 - \bar{p}_3)^2 \ . \end{aligned} \tag{II-6}$$

Two sets of OBE pp processes, which will be used as the source graphs to generate bremsstrahlung diagrams, are shown in Fig. 1. Note that the amplitude corresponding to Fig.1 , which involves a direct process minus an exchange process,

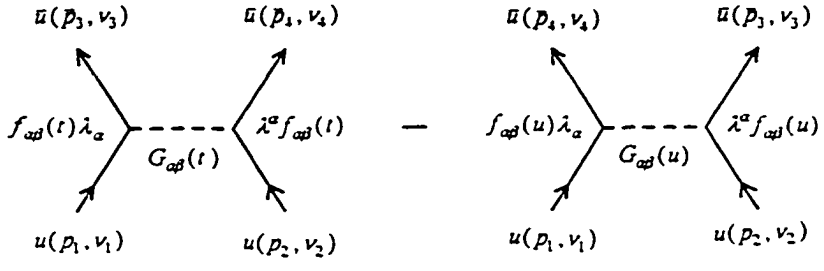

Fig.1. Feynman diagrams for the pp elastic scattering process in the OBE model.

satisfies the Pauli principle. In this work, we use Horowitz's OBE model with ten neutral "mesons" exchanged between the two protons [35]. The elastic amplitude corresponding to Fig. 1, valid for both ps and pv couplings, has the form

$$M_{pp}(u,t) = \sum_{\alpha=1}^{5}\sum_{\beta=1}^{4}\Big\{ G_{\alpha\beta}(t) f_{\alpha\beta}^2(t)\,\bar{u}(\bar{p}_3,\nu_3)\lambda_\alpha u(p_1,\nu_1)\,\bar{u}(\bar{p}_4,\nu_4)\lambda^\alpha u(p_2,\nu_2)$$
$$- G_{\alpha\beta}(u) f_{\alpha\beta}^2(u)\,\bar{u}(\bar{p}_4,\nu_4)\lambda_\alpha u(p_1,\nu_1)\,\bar{u}(\bar{p}_3,\nu_3)\lambda^\alpha u(p_2,\nu_2)\Big\}, \quad \text{(II-7)}$$

where

$$(\lambda_1,\lambda_2,\lambda_3,\lambda_4,\lambda_5) \equiv (1,\sigma_{\mu\nu},\gamma_5\gamma_\mu,\gamma_\mu,\gamma_5), \quad \text{(II-8a)}$$

$$(\lambda^1,\lambda^2,\lambda^3,\lambda^4,\lambda^5) \equiv (1,\sigma^{\mu\nu},\gamma_5\gamma^\mu,\gamma^\mu,\gamma_5), \quad \text{(II-8b)}$$

$$f_{\alpha\beta}(x) = \frac{\Lambda_{\alpha\beta}^2}{x-\Lambda_{\alpha\beta}^2}, \quad \text{(II-8c)}$$

$$G_{\alpha\beta}(x) = 4\pi g^2_{\alpha\beta} \frac{i}{x - m^2_{\alpha\beta} + i\epsilon_{\alpha\beta}} , \qquad x = t , u . \qquad \text{(II-8d)}$$

Horowitz's parameters, which involve the complex coupling constants $g^2_{\alpha\beta}$, the cut-off parameters $\Lambda_{\alpha\beta}$, and the meson masses $m_{\alpha\beta}$, are defined in Appendix. Note that $t = -q^2$ and $u = -Q^2$, where q and Q are respectively the direct momentum transfer and the exchange momentum transfer used by Horowitz. Let us briefly explain why the amplitude $M_{pp}(u,t)$ given by Eq.(II-7) is correct for pv coupling. For π-exchange corresponding to λ_5 and λ^5 in Eq.(II-7), those in the first term should be replaced by $\lambda_5(\not{p}_1 - \not{p}_3)/(2m)$ and $\lambda^5(\not{p}_2 - \not{p}_4)/(2m)$, respectively, while those in the second term should be replaced by $\lambda_5(\not{p}_1 - \not{p}_4)/(2m)$ and $\lambda^5(\not{p}_2 - \not{p}_3)/(2m)$, respectively. However, using the Dirac equation and the relation $\gamma_\mu\gamma_5 + \gamma_5\gamma_\mu = 0$, all extra factors introduced to modify λ_5 and λ^5 are exactly equal to 1. Thus the elastic amplitude for pv coupling is identical to the elastic amplitude for ps coupling.

Our choice of Horowitz's model as the input for our $pp\gamma$ calculation is motivated by the following considerations. A relativistic pp elastic amplitude, which is consistent with parity invariance, time-reversal invariance, charge symmetry and the Pauli principle, has been proposed by Goldberger, Grisaru, MacDowell and Wong [39]. If the Fierz transformation is used to transform those exchange (interchange) terms, this GGMW amplitude can be characterized in terms of five Lorentz invariant amplitudes (scalar F_S, vector F_V, pseudoscalar F_{PS}, axialvector F_A and tensor F_T) and the associated five Fermi covariants ($S \equiv \bar{u}(p_3)u(p_1)\bar{u}(p_4)u(p_2)$, $A \equiv \bar{u}(p_3)i\gamma_5\gamma_\mu u(p_1)\bar{u}(p_4)i\gamma_5\gamma^\mu u(p_2)$, $T \equiv (1/2)\,\bar{u}(p_3)\sigma_{\mu\nu}u(p_1)\,\bar{u}(p_4)\sigma^{\mu\nu}u(p_2)$, $V \equiv \bar{u}(p_3)\gamma_\mu u(p_1)\bar{u}(p_4)\gamma^\mu u(p_2)$, $PS \equiv \bar{u}(p_3)\gamma_5 u(p_1)\bar{u}(p_4)\gamma_5 u(p_2)$). The five

invariant amplitudes F_i (i=S, A, T, V, PS) can be directly expressed in terms of the five helicity amplitudes, which are explicit functions of phase shifts. If we write Horowitz's amplitude (Eq. (II-7)) in the same form as the GGMW amplitude, the five invariant amplitudes F_i can be identified and they can be expressed in terms of a set of OBE-parameters (masses, complex coupling constants and cut-off parameters). The values of these parameters have been determined by fitting to the Arndt amplitudes directly without iteration of the meson exchanges. Complex meson couplings are required and they have played an essential role in the description of the NN (pp and np) and $NN\gamma$ analyzing powers. Like phase shifts, all OBE-parameters are energy dependent. Thus, Horowitz's model, which has replaced phase shifts by OBE-parameters, is an alternative representation of the pp elastic amplitude. It is a realistic OBE model since it describes the nucleon-nucleon elastic data (both cross sections and analyzing powers) very well. We should emphasize that Horowitz's model (which introduces complex coupling constants) is quite different from any other simple OBE models (which uses real coupling constants). There is an important difference between Horowitz's model and those simple OBE models: Our $pp\gamma$ amplitude generated from Horowitz's model can be used to calculate $pp\gamma$ analyzing powers, while the $pp\gamma$ amplitudes constructed from the simple OBE models always give vanishing (zero) analyzing powers. Generally speaking, our amplitude describes the $NN\gamma$ ($pp\gamma$ and $np\gamma$) data very well and our predictions are in agreement with other calculations. As demonstrated in our recent work [21], our calculated $pp\gamma$ and $np\gamma$ cross sections (using the on-shell $p\gamma p$ vertex) are in close agreement with the results calculated using the Bonn OBEPQ potential [12] and the HJ potential ([40] and the results

obtained in Ref. [12]). Furthermore, our $pp\gamma$ cross sections are also in very good agreement with the results calculated using a two-u-two-t soft-photon amplitude constructed from the GGMW amplitude and phase shifts from the latest Nijmegen pp partial-wave analysis [19]. Here, in this work, we present more evidence that the $pp\gamma$ amplitude constructed from Horowitz's model can indeed provide a very good description of the $pp\gamma$ data, both cross sections and analyzing powers.

In constructing the $pp\gamma$ amplitude from Horowitz's model, we have used Horowitz's OBE diagrams with OBE parameters. We do not generate the $pp\gamma$ amplitude directly from the five-term representation of the pp amplitude. This is because additional terms are required if one of the two protons is off-mass shell [41]. Therefore, this procedure is much more complicated than our alternative approach which generates the $pp\gamma$ amplitude from Horowitz's OBE diagrams with OBE parameters. Moreover, our approach allows us to single out only the pion to have ps or pv coupling to the proton. Thus, our $pp\gamma$ amplitude is general and valid for investigating the ps-pv problem.

II.2 The Off-Shell $p_\gamma p$ Vertex

The off-shell $p\gamma p$ vertex has been investigated by many authors [36,42-46]. It has the form

$$\bar{u}(p)\Gamma^{1}_{\mu}(p,\ p+K)$$

$$= \bar{u}(p)\left\{\gamma_\mu - \frac{i\sigma_{\mu\nu}K^\nu}{2m}\left[F_2^+(\omega^2)\frac{\not p + \not K + m}{2m} + F_2^-(\omega^2)\frac{-\not p - \not K + m}{2m}\right]\right\}, \quad \text{(II-9)}$$

where $F_2^+(\omega^2)$ and $F_2^-(\omega^2)$ are two real electromagnetic form factors. As shown by Bincer [42], these two form factors satisfy dispersion relations in $\omega^2 = (p + K)^2$, with the cut starting at $\omega^2 = (m + m_\pi)^2$:

$$F_2^{\pm}(\omega^2) = \frac{1}{\pi} \int_{(m+m_\pi)^2}^{N^2} \frac{Im F_2^{\pm}(\omega'^2)}{\omega'^2 - \omega^2} d\omega'^2 , \qquad \text{(II-10)}$$

where N is a cutoff parameter. In terms of a once-subtracted dispersion relation, we have alternate expressions for $F_2^{\pm}(\omega^2)$,

$$F_2^+(\omega^2) = \kappa_p + \frac{\omega^2 - m^2}{\pi} \int_{(m+m_\pi)^2}^{N^2} \frac{Im F_2^+(\omega'^2) d\omega'^2}{(\omega'^2 - m^2)(\omega'^2 - \omega^2)} \qquad \text{(II-11)}$$

and

$$F_2^-(\omega^2) = \kappa_p^- + \frac{\omega^2 - m^2}{\pi} \int_{(m+m_\pi)^2}^{N^2} \frac{Im F_2^-(\omega'^2) d\omega'^2}{(\omega'^2 - m^2)(\omega'^2 - \omega^2)} , \qquad \text{(II-12)}$$

where $\kappa_p = F_2^+(m^2)$ is the anomalous magnetic moment of the proton and $\kappa_p^- = F_2^-(m^2)$ is an unknown constant. On the mass shell, the term involving F_2^- in Eq.(II-9) vanishes due to the Dirac equation and therefore the off-shell vertex $\bar{u}(p)\Gamma_\mu^1(p, p+K)$ reduces to the on-shell vertex $\bar{u}(p)\Gamma_\mu^p$,

$$\Gamma_\mu^p = \gamma_\mu - \frac{i\kappa_p}{2m} \sigma_{\mu\nu} K^\nu . \qquad \text{(II-13)}$$

The form factors $F_2^{\pm}$ have been studied by Nyman [26]. Using

$$Im F_2^{+v}(\omega^2) \approx \frac{g_\pi^2}{4\pi} \frac{|\vec{q}|}{\omega} \qquad \text{(II-14)}$$

and

$$\mathrm{Im}F_2^{+s}(\omega^2) \approx -\frac{3}{4}\frac{m_\pi}{m}\frac{g_\pi^2}{4\pi}\frac{|\vec{q}|}{\omega} , \tag{II-15}$$

where

$$\frac{|\vec{q}|}{\omega} = \frac{1}{2\omega^2}\left\{\left[\omega^2-(m+m_\pi)^2\right]\left[\omega^2-(m-m_\pi)^2\right]\right\}^{\frac{1}{2}} , \tag{II-16}$$

he obtained an expression for the off-mass shell anomalous magnetic isoscalar form factor,

$$F_2^{+s}(\omega^2) = \frac{1}{\pi}\int_{(m+m_\pi)^2}^{N_s^2}\frac{\mathrm{Im}F_2^{+s}(\omega'^2)}{\omega'^2-\omega^2}d\omega'^2 , \tag{II-17}$$

and another expression for the off-mass shell anomalous magnetic isovector form factor,

$$F_2^{+v}(\omega^2) = \frac{1}{\pi}\int_{(m+m_\pi)^2}^{N_v^2}\frac{\mathrm{Im}F_2^{+v}(\omega'^2)}{\omega'^2-\omega^2}d\omega'^2 . \tag{II-18}$$

The cutoff parameters N_s and N_v are determined by imposing the conditions,

$$F_2^{+v}(m^2) = 1.85 \tag{II-19a}$$

and

$$F_2^{+s}(m^2) = -0.06 . \tag{II-19b}$$

Note that

$$\kappa_p = F_2^{+v}(m^2) + F_2^{+s}(m^2) = 1.79 \tag{II-20}$$

Nyman found $N_s = 1.26$ GeV and $N_v = 1.74$ GeV. We have obtained the same value for N_s but our value for N_v is slightly less than Nyman's value, i.e., $N_v = 1.695$ GeV.

For the proton case,

$$F_2^+(\omega^2) = F_2^{+v}(\omega^2) + F_2^{+s}(\omega^2) \ . \tag{II-21}$$

The same result can also be obtained from the once-subtracted dispersion relation,

$$\begin{aligned} F_2^+(\omega^2) = \kappa_p + \frac{\omega^2 - m^2}{\pi} \int_{(m+m_\pi)^2}^{N_v^2} \frac{\mathrm{Im} F_2^{+v}(\omega'^2) d\omega'^2}{(\omega'^2 - \omega^2)(\omega'^2 - m^2)} \\ + \frac{\omega^2 - m^2}{\pi} \int_{(m+m_\pi)^2}^{N_s^2} \frac{\mathrm{Im} F_2^{+s}(\omega'^2) d\omega'^2}{(\omega'^2 - \omega^2)(\omega'^2 - m^2)} \ . \end{aligned} \tag{II-22}$$

If we let $N_v = N_s = N$ in Eq. (II-22) and use

$$\mathrm{Im} F_2^+ = \mathrm{Im} F_2^{+v}(\omega^2) + \mathrm{Im} F_2^{+s}(\omega^2) \ , \tag{II-23}$$

then we obtain Eq. (II-11). As shown in Fig. 2, Eqs. (II-22) and (II-11) (with $N^2 \geq 40\ \mathrm{GeV}^2$) do give similar results for $F_2^+(\omega^2)$. In this work, we have used Eq. (II-22) to calculate $F_2^+(\omega^2)$.

Equation (II-12) can be written in the form

$$F_2^-(\omega^2) = \kappa_p^- + \frac{\omega^2 - m^2}{\pi} \int_{(m+m_\pi)^2}^{N^2} \left[\frac{\mathrm{Im} F_2^-(\omega'^2)}{\mathrm{Im} F_2^+(\omega'^2)} \right] \frac{\mathrm{Im} F_2^+(\omega'^2) d\omega'^2}{(\omega'^2 - m^2)(\omega'^2 - \omega^2)} \ . \tag{II-24}$$

Applying the second mean value theorem to the integral, we can rewrite Eq. (II-24) as

$$F_2^-(\omega^2) = \kappa_p^- + \left[\frac{\omega^2 - m^2}{\pi} \right] \left[\frac{\mathrm{Im} F_2^-(\bar{\omega}^2)}{\mathrm{Im} F_2^+(\bar{\omega}^2)} \right] \int_{(m+m_\pi)^2}^{N^2} \frac{\mathrm{Im} F_2^+(\omega'^2) d\omega'^2}{(\omega'^2 - m^2)(\omega'^2 - \omega^2)} \ , \tag{II-25}$$

where

$$\bar{\omega}^2 = (m + m_\pi)^2 + \xi \left[N^2 - (m + m_\pi)^2 \right], \ 0 \leq \xi \leq 1 \ . \tag{II-26}$$

Substitution of Eq. (II-11) into Eq. (II-25) yields the expression

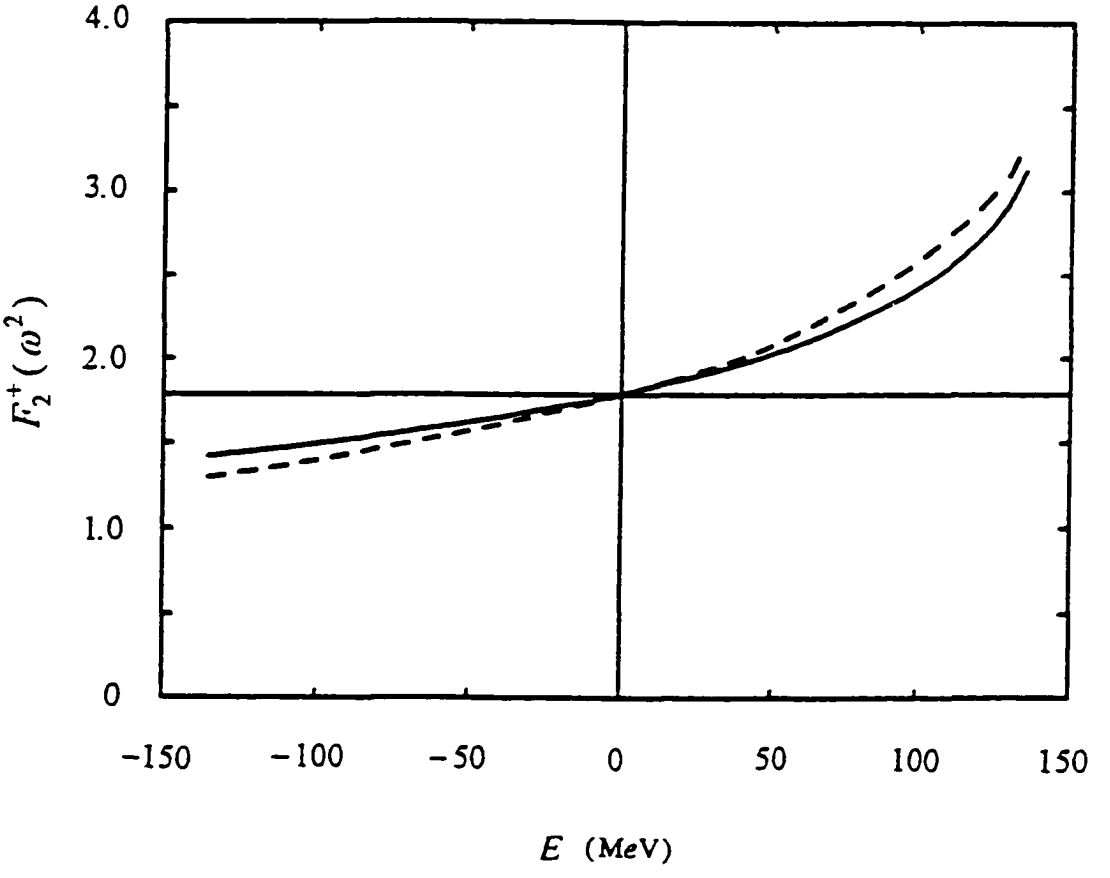

Fig.2. The proton electromagnetic form factor $F_2^+(\omega^2)$ as a function of E, $\omega = m + E$. The solid and dashed curves are calculated using Eqs.(II-22) and (II-11) (with $N^2 \geq 40\ GeV^2$) , respectively.

$$F_2^-(\omega^2) = \kappa_p^- + \left[\frac{\mathrm{Im}\, F_2^-(\bar{\omega}^2)}{\mathrm{Im}\, F_2^+(\bar{\omega}^2)}\right]\left[F_2^+(\omega^2) - \kappa_p\right]. \qquad \text{(II-27)}$$

The threshold dominance assumption is equivalent to choosing $\xi = 0$ and using the exact expression

$$\frac{\mathrm{Im}\, F_2^-\left[(m + m_\pi)^2\right]}{\mathrm{Im}\, F_2^+\left[(m + m_\pi)^2\right]} = \frac{2m + m_\pi}{m_\pi}. \qquad \text{(II-28)}$$

Applying this assumption to Eq. (II-27), we obtain

$$F_2^-(\omega^2) \approx \kappa_p^- + \frac{2m + m_\pi}{m_\pi}\left[F_2^+(\omega^2) - \kappa_p\right] \qquad \text{(II-29a)}$$

$$\approx \kappa_p^- + \frac{2m}{m_\pi}\left[F_2^+(\omega^2) - \kappa_p\right]. \qquad \text{(II-29b)}$$

Equation (II-29b) is the expression used by Nyman.

Our calculations indicate that Eq.(II-29b) or (II-29a) is not a good approximation for the following reason: Although $[\mathrm{Im}\, F_2^-(\bar{\omega}^2)/\mathrm{Im}\, F_2^+(\bar{\omega}^2)]$ should be a constant for a given value of ω^2, it is actually a function of ω^2. Now, there are four photon emission processes for the ppγ case (photon emission from two incoming and two outgoing protons). Thus, the ppγ amplitude is a sum of four amplitudes corresponding to those four processes. These four amplitudes will depend on four different values of ω^2. By using Eq. (II-28) for all four amplitudes, one has completely ignored the ω^2 dependence of these amplitudes. This is certainly not a good approximation for those cases with higher-photon energies when the incident energies are greater than 150 MeV.

One way of improving this approximation is to find an improved expression which has more explicit ω^2 dependence for $F_2^-(\omega^2)$. This can be done using the

following expansion

$$\frac{1}{\omega'^2-\omega^2} = \frac{1}{\omega'^2-m^2}\left[1+\frac{\omega^2-m^2}{\omega'^2-m^2}+\left[\frac{\omega^2-m^2}{\omega'^2-m^2}\right]^2+\cdots\right] \qquad \text{(II-30)}$$

$$= \frac{1}{\omega'^2-m^2}\sum_{n=0}^{\infty}\left[\frac{\omega^2-m^2}{\omega'^2-m^2}\right]^n \quad , \quad \omega^2 < \omega'^2 \, .$$

Substituting Eq. (II-30) into Eq. (II-12) [or Eq. (II-24)] gives

$$F_2^-(\omega^2) = \kappa_p^- + \sum_{n=0}^{\infty}\frac{(\omega^2-m^2)^{n+1}}{\pi} I_{n+1} \, , \qquad \text{(II-31a)}$$

where

$$I_{n+1} = \int_{(m+m_\pi)^2}^{N^2} \frac{\mathrm{Im}\, F_2^-(\omega'^2)\, d\omega'^2}{(\omega'^2-m^2)^{n+2}} \, . \qquad \text{(II-31b)}$$

The coefficients I_n are unknown constants, independent of ω^2. In order to understand more about I_n, we write I_n in the form

$$I_{n+1} = \int_{(m+m_\pi)^2}^{N^2} \left[\frac{\mathrm{Im}\, F_2^-(\omega'^2)}{\mathrm{Im}\, F_2^+(\omega'^2)}\right] \frac{\mathrm{Im}\, F_2^+(\omega'^2)\, d\omega'^2}{(\omega'^2-m^2)^{n+2}} \, . \qquad \text{(II-32)}$$

Applying the mean value theorem to the integral again, we obtain

$$I_{n+1} = \left[\frac{\mathrm{Im}\, F_2^-(\bar{\omega}'^2)}{\mathrm{Im}\, F_2^+(\bar{\omega}'^2)}\right]_{n+1} J_{n+1} \, , \qquad \text{(II-33a)}$$

where

$$J_{n+1} = \int_{(m+m_\pi)^2}^{N^2} \frac{\mathrm{Im}\, F_2^+(\omega'^2)\, d\omega'^2}{(\omega'^2-m^2)^{n+2}} \qquad \text{(II-33b)}$$

and

$$\bar{\omega}'^2 = (m + m_\pi)^2 + \xi'\left[N^2 - (m + m_\pi)^2\right], \qquad 0 \le \xi' \le 1 \ . \tag{II-33c}$$

The constants J_n can be calculated if we use Eq. (II-23) and $N^2 = 40\ \mathrm{GeV}^2$. However, it is not necessary to worry about the accuracy of J_n if we wish to treat the I_n as free parameters and to determine them from the experimental ppγ data. Referring to Eq.(II-28), we can write

$$\left[\frac{\mathrm{Im}\, F_2^-(\bar{\omega}'^2)}{\mathrm{Im}\, F_2^+(\bar{\omega}'^2)}\right]_{n+1} = C'_{n+1}\left[\frac{2m + m_\pi}{m_\pi}\right] \ . \tag{II-34}$$

For a given n, C'_{n+1} is expected to be a positive constant independent of ω^2 in line with the threshold dominance assumption. Inserting Eq. (II-34) into Eq. (II-33a) yields

$$I_{n+1} = C'_{n+1}\left[\frac{2m + m_\pi}{m_\pi}\right] J_{n+1} \tag{II-35}$$

which represent positive constants since J_n and C'_{n+1} are each positive. Using Eq. (II-35), $F_2^-(\omega^2)$ given by Eq. (II-31a) can be written as

$$F_2^-(\omega^2) = \kappa_p^- + \sum_{n=0}^{\infty} C_{n+1}\left[\frac{2m + m_\pi}{m_\pi}\right]\left[\frac{\omega^2}{m^2} - 1\right]^{n+1} , \tag{II-36a}$$

where the C_{n+1} denote the positive coefficients

$$C_{n+1} = C'_{n+1} J_{n+1} m^{2n+2}/\pi \ . \tag{II-36b}$$

For $K < 100$ MeV, the series given by Eq. (II-36a) converges rapidly. (To insure that the series converges, we must have $K < m_\pi$.) Thus

$$F_2^-(\omega^2) \approx \kappa_p^- + C_1\left[\frac{2m + m_\pi}{m_\pi}\right]\left[\frac{\omega^2}{m^2} - 1\right] + C_2\left[\frac{2m + m_\pi}{m_\pi}\right]\left[\frac{\omega^2}{m^2} - 1\right]^2 \tag{II-37}$$

will be a good approximation. This equation has been used in this work. There are

three unknown constants (κ_p^-, C_1 and C_2) in Eq.(II-37). We have determined them by fitting to the analyzing powers measured at 280 MeV by the TRIUMF group [7].

II.3 Bremsstrahlung Amplitudes

A. Bremsstrahlung Amplitude Using the Off-Shell pγp Vertex

We use the two sets of pp elastic scattering diagrams exhibited in Fig. 1 to generate eight bremsstrahlung diagrams as shown in Fig. 3. There is no internal

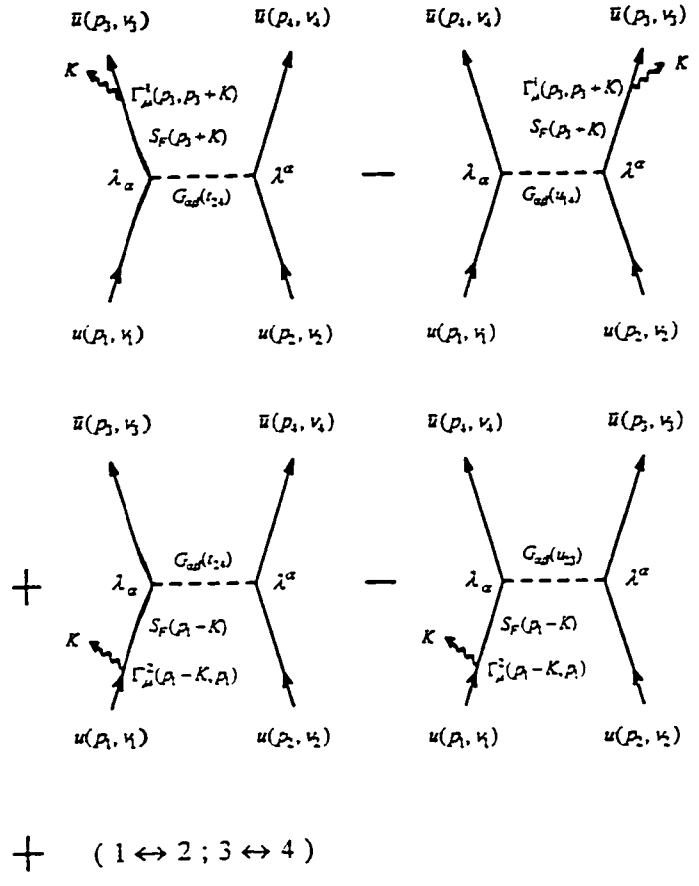

Fig.3. Feynman diagrams for the $pp\gamma$ process in the OBE model. $S_F(p) = (\not{p} - m + i\epsilon)^{-1}$ is the proton propagator. These diagrams are generated from the source graphs, Fig. 1.

emission diagram since no charged meson can be exchanged between two protons. The pp bremsstrahlung amplitude corresponding to Fig. 3 for ps coupling has the form

$$\bar{M}_{\mu}^{ps}(u_{14},u_{23};t_{13},t_{24}) = i\sum_{\alpha=1}^{5}\sum_{\beta=1}^{4}\Big\{G_{\alpha\beta}(t_{24})f_{\alpha\beta}^{2}(t_{24})\bar{u}(p_3,v_3)X_{\alpha\mu}u(p_1,v_1)\bar{u}(p_4,v_4)\lambda^{\alpha}u(p_2,v_2)$$

$$+\ G_{\alpha\beta}(t_{13})f_{\alpha\beta}^{2}(t_{13})\bar{u}(p_3,v_3)\lambda_{\alpha}u(p_1,v_1)\bar{u}(p_4,v_4)\,Y_{\mu}^{\alpha}u(p_2,v_2)$$

$$-\ G_{\alpha\beta}(u_{14})f_{\alpha\beta}^{2}(u_{14})\bar{u}(p_4,v_4)\lambda_{\alpha}u(p_1,v_1)\bar{u}(p_3,v_3)Z_{\mu}^{\alpha}u(p_2,v_2)$$

$$-\ G_{\alpha\beta}(u_{23})f_{\alpha\beta}^{2}(u_{23})\bar{u}(p_4,v_4)\,T_{\alpha\mu}u(p_1,v_1)\bar{u}(p_3,v_3)\lambda^{\alpha}u(p_2,v_2)\Big\}, \tag{II-38}$$

where

$$\begin{aligned}
X_{\alpha\mu} &= \lambda_{\alpha}\frac{1}{\not p_1 - \not K - m + i\epsilon}\Gamma_{\mu}^{2}(p_1-K,p_1)+\Gamma_{\mu}^{1}(p_3,p_3+K)\frac{1}{\not p_3+\not K-m+i\epsilon}\lambda_{\alpha},\\
Y_{\mu}^{\alpha} &= \lambda^{\alpha}\frac{1}{\not p_2 - \not K - m + i\epsilon}\Gamma_{\mu}^{2}(p_2-K,p_2)+\Gamma_{\mu}^{1}(p_4,p_4+K)\frac{1}{\not p_4+\not K-m+i\epsilon}\lambda^{\alpha},\\
Z_{\mu}^{\alpha} &= \lambda^{\alpha}\frac{1}{\not p_2 - \not K - m + i\epsilon}\Gamma_{\mu}^{2}(p_2-K,p_2)+\Gamma_{\mu}^{1}(p_3,p_3+K)\frac{1}{\not p_3+\not K-m+i\epsilon}\lambda^{\alpha},\\
T_{\alpha\mu} &= \lambda_{\alpha}\frac{1}{\not p_1 - \not K - m + i\epsilon}\Gamma_{\mu}^{2}(p_1-K,p_1)+\Gamma_{\mu}^{1}(p_4,p_4+K)\frac{1}{\not p_4+\not K-m+i\epsilon}\lambda_{\alpha}.
\end{aligned} \tag{II-39}$$

Referring to Eq. (II-9), the off-shell pγp vertices have the following expressions:

$$\Gamma_{\mu}^{1}(p_j,p_j+K) = \gamma_{\mu} - \frac{i}{2m}\sigma_{\mu\nu}K^{\nu}\left[F_2^{+}(\omega_j^2)\frac{\not p_j+\not K+m}{2m}+F_2^{-}(\omega_j^2)\frac{-\not p_j-\not K+m}{2m}\right] \tag{II-40a}$$

and

$$\Gamma_{\mu}^{2}(p_l-K,p_l) = \gamma_{\mu} - \frac{i}{2m}\left[F_2^{+}(\omega_l^2)\frac{\not p_l-\not K+m}{2m}+F_2^{-}(\omega_l^2)\frac{-\not p_l+\not K+m}{2m}\right]\sigma_{\mu\nu}K^{\nu}, \tag{II-40b}$$

where $\omega_j^2 = (p_j + K)^2$ and $\omega_l^2 = (p_l - K)^2$ with $j = 3,4$ and $l = 1,2$. It is obvious that

the gauge condition $K^\mu \bar{M}^{ps}_\mu = 0$ is satisfied. To see this, for example, we write $\bar{u}(p_3,v_3) X_{\alpha\mu} u(p_1,v_1)$ in another form, i.e.

$$\bar{u}(p_3,v_3) X_{\alpha\mu} u(p_1,v_1) = \bar{u}(p_3,v_3)\left[\left[\frac{p_{3\mu}+R_{3\mu}}{p_3\cdot K}\right]\lambda_\alpha - \lambda_\alpha \left[\frac{p_{1\mu}+R_{1\mu}}{p_1\cdot K}\right]\right] u(p_1,v_1), \quad \text{(II-41)}$$

where

$$R_{1\mu} = \frac{1}{4}[\gamma_\mu, K] + \frac{1}{8m}\left\{ [\gamma_\mu, K], F_2^+(\omega_1^2)\not{p}_1 - F_2^+(\omega_1^2)\frac{p_1\cdot K}{2m} + F_2^-(\omega_1^2)\frac{p_1\cdot K}{2m}\right\}, \quad \text{(II-42a)}$$

$$R_{3\mu} = \frac{1}{4}[\gamma_\mu, K] + \frac{1}{8m}\left\{ [\gamma_\mu, K], F_2^+(\omega_3^2)\not{p}_3 + F_2^+(\omega_3^2)\frac{p_3\cdot K}{2m} - F_2^-(\omega_3^2)\frac{p_3\cdot K}{2m}\right\}. \quad \text{(II-42b)}$$

Here, $\omega_1^2 = (p_1 - K)^2$, $\omega_3^2 = (p_3 + K)^2$, and we have used the commutation relations [A,B] $\equiv$ AB − BA and {A,B} $\equiv$ AB + BA. Since $K^\mu R_{1\mu} = K^\mu R_{3\mu} = 0$, we have $K^\mu \bar{u} X_{\alpha\mu} u = 0$. Similarly, we can also show that $K^\mu \bar{u} Y^\alpha_\mu u = 0$, $K^\mu \bar{u} Z^\alpha_\mu u = 0$, and $K^\mu \bar{u} T_{\alpha\mu} u = 0$. We have also verified the gauge invariance of our numerical calculation, i.e. $K^\mu \bar{M}^{ps}_\mu \sim 10^{-20}$.

The pp bremsstrahlung amplitude for pv coupling can be written in terms of the amplitude $\bar{M}^{ps}_\mu$ as

$$\bar{M}^{pv}_\mu(u_{14},u_{23};t_{13},t_{24}) = \bar{M}^{ps}_\mu + \Delta\bar{M}^{\pi(1)}_\mu + \Delta\bar{M}^{\pi(2)}_\mu + \Delta\bar{M}^{\pi(3)}_\mu + \Delta\bar{M}^{\pi(4)}_\mu, \quad \text{(II-43)}$$

where

$$\Delta\bar{M}_{\mu}^{\pi(1)} = \sum_{\beta=1}^{2} \Bigg\{ G_{5\beta}(t_{24}) \Bigg[\bar{u}(p_3,\nu_3)\lambda_5 \left(\frac{\not p_1 - \not K - \not p_3}{2m}\right) \frac{1}{\not p_1 - \not K - m + i\epsilon} \Gamma_{\mu}^{2}(p_1 - K, p_1)\, u(p_1,\nu_1)$$
$$\cdot\, \bar{u}(p_4,\nu_4)\, \lambda^5 \left(\frac{\not p_2 - \not p_4}{2m}\right) u(p_2,\nu_2)$$
$$- \bar{u}(p_3,\nu_3)\lambda_5 \frac{1}{\not p_1 - \not K - m + i\epsilon} \Gamma_{\mu}^{2}(p_1 - K, p_1)\, u(p_1,\nu_1)\bar{u}(p_4,\nu_4)\lambda^5 u(p_2,\nu_2) \Bigg]$$
$$- G_{5\beta}(u_{23}) \Bigg[\bar{u}(p_4,\nu_4)\lambda_5 \left(\frac{\not p_1 - \not K - \not p_4}{2m}\right) \frac{1}{\not p_1 - \not K - m + i\epsilon} \Gamma_{\mu}^{2}(p_1 - K, p_1)\, u(p_1,\nu_1)$$
$$\cdot\, \bar{u}(p_3,\nu_3)\, \lambda^5 \left(\frac{\not p_2 - \not p_3}{2m}\right) u(p_2,\nu_2)$$
$$- \bar{u}(p_4,\nu_4)\lambda_5 \frac{1}{\not p_1 - \not K - m + i\epsilon} \Gamma_{\mu}^{2}(p_1 - K, p_1)\, u(p_1,\nu_1)\bar{u}(p_3,\nu_3)\lambda^5 (p_2,\nu_2) \Bigg] \Bigg\}, \tag{II-44a}$$

$$\Delta\bar{M}_{\mu}^{\pi(2)} = \Delta\bar{M}_{\mu}^{\pi(1)} \quad (1 \leftrightarrow 2,\ 3 \leftrightarrow 4), \tag{II-44b}$$

$$\Delta\bar{M}_{\mu}^{\pi(3)} = \sum_{\beta=1}^{2} \Bigg\{ G_{5\beta}(t_{24}) \Bigg[\bar{u}(p_3,\nu_3)\Gamma_{\mu}^{1}(p_3, p_3+K) \frac{1}{\not p_3 + \not K - m + i\epsilon} \lambda_5 \left(\frac{\not p_1 - \not K - \not p_3}{2m}\right) u(p_1,\nu_1)$$
$$\cdot\, \bar{u}(p_4,\nu_4)\, \lambda^5 \left(\frac{\not p_2 - \not p_4}{2m}\right) u(p_2,\nu_2)$$
$$- \bar{u}(p_3,\nu_3)\Gamma_{\mu}^{1}(p_3, p_3+K) \frac{1}{\not p_3 + \not K - m + i\epsilon} \lambda_5 u(p_1,\nu_1)\bar{u}(p_4,\nu_4)\lambda^5 u(p_2,\nu_2) \Bigg]$$
$$- G_{5\beta}(u_{14}) \Bigg[\bar{u}(p_4,\nu_4)\lambda_5 \left(\frac{\not p_1 - \not p_4}{2m}\right) u(p_1,\nu_1)$$
$$\cdot \bar{u}(p_3,\nu_3)\Gamma_{\mu}^{1}(p_3, p_3+K) \frac{1}{\not p_3 + \not K - m + i\epsilon} \lambda^5 \left(\frac{\not p_2 - \not p_3 - \not K}{2m}\right) u(p_2,\nu_2)$$
$$- \bar{u}(p_4,\nu_4)\lambda_5 u(p_1,\nu_1)\bar{u}(p_3,\nu_3)\Gamma_{\mu}^{1}(p_3, p_3+K) \frac{1}{\not p_3 + \not K - m + i\epsilon} \lambda^5 u(p_2,\nu_2) \Bigg] \Bigg\}, \tag{II-44c}$$

and

$$\Delta \bar{M}_{\mu}^{\pi(4)} = \Delta \bar{M}_{\mu}^{\pi(3)} \quad (1 \leftrightarrow 2, 3 \leftrightarrow 4) \ . \tag{II-44d}$$

B. Bremsstrahlung Amplitude Using the On-Shell pγp Vertex

If the on-shell pγp vertex Γ_{μ}^{p} defined by Eq. (II-13) is used, the ppγ amplitude for ps coupling, M_{μ}^{ps}, is given by the same expression as the amplitude $\bar{M}_{\mu}^{ps}$ in Eqs. (II-38) and (II-39) but with all off-shell vertices Γ_{μ}^{1} and Γ_{μ}^{2} in Eq. (II-39) replaced by the on-shell vertex Γ_{μ}^{p}. Specifically,

$$M_{\mu}^{ps}(u_{14}, u_{23}; t_{13}, t_{24}) = \bar{M}_{\mu}^{ps}(u_{14}, u_{23}; t_{13}, t_{24}) \ , \tag{II-45}$$

where the expressions for $X_{\alpha\mu}$, Y_{μ}^{α}, Z_{μ}^{α} and $T_{\alpha\mu}$ remain the same but with $\Gamma_{\mu}^{1}(p_3, p_3 + K)$, $\Gamma_{\mu}^{1}(p_4, p_4 + K)$, $\Gamma_{\mu}^{2}(p_1 - K, p_1)$ and $\Gamma_{\mu}^{2}(p_2 - K, p_2)$ replaced by Γ_{μ}^{p}. Similarly, when the on-shell vertex Γ_{μ}^{p} is used, the ppγ amplitude for pv coupling, M_{μ}^{pv}, can be defined as

$$\begin{aligned} M_{\mu}^{pv}(u_{14}, u_{23}; t_{13}, t_{24}) &= M_{\mu}^{ps}(u_{14}, u_{23}; t_{13}, t_{24}) \\ &\quad + \Delta M_{\mu}^{\pi(1)} + \Delta M_{\mu}^{\pi(2)} + \Delta M_{\mu}^{\pi(3)} + \Delta M_{\mu}^{\pi(4)} \ . \end{aligned} \tag{II-46}$$

Here $\Delta M_{\mu}^{\pi(i)} (i = 1, 2, 3, 4)$ is given by the same expression as $\Delta \bar{M}_{\mu}^{\pi(i)}$ defined by Eqs. (II-44) but with all off-shell vertices, $\Gamma_{\mu}^{1}(p_3, p_3 + K)$, $\Gamma_{\mu}^{1}(p_4, p_4 + K)$, $\Gamma_{\mu}^{2}(p_1 - K, p_1)$ and $\Gamma_{\mu}^{2}(p_2 - K, p_2)$ replaced by the on-shell vertex Γ_{μ}^{p}.

The expression for ΔM_{μ}^{π},

$$\Delta M_{\mu}^{\pi} = \Delta M_{\mu}^{\pi(1)} + \Delta M_{\mu}^{\pi(2)} + \Delta M_{\mu}^{\pi(3)} + \Delta M_{\mu}^{\pi(4)} \ , \tag{II-47a}$$

can be simplified by using the following relations

$$\bar{u}(p_i,\nu_i)\,\Gamma_\mu\,\frac{1}{\not p_i+\not K-m}\,\gamma_5\left[\frac{\not p_j-\not p_i-\not K}{2m}\right]u(p_j,\nu_j)$$

$$=\bar{u}(p_i,\nu_i)\,\Gamma_\mu\,\frac{1}{\not p_i+\not K-m}\,\gamma_5\,u(p_j,\nu_j)+\frac{1}{2m}\,\bar{u}(p_i,\nu_i)\,\Gamma_\mu\,\gamma_5\,u(p_j,\nu_j)\qquad\text{(II-47b)}$$

and

$$\bar{u}(p_i,\nu_i)\,\gamma_5\left[\frac{\not p_j-\not p_i-\not K}{2m}\right]\frac{1}{\not p_j-\not K-m}\,\Gamma_\mu\,u(p_j,\nu_j)$$

$$=\bar{u}(p_i,\nu_i)\,\gamma_5\,\frac{1}{\not p_j-\not K-m}\,\Gamma_\mu\,u(p_j,\nu_j)+\frac{1}{2m}\,\bar{u}(p_i,\nu_i)\,\gamma_5\,\Gamma_\mu\,u(p_j,\nu_j)\qquad\text{(II-47c)}$$

(i=3,4 and j=1,2). We obtain

$$\begin{aligned}\Delta M_\mu^{\pi} &= M_\mu^{pv}-M_\mu^{ps}\\ &=\frac{-i\,\kappa_p}{2m^2}\sum_{\beta=1}^{2}\Big\{f_{5\beta}^2(t_{24})\,G_{5\beta}(t_{24})\,[\,\bar{u}(p_3,\nu_3)\,\sigma_{\mu\nu}\,K^\nu\gamma_5\,u(p_1,\nu_1)\,\bar{u}(p_4,\nu_4)\,\gamma_5\,u(p_2,\nu_2)\,]\\ &\quad+f_{5\beta}^2(t_{13})\,G_{5\beta}(t_{13})\,[\,\bar{u}(p_3,\nu_3)\,\gamma_5\,u(p_1,\nu_1)\,\bar{u}(p_4,\nu_4)\,\sigma_{\mu\nu}\,K^\nu\,\gamma_5\,u(p_2,\nu_2)\,]\\ &\quad-f_{5\beta}^2(u_{23})\,G_{5\beta}(u_{23})\,[\,\bar{u}(p_4,\nu_4)\,\sigma_{\mu\nu}\,K^\nu\gamma_5\,u(p_1,\nu_1)\,\bar{u}(p_3,\nu_3)\,\gamma_5\,u(p_2,\nu_2)\,]\\ &\quad-f_{5\beta}^2(u_{14})\,G_{5\beta}(t_{14})\,[\,\bar{u}(p_4,\nu_4)\,\gamma_5\,u(p_1,\nu_1)\,\bar{u}(p_3,\nu_3)\,\sigma_{\mu\nu}\,K^\nu\,\gamma_5\,u(p_2,\nu_2)\,]\Big\}\qquad\text{(II-47d)}\end{aligned}$$

Eq.(II-47d) shows the direct proportionality of ΔM_μ^{π} to κ_p. This means that ΔM_μ^{π} does not vanish for $pp\gamma$, and that its contribution increases as the proton scattering angles decrease. The last statement results because of the following: For a given incident energy, K increases as the outgoing proton scattering angles decrease, and the $pp\gamma$ cross section for very small scattering angles is dominated by those terms involving κ_p.

II.4 Bremsstrahlung Cross Sections and Analyzing Powers

A. Cross Sections

In Section II.3, we have obtained four amplitudes $\bar{M}_{\mu}^{ps}$, $\bar{M}_{\mu}^{pv}$, M_{μ}^{ps} and M_{μ}^{pv} (given by Eqs. (II-38), (II-43), (II-45) and (II-46), respectively). These amplitudes can be used to calculate $pp\gamma$ cross sections and analyzing powers. Both coplanar and (symmetric) noncoplanar cases are considered; the Harvard geometry [27,29] is used in this work. We follow the definition and the formulas given in the Appendix of Ref. [40]. ($\vec{p}'_1$ and $\vec{p}'_2$ used in Ref.[40] have been changed to $\vec{p}_3$ and $\vec{p}_4$, respectively, in this work.)

In the Harvard noncoplanar coordinate system (see Fig. 15 of Ref. [40]), p_1^{μ}, p_2^{μ}, p_3^{μ}, p_4^{μ} and K^{μ} in the laboratory system can be written as

$$
\begin{aligned}
p_1^{\mu} &= (E_1,\ 0,\ 0,\ p_1)\ , \\
p_2^{\mu} &= (m,\ 0,\ 0,\ 0)\ , \\
p_3^{\mu} &= (E_3,\ p_3 \cos\bar{\phi}_3 \sin\bar{\theta}_3,\ p_3 \sin\bar{\phi}_3,\ p_3 \cos\bar{\phi}_3 \cos\bar{\theta}_3)\ , \\
p_4^{\mu} &= (E_4,\ -p_4 \cos\bar{\phi}_4 \sin\bar{\theta}_4,\ p_4 \sin\bar{\phi}_4,\ p_4 \cos\bar{\phi}_4 \cos\bar{\theta}_4)\ , \\
K^{\mu} &= (K,\ K \cos\bar{\phi}_{\gamma} \sin\bar{\theta}_{\gamma},\ -K \sin\bar{\phi}_{\gamma},\ K \cos\bar{\phi}_{\gamma} \cos\bar{\theta}_{\gamma})\ ,
\end{aligned}
\qquad \text{(II-48)}
$$

where $E_i = (\vec{p}_i^{\,2} + m^2)^{1/2}$, $(i = 1, 3, 4)$.

In Eq.(II-48), there are three noncoplanar angles, $\bar{\phi}_3$, $\bar{\phi}_4$, and $\bar{\phi}_{\gamma}$. The kinematically allowed limit of the angle $\bar{\phi} = (\bar{\phi}_3 + \bar{\phi}_4)/2$ is called the maximum noncoplanarity angle $\bar{\phi}_{\max}$. In this limiting case, the gamma ray has a momentum $\vec{q}$ in the Harvard coordinate system ($\bar{\phi}_{\gamma} = \bar{\phi}_0$, $\bar{\theta}_{\gamma} = \bar{\theta}_0$),

$$\bar{q} = q \cos \bar{\phi}_0 \sin \bar{\theta}_0 \, \hat{e}_x - q \sin \bar{\phi}_0 \, \hat{e}_y + q \cos \bar{\phi}_0 \cos \bar{\theta}_0 \, \hat{e}_z \, . \qquad \text{(II-49)}$$

The momentum $\bar{q}$ can be used to define a new polar angle ψ_γ. This is done by requiring the momentum $\vec{K}'$,

$$\vec{K}' = \vec{K} - \alpha \vec{q} \, , \qquad \text{(II-50)}$$

lie in the reference x-z plane, i.e.,

$$\vec{K}' = K' \sin \psi_\gamma \, \hat{e}_x + K' \cos \psi_\gamma \, \hat{e}_z \, . \qquad \text{(II-51)}$$

To determine the complete kinematics, we first calculate three angles $(\bar{\theta}_0, \bar{\phi}_0, \bar{\phi}_{max})$ for the limiting gamma ray from a given set of conditions ($T = E_1 - m$, $\bar{\theta}_3 = \bar{\theta}_4 = \bar{\theta}$ for the symmetric case). We then use a set of known values $(\bar{T}, \bar{\theta}_3, \bar{\phi}_3, \bar{\theta}_4, \bar{\phi}_4, \bar{\phi}_{max}, \bar{\theta}_0, \bar{\phi}_0, \bar{\psi}_\gamma)$ to calculate p_3, p_4, $\bar{K}$, $\bar{\theta}_\gamma$ and $\bar{\phi}_\gamma$. Note that the four equations of energy-momentum conservation are used in each of these calculations, and we vary $\bar{\phi}$ from zero to $\bar{\phi}_{max}$. For the symmetric noncoplanar case, we have $\bar{\theta}_3 = \bar{\theta}_4 = \bar{\theta}$ and $\bar{\phi}_3 = \bar{\phi}_4 = \bar{\phi}$.

Since the independent variables are $\bar{\theta}_3$, $\bar{\phi}_3$, $\bar{\theta}_4$, $\bar{\phi}_4$ and ψ_γ, four differential cross sections, $\bar{\sigma}^{ps}_{pp\gamma}$ and $\sigma^{ps}_{pp\gamma}$ for ps coupling as well as $\bar{\sigma}^{pv}_{pp\gamma}$ and $\sigma^{pv}_{pp\gamma}$ for pv coupling, can be obtained from the following expressions:

$$\bar{\sigma}^{ps(pv)}_{pp\gamma} \equiv \frac{d^3 \bar{\sigma}^{ps(pv)}}{d\Omega_3 \, d\Omega_4 \, d\psi_\gamma} = c \, \bar{Q}^{ps(pv)} \, , \qquad \text{(II-52a)}$$

$$\sigma^{ps(pv)}_{pp\gamma} \equiv \frac{d^3 \sigma^{ps(pv)}}{d\Omega_3 \, d\Omega_4 \, d\psi_\gamma} = c \, Q^{ps(pv)} \, , \qquad \text{(II-52b)}$$

where

$$\bar{Q}^{ps(pv)} = \sum_{spin} \sum_{pol} (\epsilon^{\mu} \bar{M}_{\mu}^{ps(pv)})^{\dagger} (\epsilon^{\nu} \bar{M}_{\nu}^{ps(v)}) , \qquad \text{(II-53a)}$$

$$Q^{ps(pv)} = \sum_{spin} \sum_{pol} (\epsilon^{\mu} M_{\mu}^{ps(pv)})^{\dagger} (\epsilon^{\nu} M_{\nu}^{ps(pv)}) , \qquad \text{(II-53b)}$$

and

$$c = \frac{m^4 e^2 |F|}{8 (2\pi)^5 [(p_1 \cdot p_2)^2 - m^4]^{1/2}} , \qquad \text{(II-53c)}$$

In Eq. (II-53c), e is the proton charge and F, which is the phase space factor, is given by Eq. (A39) of Ref. [40].

Referring to the expression for K^{μ} given in Eq. (II-48), two photon polarization four-vectors can be chosen,

$$\epsilon_{(1)}^{\mu} = (0, \cos \bar{\theta}_{\gamma}, 0, -\sin \bar{\theta}_{\gamma}) , \qquad \text{(II-54a)}$$

$$\epsilon_{(2)}^{\mu} = (0, \sin \bar{\phi}_{\gamma} \sin \bar{\theta}_{\gamma}, \cos \bar{\phi}_{\gamma}, \sin \bar{\phi}_{\gamma} \cos \bar{\theta}_{\gamma}) . \qquad \text{(II-54b)}$$

They satisfy the conditions $K_{\mu} \epsilon_{(1)}^{\mu} = K_{\mu} \epsilon_{(2)}^{\mu} = 0$. Using these two polarization vectors, we can write $\bar{Q}^{ps}$, $\bar{Q}^{pv}$, Q^{ps} and Q^{pv} in the forms

$$\bar{Q}^{ps(pv)} = \sum\!\!\!\!\!\!\int_{\nu_1,\nu_2,\nu_3,\nu_4} \bar{Q}^{ps(pv)} (\nu_1, \nu_2, \nu_3, \nu_4) , \qquad \text{(II-55a)}$$

$$Q^{ps(pv)} = \sum\!\!\!\!\!\!\int_{\nu_1,\nu_2,\nu_3,\nu_4} Q^{ps(pv)} (\nu_1, \nu_2, \nu_3, \nu_4) , \qquad \text{(II-55b)}$$

where

$$\bar{Q}^{ps(pv)}(\nu_1,\nu_2,\nu_3,\nu_4) = (\epsilon_{(1)}^{\mu} \bar{M}_{\mu}^{ps(pv)})^{\dagger} (\epsilon_{(1)}^{\nu} \bar{M}_{\nu}^{ps(pv)}) + (\epsilon_{(2)}^{\mu} \bar{M}_{\mu}^{ps(pv)})^{\dagger} (\epsilon_{(2)}^{\nu} \bar{M}_{\nu}^{ps(pv)}) , \qquad \text{(II-56a)}$$

$$Q^{ps(pv)}(\nu_1,\nu_2,\nu_3,\nu_4) = (\epsilon^{\mu}_{(1)} M^{ps(pv)}_{\mu})^{\dagger} (\epsilon^{\nu}_{(1)} M^{ps(pv)}_{\nu}) + (\epsilon^{\mu}_{(2)} M^{ps(pv)}_{\mu})^{\dagger} (\epsilon^{\nu}_{(2)} M^{ps(pv)}_{\nu}) \ , \quad \text{(II-56b)}$$

A computer program has been developed for the numerical evaluation of $\bar{Q}^{ps}(\nu_1, \nu_2, \nu_3, \nu_4)$, $\bar{Q}^{pv}(\nu_1, \nu_2, \nu_3, \nu_4)$, $Q^{ps}(\nu_1, \nu_2, \nu_3, \nu_4)$ and $Q^{pv}(\nu_1, \nu_2, \nu_3, \nu_4)$. Since each ν has two values, there are a total of 16 different $\bar{Q}^{ps(pv)}(\nu_1, \nu_2, \nu_3, \nu_4)$ and $Q^{ps(pv)}(\nu_1, \nu_2, \nu_3, \nu_4)$ to be evaluated. Thus, each individual evaluation yields the differential cross section for a particular polarization.

B. Analyzing Powers and Spin-Correlation Coefficients

Our calculation has been designed to calculate first the $pp\gamma$ cross section for four polarized protons (beam, target and two outgoing protons). In order to calculate $\bar{Q}^{ps(pv)}(\nu_1, \nu_2, \nu_3, \nu_4)$ and $Q^{ps(pv)}(\nu_1, \nu_2, \nu_3, \nu_4)$ for protons polarized along the x, y, or z axes, we introduce the following six different forms of $u(p_i, \nu_i)$:

$$u_{\beta}(p_i,\nu_i) = \sqrt{\frac{E_i + m}{2m}} \begin{bmatrix} x^{\nu i}_{\beta} \\ \dfrac{\vec{\sigma} \cdot \vec{p}_i}{E_i + m} \, x^{\nu i}_{\beta} \end{bmatrix} , \quad (\beta = x, y, z \text{ and } \nu_i = 1, 2) \quad \text{(II-57)}$$

where

$$\chi^1_x = \frac{1}{\sqrt{2}} \begin{bmatrix} 1 \\ 1 \end{bmatrix} , \ \chi^2_x = \frac{1}{\sqrt{2}} \begin{bmatrix} 1 \\ -1 \end{bmatrix} ,$$

$$\chi^1_y = \frac{1}{\sqrt{2}} \begin{bmatrix} 1 \\ i \end{bmatrix} , \ \chi^2_y = \frac{1}{\sqrt{2}} \begin{bmatrix} 1 \\ -i \end{bmatrix} , \quad \text{(II-58)}$$

$$\chi^1_z = \begin{bmatrix} 1 \\ 0 \end{bmatrix} , \quad \chi^2_z = \begin{bmatrix} 0 \\ 1 \end{bmatrix} .$$

We define $\bar{Q}^{ps(pv)}_{0\beta}(\nu_1, \nu_2, \nu_3, \nu_4)$ and $Q^{ps(pv)}_{0\beta}(\nu_1, \nu_2, \nu_3, \nu_4)$ $(\beta = x, y, z)$ for

the case where the target proton alone is polarized along the $(\pm x)$, $(\pm y)$, or $(\pm z)$ directions. $\bar{Q}_{0\beta}^{ps\,(pv)}(\nu_1, \nu_2, \nu_3, \nu_4)$ and $Q_{0\beta}^{ps\,(pv)}(\nu_1, \nu_2, \nu_3, \nu_4)$ are given by the same expressions as those for $\bar{Q}^{ps\,(pv)}(\nu_1, \nu_2, \nu_3, \nu_4)$ and $Q^{ps\,(pv)}(\nu_1, \nu_2, \nu_3, \nu_4)$ in Eqs. (II-56a) and (II-56b), respectively, but with $u(p_2, \nu_2)$ in the expressions for both $\bar{M}_{\mu}^{ps(pv)}$ and $M_{\mu}^{ps(pv)}$ replaced by $u_{\beta}(p_2, \nu_2)$. In terms of $\bar{Q}_{0\beta}^{ps(pv)}(\nu_1, \nu_2, \nu_3, \nu_4)$ and $Q_{0\beta}^{ps(pv)}(\nu_1, \nu_2, \nu_3, \nu_4)$, the $pp\gamma$ analyzing powers for a polarized target proton are

$$\bar{A}_{\beta}^{ps(pv)} = \frac{\bar{Q}_{0\beta}^{ps(pv)}(1) - \bar{Q}_{0\beta}^{ps(pv)}(2)}{\bar{Q}_{0\beta}^{ps(pv)}(1) + \bar{Q}_{0\beta}^{ps(pv)}(2)}, \quad (\beta = x, y, z) \tag{II-59a}$$

and

$$A_{\beta}^{ps(pv)} = \frac{Q_{0\beta}^{ps(pv)}(1) - Q_{0\beta}^{ps(pv)}(2)}{Q_{0\beta}^{ps(pv)}(1) + Q_{0\beta}^{ps(pv)}(2)}, \tag{II-59b}$$

where

$$\bar{Q}_{0\beta}^{ps(pv)}(i) = \sum_{\nu_1=1}^{2} \sum_{\nu_3=1}^{2} \sum_{\nu_4=1}^{2} \bar{Q}_{0\beta}^{ps(pv)}(\nu_1, i, \nu_3, \nu_4), \tag{II-60a}$$

$$Q_{0\beta}^{ps(pv)}(i) = \sum_{\nu_1=1}^{2} \sum_{\nu_3=1}^{2} \sum_{\nu_4=1}^{2} Q_{0\beta}^{ps(pv)}(\nu_1, i, \nu_3, \nu_4), \tag{II-60b}$$

$$i = 1, 2.$$

For the case in which both the beam and the target are polarized, we can define $\bar{C}_{\alpha\beta}(\nu_1, \nu_2)$ and $C_{\alpha\beta}(\nu_1, \nu_2)$ as follows:

$$\bar{C}_{\alpha\beta}^{ps(pv)}(\nu_1, \nu_2) = \sum_{\nu_3=1}^{2} \sum_{\nu_4=1}^{2} \bar{Q}_{\alpha\beta}^{ps\,(pv)}(\nu_1, \nu_2, \nu_3, \nu_4) \tag{II-61a}$$

and

$$C_{\alpha\beta}^{ps(pv)}(\nu_1, \nu_2) = \sum_{\nu_3 = 1}^{2} \sum_{\nu_4 = 1}^{2} Q_{\alpha\beta}^{ps(pv)}(\nu_1, \nu_2, \nu_3, \nu_4) \ , \qquad \text{(II-61b)}$$

where $\bar{Q}_{\alpha\beta}^{ps(pv)}(\nu_1, \nu_2, \nu_3, \nu_4)$ and $Q_{\alpha\beta}^{ps(pv)}(\nu_1, \nu_2, \nu_3, \nu_4)$ are given by the same expression as those for $\bar{Q}^{ps(pv)}(\nu_1, \nu_2, \nu_3, \nu_4)$ and $Q^{ps(pv)}(\nu_1, \nu_2, \nu_3, \nu_4)$ in Eqs. (II-56a) and (II-56b), respectively, but with $u(p_1, \nu_1)$ and $u(p_2, \nu_2)$ in the expressions for both $\bar{M}_{\mu}^{ps(pv)}$ and $M_{\mu}^{ps(pv)}$ replaced by $u_{\alpha}(p_1, \nu_1)$ and $u_{\beta}(p_2, \nu_2)$, respectively. $\bar{C}_{\alpha\beta}(\nu_1, \nu_2)$ and $C_{\alpha\beta}(\nu_1, \nu_2)$ can be used to calculate quantities such as spin-correlation coefficients or tensor powers.

II.5 Results

Equations (II-52a)-(II-52b) have been used to calculate the coplanar and noncoplanar differential cross sections, $\bar{\sigma}_{pp\gamma}^{ps}$ and $\sigma_{pp\gamma}^{ps}$ for ps coupling and $\bar{\sigma}_{pp\gamma}^{pv}$ and $\sigma_{pp\gamma}^{pv}$ for pv coupling. Both $\bar{\sigma}_{pp\gamma}^{ps}$ and $\bar{\sigma}_{pp\gamma}^{pv}$ are calculated using the off-shell $p\gamma p$ vertices Γ_{μ}^{1} and Γ_{μ}^{2} defined by Eqs.(II-40), while $\sigma_{pp\gamma}^{ps}$ and $\sigma_{pp\gamma}^{pv}$ are calculated using the on-shell $p\gamma p$ vertex Γ_{μ}^{p} given by Eq.(II-13). Some results at 157, 200 and 280 MeV are shown in Figs.4-12. We have used Horowitz's published parameters at 135 and 200 MeV for the calculation of the $pp\gamma$ cross sections at 157 and 200 MeV. These two sets of parameters yield very similar results for the case at 157 MeV. The cross sections at 280 MeV, on the other hand, are calculated using Horowitz's unpublished parameters at 300 MeV. Since the data at 280 MeV involve an ambiguity due to the $\frac{2}{3}$-normalization factor used by the TRIUMF group [7], the data at 157 and 200 MeV have served as an important check of our calculations.

The differential cross section has been expressed as a function of the photon

angle ψ_γ (from 0° to 180°) and the noncoplanarity angle $\bar{\phi}$ (from 0° to $\bar{\phi}_{max}$). The value $\bar{\phi} = 0$ gives the coplanar case. Our calculated noncoplanar cross sections are compared with the Harvard data at 157 MeV [37]. We have also integrated the 3-fold differential cross sections ($d^3\bar{\sigma}^{ps(pv)}/d\Omega_3 d\Omega_4 d\psi_\gamma$ and $d^3\sigma^{ps(pv)}/d\Omega_3 d\Omega_4 d\psi_\gamma$) over ψ_γ to obtain the 2-fold differential cross sections ($d^2\bar{\sigma}^{ps(pv)}/d\Omega_3 d\Omega_4$ and $d^2\sigma^{ps(pv)}/d\Omega_3 d\Omega_4$) as functions of $\bar{\phi}$.

We have also applied Eqs. (II-59a) and (II-59b) to calculate analyzing powers, $\bar{A}_\beta^{ps}$ and A_β^{ps} ($\beta = x, y, z$) for ps coupling and $\bar{A}_\beta^{pv}$ and A_β^{pv} for pv coupling. Again, $\bar{A}_\beta^{ps}$ and $\bar{A}_\beta^{pv}$ are calculated using the off-shell pγp vertices, while A_β^{ps} and A_β^{pv} are calculated using the on-shell pγp vertex. These analyzing powers are calculated using $\bar{\phi} = 0$, and they are expressed as a function of ψ_γ. The measured analyzing powers are available only at 280 MeV [7].

As mentioned in the introduction and will be shown in this section, our calculations clearly indicate that the off-shell pγp vertices must be used to describe the measured analyzing powers because a large discrepancy has been found between the predictions calculated using the on-shell pγp vertex and the TRIUMF data. In order to demonstrate this fact, our results obtained from the on-shell pγp vertex are always compared with those obtained from the off-shell vertices.

The off-shell vertices Γ_μ^1 and Γ_μ^2, which have been used to calculate $\bar{\sigma}_{pp\gamma}^{ps}$, $\bar{\sigma}_{pp\gamma}^{pv}$, $\bar{A}_\beta^{ps}$ and $\bar{A}_\beta^{pv}$, are determined by two form factors $F_2^+(\omega^2)$ and $F_2^-(\omega^2)$. $F_2^+(\omega^2)$ can be calculated using either Eq. (II-22) or Eqs. (II-17), (II-18) and (II-21), while $F_2^-(\omega^2)$ has been calculated using Eq. (II-37). In Eq. (II-37), κ_p^-, C_1 and C_2 are three unspecified parameters. These parameters have been determined by fitting to the

TRIUMF analyzing powers. Since a unique result can be obtained for C_1 and C_2 if κ_p^- is given, we have postulated various values for κ_p^- and used ten sets of TRIUMF analyzing powers to find C_1 and C_2. The analyzing powers shown in Figs. 10 correspond to the ten sets of data used in this work to fit C_1 and C_2. For a given κ_p^-, we obtain the parameters C_1 and C_2 from $\bar{A}_y^{ps}$ and $\bar{A}_y^{pv}$. In Table I, we present four sets of fitted parameters which are determined by using $\bar{A}_y^{pv}$. The values of κ_p^- in Table I lie in the range between -5 and 5, since good results can be obtained in this range. In Table II, using $\bar{A}_y^{ps}$ to fit C_1 and C_2, we also show two sets of parameters. Only two sets of parameters are given here because most cross sections $\bar{\sigma}_{pp\gamma}^{ps}$ calculated

TABLE I. Parameters κ_p^-, C_1 and C_2 for the form factor $F_2^-(\omega^2)$ given by Eq. (II-37). They are determined by fitting to TRIUMF's analyzing powers. This table gives four sets of κ_p^-, C_1 and C_2 for the pv-coupling case, in which $\bar{A}_y^{pv}$ is used to calculate analyzing powers.

parameter	κ_p^-	C_1	C_2
set I_a	5.00	4.51	0.91
set I_b	1.79	4.09	3.37
set I_c	0.00	3.88	4.87
set I_d	-4.00	3.29	7.65

using any of the sets of parameters given in Table I or II are in poor agreement with the experimental data at 200 and 280 MeV. In most cases, we have used the set I_b and the set II_a to calculate the cross sections $\bar{\sigma}^{pv}_{pp\gamma}$ and $\bar{\sigma}^{ps}_{pp\gamma}$, respectively, which have then been compared with the data at 157, 200 and 280 MeV.

TABLE II. Same as Table I except this table shows two sets of $\bar{\kappa}_p$, C_1 and C_2 for the ps-coupling case, in which $\bar{A}^{ps}_y$ is used to calculate analyzing powers.

parameter	$\bar{\kappa}_p$	C_1	C_2
set II_a	1.79	4.42	2.44
set II_b	-4.00	5.59	1.60

In Fig. 4, we present the noncoplanar cross section as a function of ψ_γ at 157 MeV for $\bar{\theta}_3 = \bar{\theta}_4 = 30°$ and several noncoplanarity angles $\bar{\phi}$. The calculated cross sections, $\bar{\sigma}^{pv}_{pp\gamma}$ (solid curve), $\bar{\sigma}^{ps}_{pp\gamma}$ (dash-dotted curve), $\sigma^{pv}_{pp\gamma}$ (dashed curve), and $\sigma^{ps}_{pp\gamma}$ (dotted curve), have a similar shape and in general the agreement with the Harvard data [37] is very good. The cross sections $\bar{\sigma}^{pv}_{pp\gamma}$ are calculated using the set I_b ($\bar{\kappa}_p = 1.79$) in Table I, while $\bar{\sigma}^{ps}_{pp\gamma}$ are calculated using the set II_a ($\bar{\kappa}_p = 1.79$) in Table II. It is easy to see that $\bar{\sigma}^{ps}_{pp\gamma} > \bar{\sigma}^{pv}_{pp\gamma}$, $\sigma^{ps}_{pp\gamma} > \sigma^{pv}_{pp\gamma}$, and $\bar{\Delta}_{pp\gamma} > \Delta_{pp\gamma}$. Here, $\bar{\Delta}_{pp\gamma} \equiv \bar{\sigma}^{ps}_{pp\gamma} - \bar{\sigma}^{pv}_{pp\gamma}$ and $\Delta_{pp\gamma} \equiv \sigma^{ps}_{pp\gamma} - \sigma^{pv}_{pp\gamma}$ are defined as the deviations in cross section. Although not shown in this figure, the cross sections $\bar{\sigma}^{pv}_{pp\gamma}$ and $\sigma^{pv}_{pp\gamma}$ are also

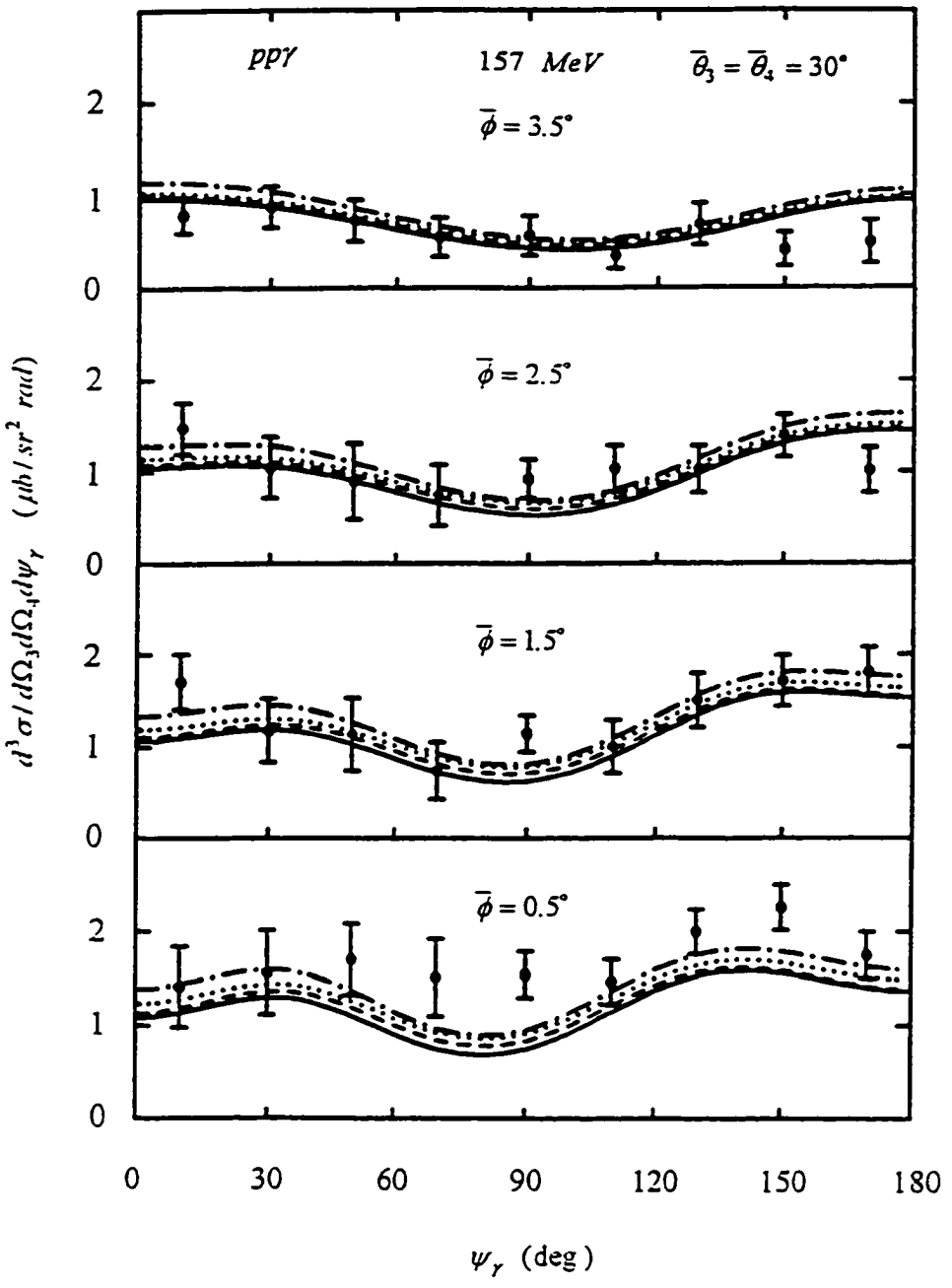

Fig.4. Noncoplanar $pp\gamma$ cross section $d^3\sigma/d\Omega_3 d\Omega_4 d\psi_\gamma$ as a function of ψ_γ at 157 MeV for $\bar{\theta}_3 = \bar{\theta}_4 = 30^\circ$ and several noncoplanarity angles $\bar{\phi}$. The results for $\bar{\sigma}^{pv}_{pp\gamma}$ (solid curve calculated using the set I_b parameters), $\bar{\sigma}^{ps}_{pp\gamma}$ (dash-dotted curve calculated using the set II_a parameters), $\sigma^{pv}_{pp\gamma}$ (dashed curve), and $\sigma^{ps}_{pp\gamma}$ (dotted curve) are compared with the Harvard data [37].

in close agreement with a potential model calculation using the Hamada-Johnston (H-J) potential [40,12]. It is important to point out that the cross section $\bar{\sigma}^{pv}_{pp\gamma}$ varies very little when the parameters given by the set I_b are replaced by the other sets I_a, I_c and I_d. In other words, $\bar{\sigma}^{pv}_{pp\gamma}$ at 157 MeV is insensitive to the variation of parameters (for $-5 < \bar{\kappa_p} < 5$), and the Harvard data cannot be used to differentiate among these parameter sets.

The noncoplanar cross sections at 157 MeV for $\bar{\theta}_3 = \bar{\theta}_4 = 35°$ have also been calculated for several values of $\bar{\phi}$. Using the set I_b for $\bar{\sigma}^{pv}_{pp\gamma}$ and the set II_a for $\bar{\sigma}^{ps}_{pp\gamma}$, as shown in Fig. 5, all calculated cross sections $\bar{\sigma}^{pv}_{pp\gamma}$, $\bar{\sigma}^{ps}_{pp\gamma}$, $\sigma^{pv}_{pp\gamma}$ and $\sigma^{ps}_{pp\gamma}$ give very similar results. This implies that both $\bar{\Delta}_{pp\gamma}$ and $\Delta_{pp\gamma}$ decrease as the proton scattering angles increase. The agreement between the calculated cross sections and the Harvard data is very good. Though not shown in the figure, we wish to point out that our OBE results are in quantitative agreement with the recent soft-photon calculations using the two-u-two-t special amplitude M_μ^{TuTts} [19] but disagree completely with the calculation using the two-s-two-t special amplitude M_μ^{TsTts} [19]. This supports the argument that the amplitude M_μ^{TuTts}, not M_μ^{TsTts}, should be used to describe the proton-proton bremsstrahlung process.

The 2-fold differential cross sections $d^2\bar{\sigma}^{ps(pv)}/d\Omega_3 d\Omega_4$ and $d^2\sigma^{ps(pv)}/d\Omega_3 d\Omega_4$ are also calculated from the 3-fold differential cross sections. The results are compared with the Harvard data in Fig. 6.

In Fig. 7(a), we present the coplanar cross sections $C_{exp}\bar{\sigma}^{pv}_{pp\gamma}$ (calculated using the set I_b), $C_{exp}\bar{\sigma}^{ps}_{pp\gamma}$ (calculated using the set II_a), $C_{exp}\sigma^{pv}_{pp\gamma}$ and $C_{exp}\sigma^{ps}_{pp\gamma}$ at 200 MeV for $\bar{\theta}_3 = \bar{\theta}_4 = 16.4°$. Here C_{exp} represents the experimental correction factor introduced by the TRIUMF group [5]. The calculated cross sections shown in Ref. [21] correspond to $\sigma^{pv}_{pp\gamma}$ and $\sigma^{ps}_{pp\gamma}$ without being multiplied by the correction factor C_{exp}.

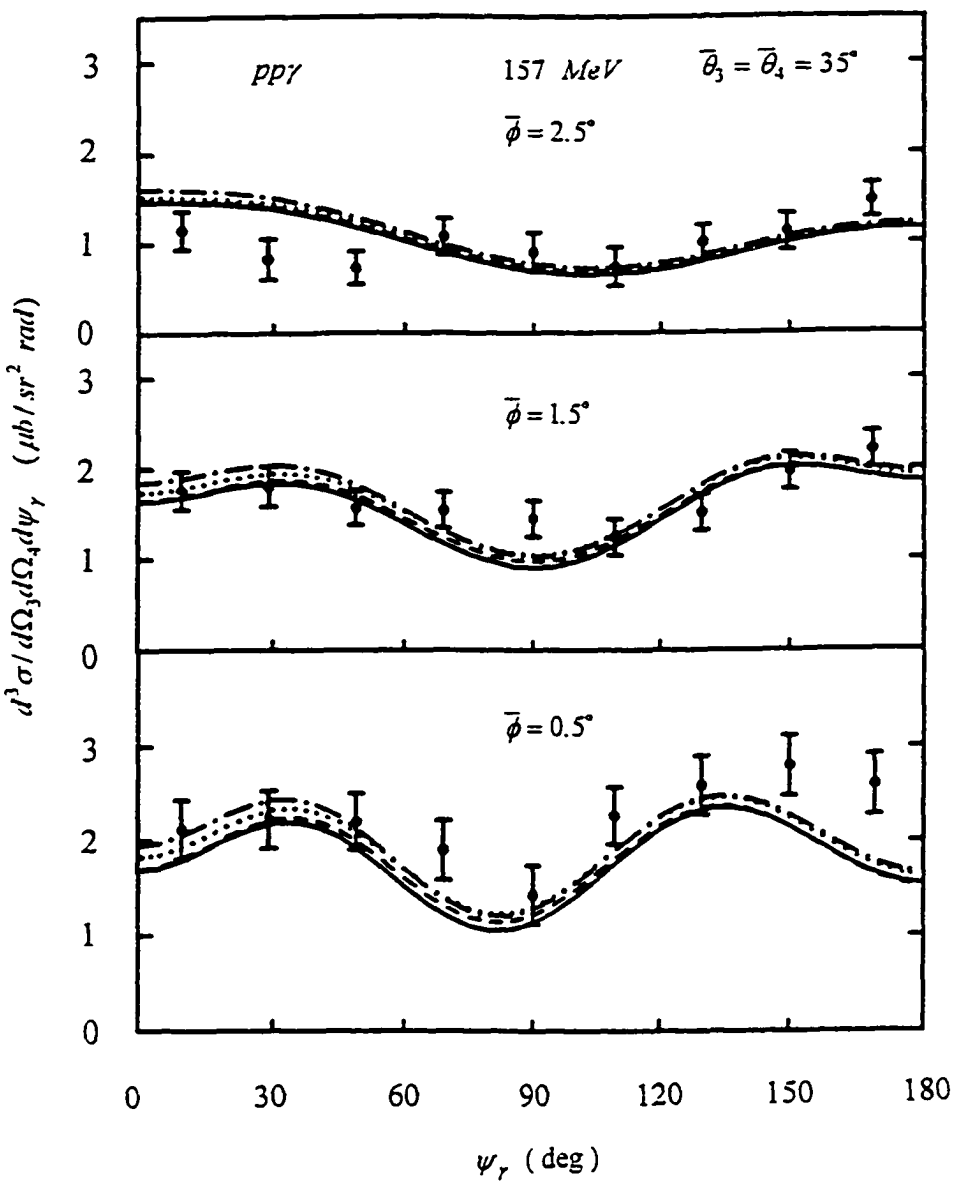

Fig.5. Same as Fig. 4, but for $\bar{\theta}_3 = \bar{\theta}_4 = 35°$.

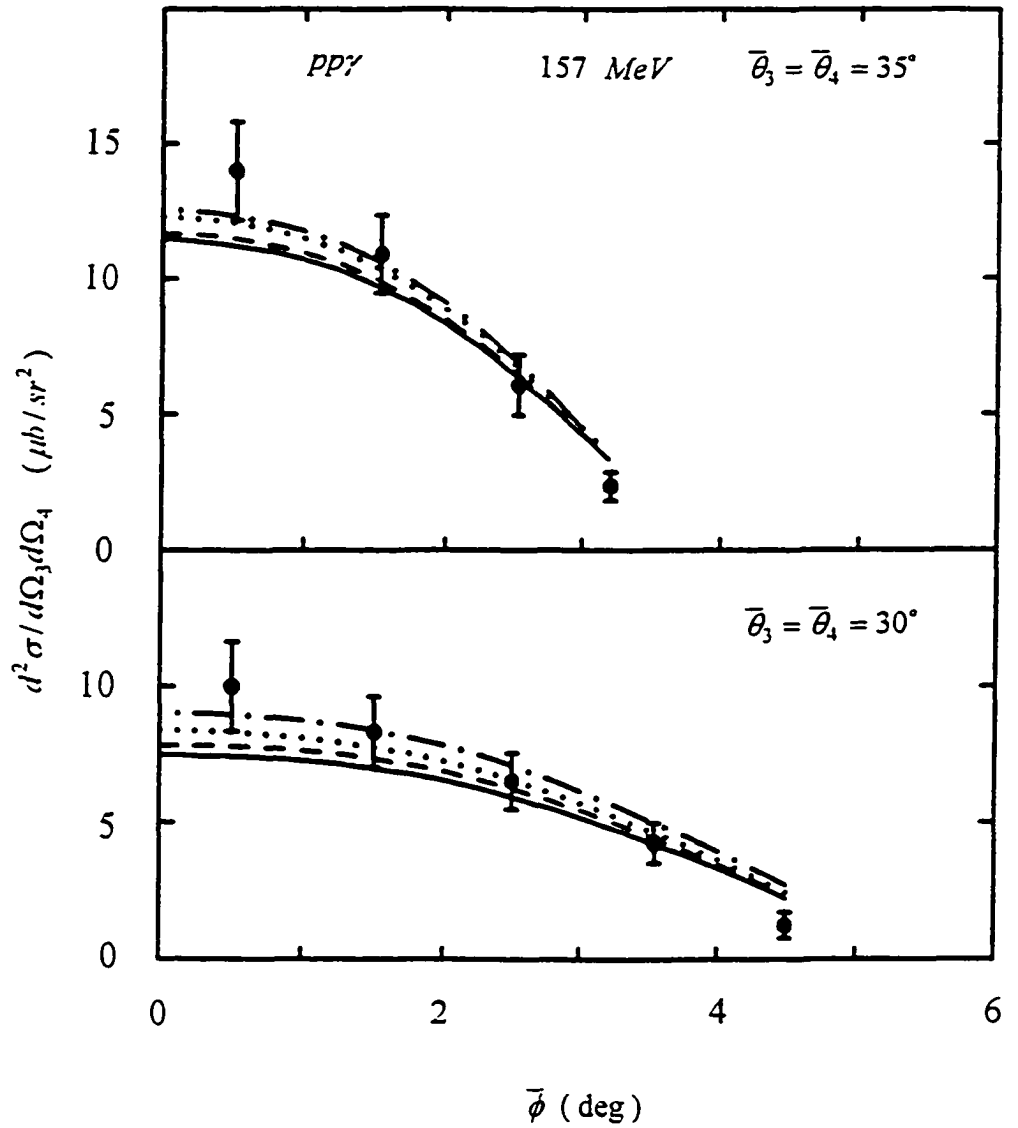

Fig.6. Integrated $pp\gamma$ cross section $d^3\sigma/d\Omega_3 d\Omega_4$ as a function of the noncoplanarity angle $\bar{\phi}$ at 157 MeV for (a) $\bar{\theta}_3 = \bar{\theta}_4 = 30°$ and (b) $\bar{\theta}_3 = \bar{\theta}_4 = 35°$. The results for $\bar{\sigma}^{pv}_{pp\gamma}$ (solid curve calculated using the set I_b parameters), $\bar{\sigma}^{ps}_{pp\gamma}$ (dash-dotted curve calculated using the set II_a parameters), $\sigma^{pv}_{pp\gamma}$ (dashed curve), and $\sigma^{ps}_{pp\gamma}$ (dotted curve) are compared with the Harvard data [37].

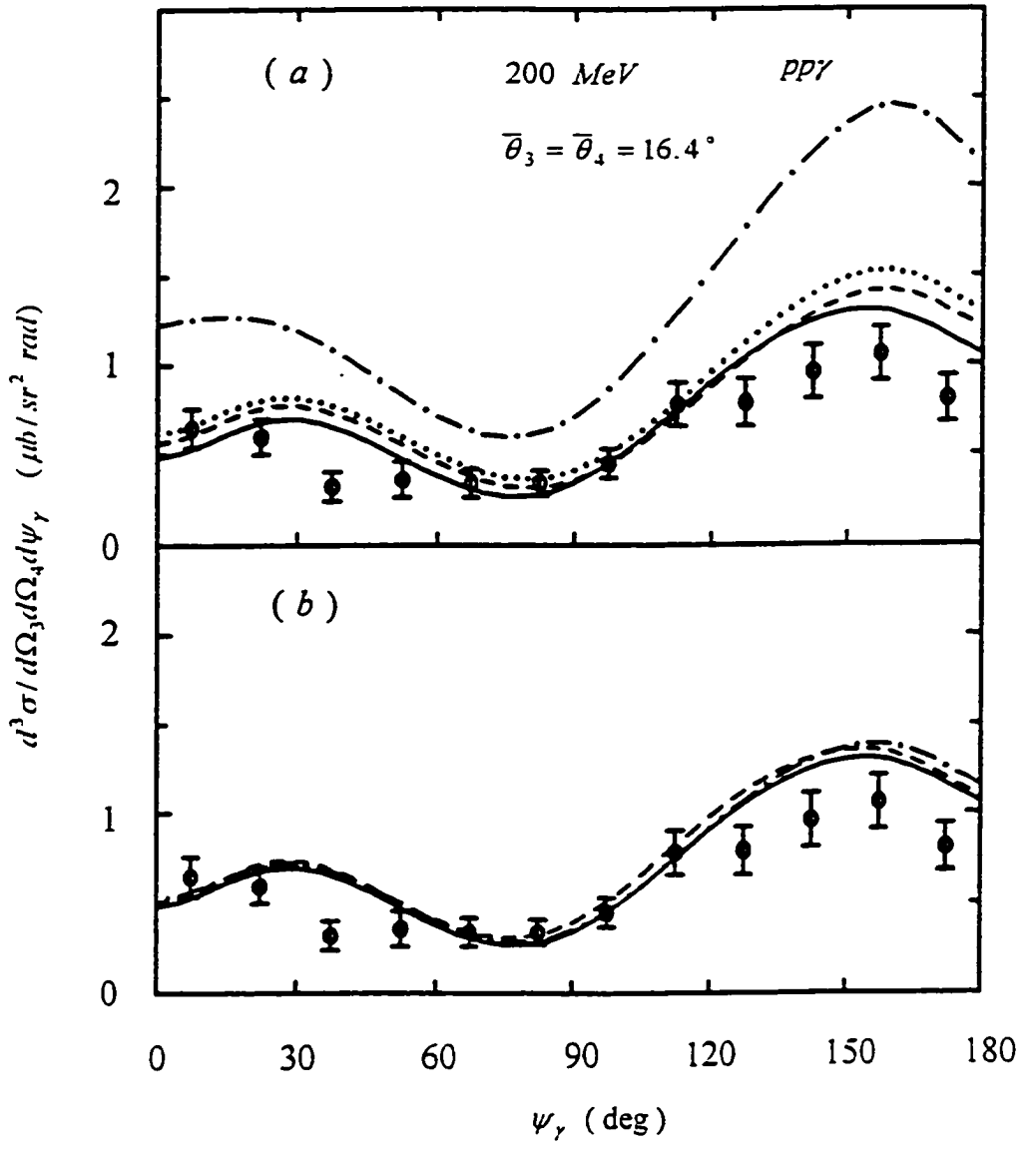

Fig.7. Coplanar $pp\gamma$ cross sections $d^3\sigma/d\Omega_3 d\Omega_4 d\psi_\gamma$ as functions of ψ_γ at 200 MeV for $\bar{\theta}_3 = \bar{\theta}_4 = 16.4°$. (a) The results for $C_{exp}\,\bar{\sigma}^{pv}_{pp\gamma}$ (solid curve calculated using the set I_b parameters), $C_{exp}\,\bar{\sigma}^{ps}_{pp\gamma}$ (dash-dotted curve calculated using the set II_a parameters), $C_{exp}\,\sigma^{pv}_{pp\gamma}$ (dashed curve), and $C_{exp}\,\sigma^{ps}_{pp\gamma}$ (dotted curve) are compared with the TRIUMF data [5]. C_{exp} represents the experimental correction factor introduced in Ref. [5]. (b) All curves represent cross sections for $C_{exp}\,\bar{\sigma}^{pv}_{pp\gamma}$ but they are calculated using three different sets of parameters, I_a (dashed curve), I_b (solid curve), and I_d (dash-dotted curve). The data are from Ref. [5].

Clearly, the cross section $C_{\exp}\bar{\sigma}^{pv}_{pp\gamma}$ (solid curve) is in better agreement with the TRIUMF data than any of the other cross sections. The data also rules out the calculation $C_{\exp}\bar{\sigma}^{ps}_{pp\gamma}$ (dash-dotted curve) because of a large discrepancy between theory and experiment. If all of the calculations shown in this figure are compared with the calculations shown in Fig. 6 of Ref. [5], we find that except for the curve corresponding to the soft-photon calculation our curve for $C_{\exp}\bar{\sigma}^{pv}_{pp\gamma}$ is in much better agreement with the TRIUMF data than those cited in Ref. [5].

In Fig. 7(b), we compare the results for the cross section $C_{\exp}\bar{\sigma}^{pv}_{pp\gamma}$ for the three different sets of parameters I_a, I_b and I_d. The difference is very small.

In Fig. 8, we show the coplanar cross section as a function of ψ_γ at 280 MeV. All theoretical cross sections are calculated using Horowitz's unpublished parameters at 300 MeV. Again, $\bar{\sigma}^{pv}_{pp\gamma}$ and $\bar{\sigma}^{ps}_{pp\gamma}$ have been calculated using the set I_b and the set II_a, respectively. The results are compared with eight sets of TRIUMF data [7], which include the $\frac{2}{3}$-normalization factor. Clearly, the calculated cross sections for $\bar{\sigma}^{ps}_{pp\gamma}$ are in gross disagreement with the data. Three other calculations for $\bar{\sigma}^{pv}_{pp\gamma}$, $\sigma^{ps}_{pp\gamma}$ and $\sigma^{pv}_{pp\gamma}$ give similar results which are in much better agreement with the data than the result for $\bar{\sigma}^{ps}_{pp\gamma}$. An important difference between those curves for $\bar{\sigma}^{pv}_{pp\gamma}$ and the other curves for $\sigma^{ps}_{pp\gamma}$ and $\sigma^{pv}_{pp\gamma}$ can be found in their shapes. The curves for $\bar{\sigma}^{pv}_{pp\gamma}$ have shapes which best describe the data.

In Fig. 9, we demonstrate that the three different sets of parameters I_a, I_b and I_d can be distinguished at 280 MeV for small proton scattering angles. As shown in Figs. 9(a) and 9(b) [$(\bar{\theta}_3, \bar{\theta}_4) = (12^o, 12.4^o)$ and $(16^o, 12.4^o)$], these three sets of parameters yield quite different results in the regions $140^o < \psi_\gamma < 180^o$ and $\psi_\gamma \leq 10^o$. The data seems to favor the value $\kappa_p^- \simeq 1.79$ (the set I_b).

In Fig. 10, we present the analyzing powers $\bar{A}^{pv}_y$ (calculated using the set I_b),

$\bar{A}_y^{ps}$ (calculated using the set Π_a), A_y^{pv} and A_y^{ps} as functions of ψ_γ at 280 MeV. Again, Horowitz's parameters at 300 MeV are used for these calculations. The results are compared with ten sets of TRIUMF data [7]. We find that the data in the region $60^o \leq \psi_\gamma \leq 120^o$ cannot be described by the calculated A_y^{pv} or A_y^{ps} (the analyzing powers calculated using the on-shell $p\gamma p$ vertex for pv coupling or ps coupling). Good agreement between theory and experiment can be achieved only if the off-shell $p\gamma p$ vertices are used. These off-shell pγp vertices depend on the two form factors $F_2^+(\omega^2)$ and $F_2^-(\omega^2)$. As will be discussed in the next section, the contribution of $F_2^-(\omega^2)$ is crucial. Without $F_2^-(\omega^2)$ it is impossible to fit the analyzing powers $\bar{A}_y^{ps}$ and $\bar{A}_y^{pv}$ to the data. Representative curves for $\bar{A}_y^{ps}$ and $\bar{A}_y^{pv}$ are shown here.

In Fig. 11, we compare the results of $\bar{A}_y^{pv}$ calculated using three different sets of parameters (I_a, I_b and I_d). The quality of the fits can be seen from these results.

Finally, we have also studied the analyzing powers at 200 MeV. In order to demonstrate that the general feature observed in Fig. 10 does not change, in Fig. 12 we show calculated $\bar{A}_y^{pv}$ (using the set I_b), $\bar{A}_y^{ps}$ (using the set II_a), A_y^{pv} and A_y^{ps} as functions of ψ_γ at 200 MeV for $\bar{\theta}_3 = \bar{\theta}_4 = 20^\circ$. Obviously, a precise measurement of analyzing powers at this energy can be used to differentiate among these calculations.

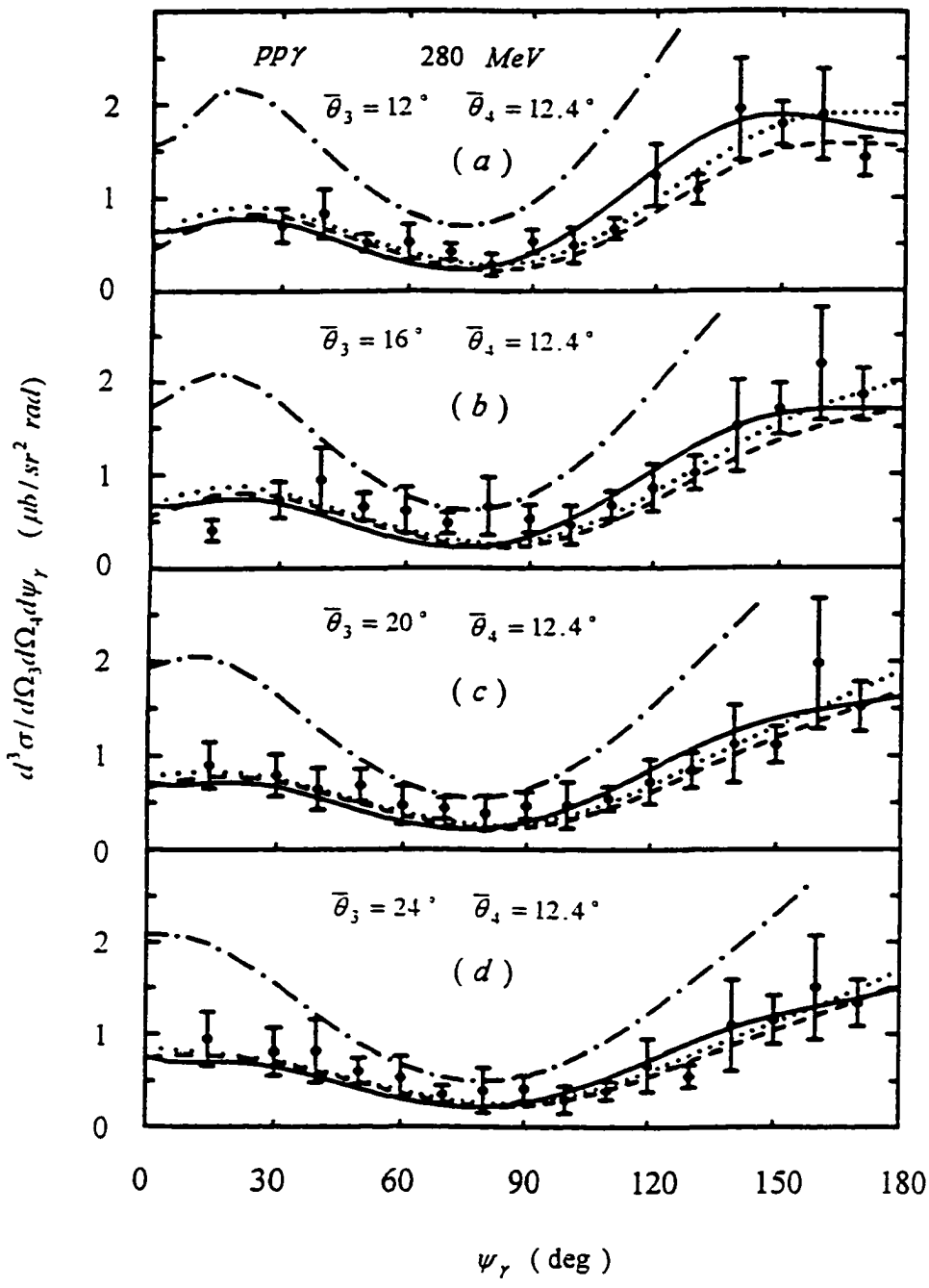

Fig.8(a-d). Coplanar $pp\gamma$ cross sections $d^3\sigma/d\Omega_3 d\Omega_4 d\psi_\gamma$ as functions of ψ_γ at 280 MeV for four sets of proton scattering angles ($\bar{\theta}_3$, $\bar{\theta}_4$). The results for $\bar{\sigma}^{pv}_{pp\gamma}$ (solid curve calculated using the set I_b parameters), $\bar{\sigma}^{ps}_{pp\gamma}$ (dash-dotted curve calculated using the set II_a parameters), $\sigma^{pv}_{pp\gamma}$ (dashed curve), and $\sigma^{ps}_{pp\gamma}$ (dotted curve) are compared with the TRIUMF data [7], which include a $\frac{2}{3}$-normalization factor.

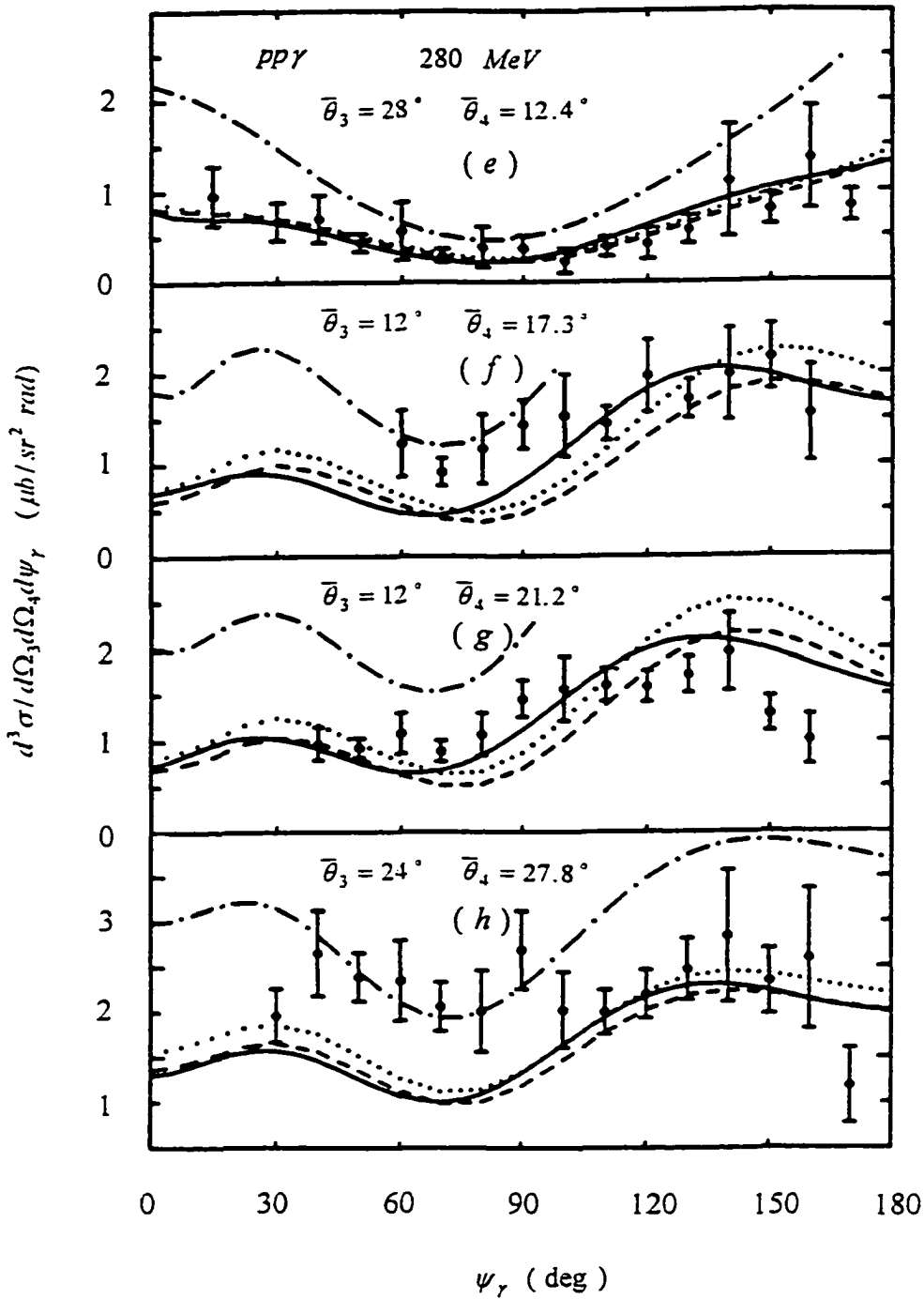

Fig.8(e-h). Same as Fig.8(a-d) but for four different sets of ($\bar{\theta}_3$, $\bar{\theta}_4$).

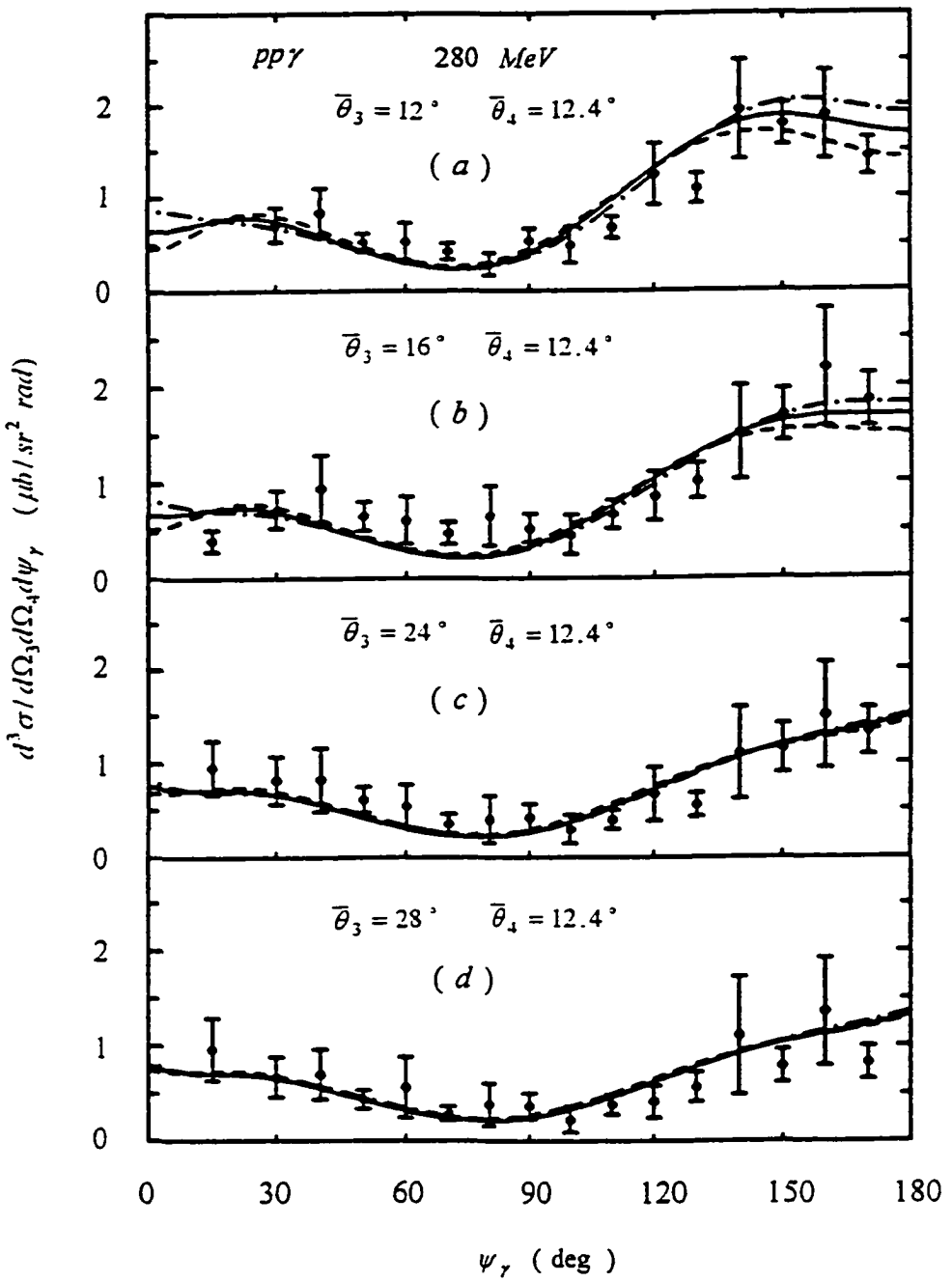

Fig.9. Coplanar $pp\gamma$ cross sections $d^3\sigma/d\Omega_3 d\Omega_4 d\psi_\gamma$ as functions of ψ_γ at 280 MeV for four sets of proton scattering angles $(\bar{\theta}_3, \bar{\theta}_4)$. All curves represent cross sections for $\bar{\sigma}^{pv}_{pp\gamma}$ but they are calculated using three different sets of parameters, I_a (dashed curve), I_b (solid curve), and I_d (dash-dotted curve). The data are from Ref. [7].

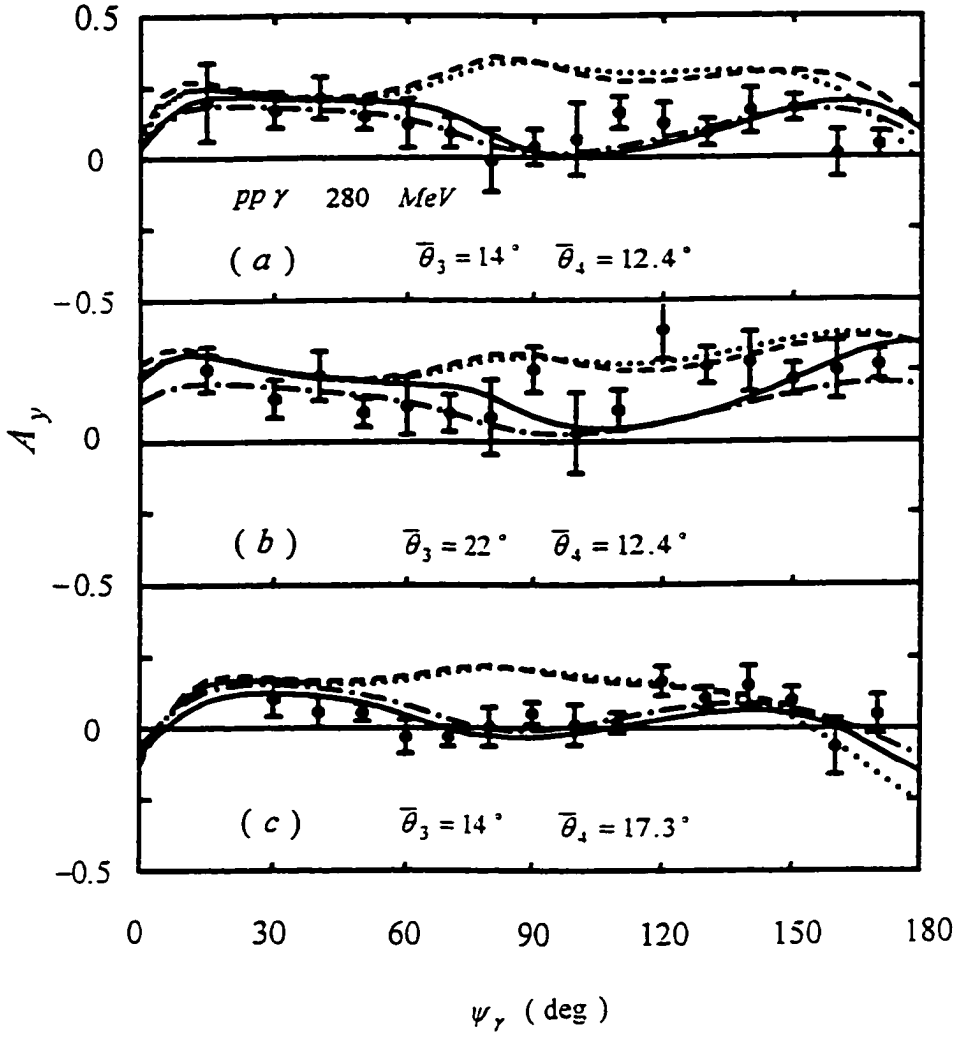

Fig. 10(a-c) Analyzing powers A_y as functions of ψ_γ at 280 MeV for three sets of proton scattering angles ($\bar{\theta}_3, \bar{\theta}_4$). The solid curves (calculated using the set I_b parameters), dash-dotted curves (calculated using the set II_a parameters), dashed curves, and dotted curves represent the results for $\bar{A}_y^{pv}$, $\bar{A}_y^{ps}$, A_y^{pv} and A_y^{ps} , respectively. The data are from Ref. [7]. These three sets of TRIUMF data have been used to determine the parameters C_1 and C_2 shown in Tables I and II.

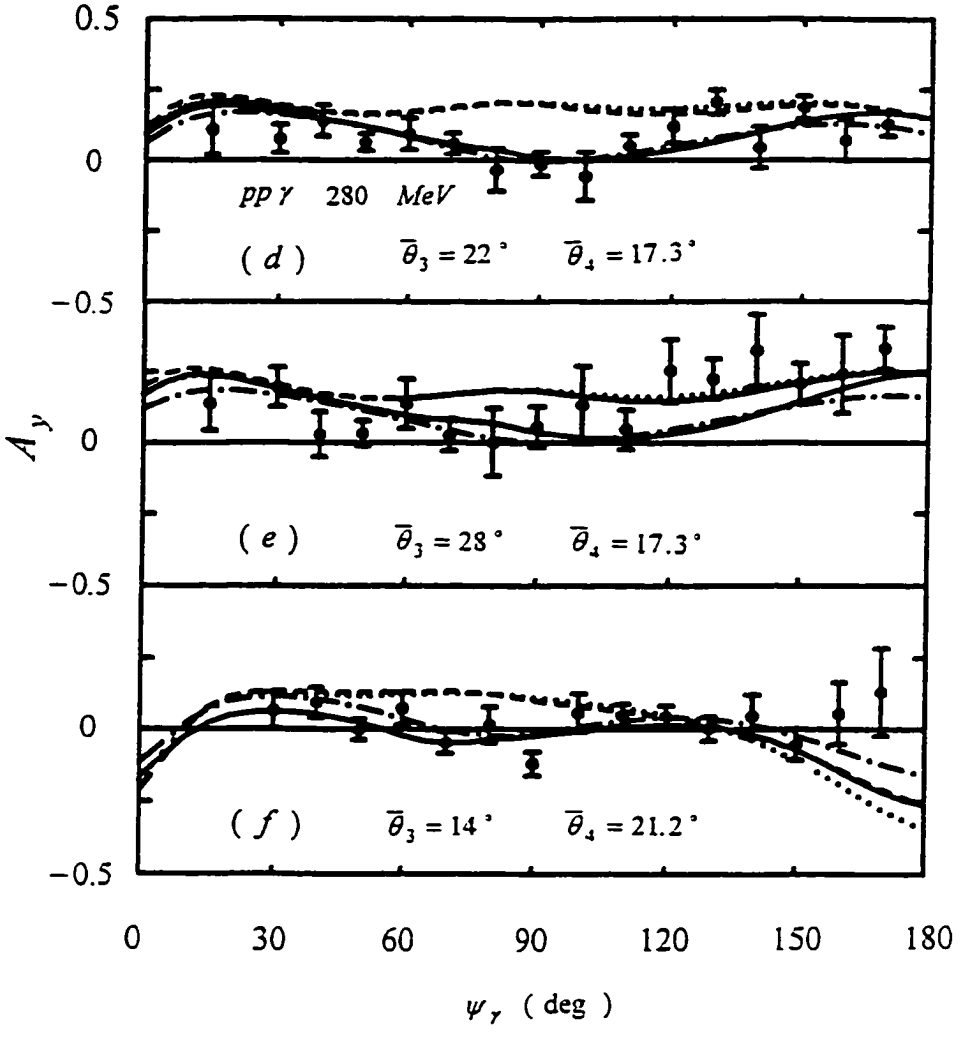

Fig. 10(d-f) Same as Fig. 10(a-c) but for three different sets of ($\bar{\theta}_3$, $\bar{\theta}_4$).

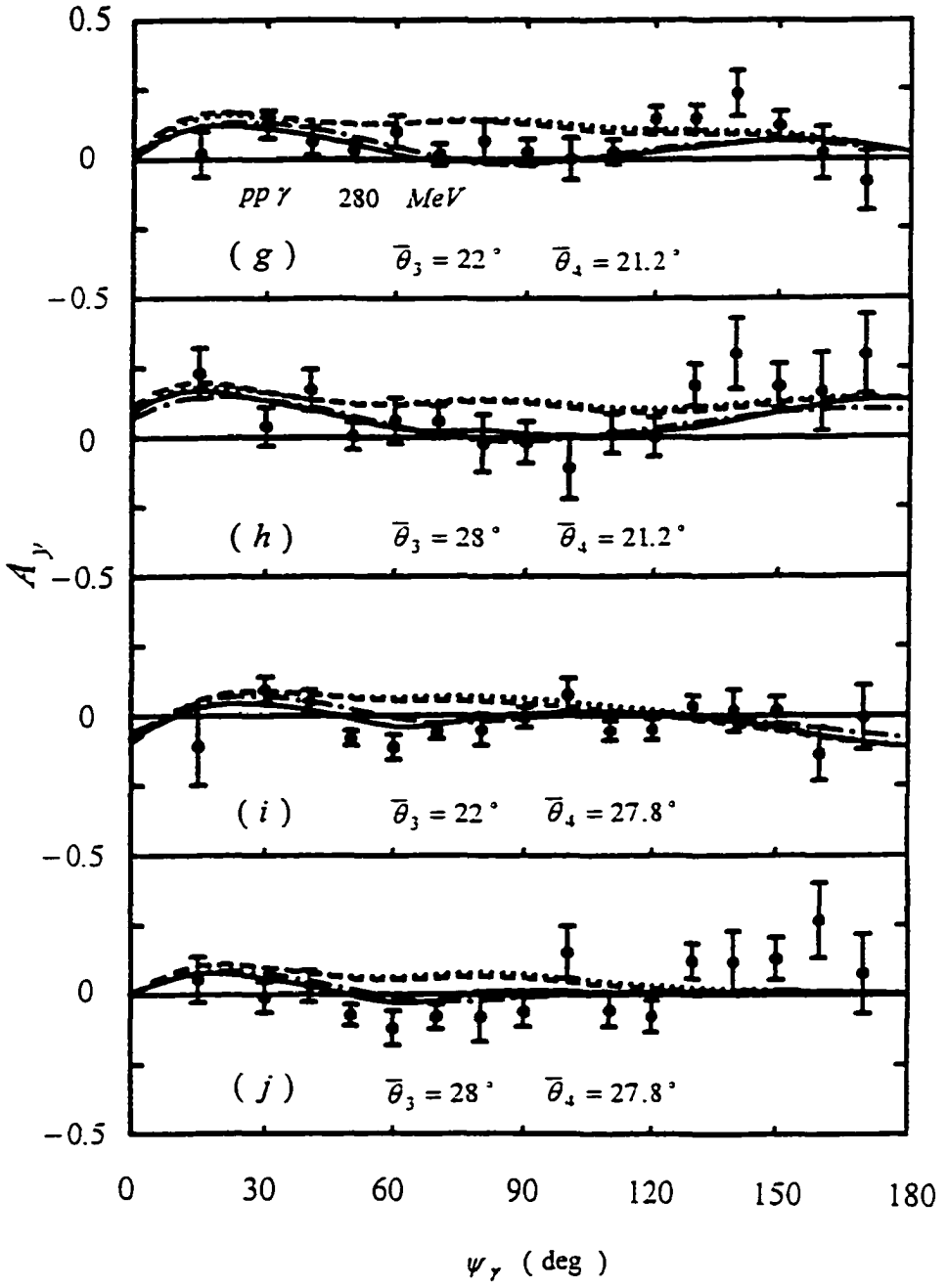

Fig.10(g-j) Same as Fig.10(a-c) but for four different sets of ($\bar{\theta}_3$, $\bar{\theta}_4$).

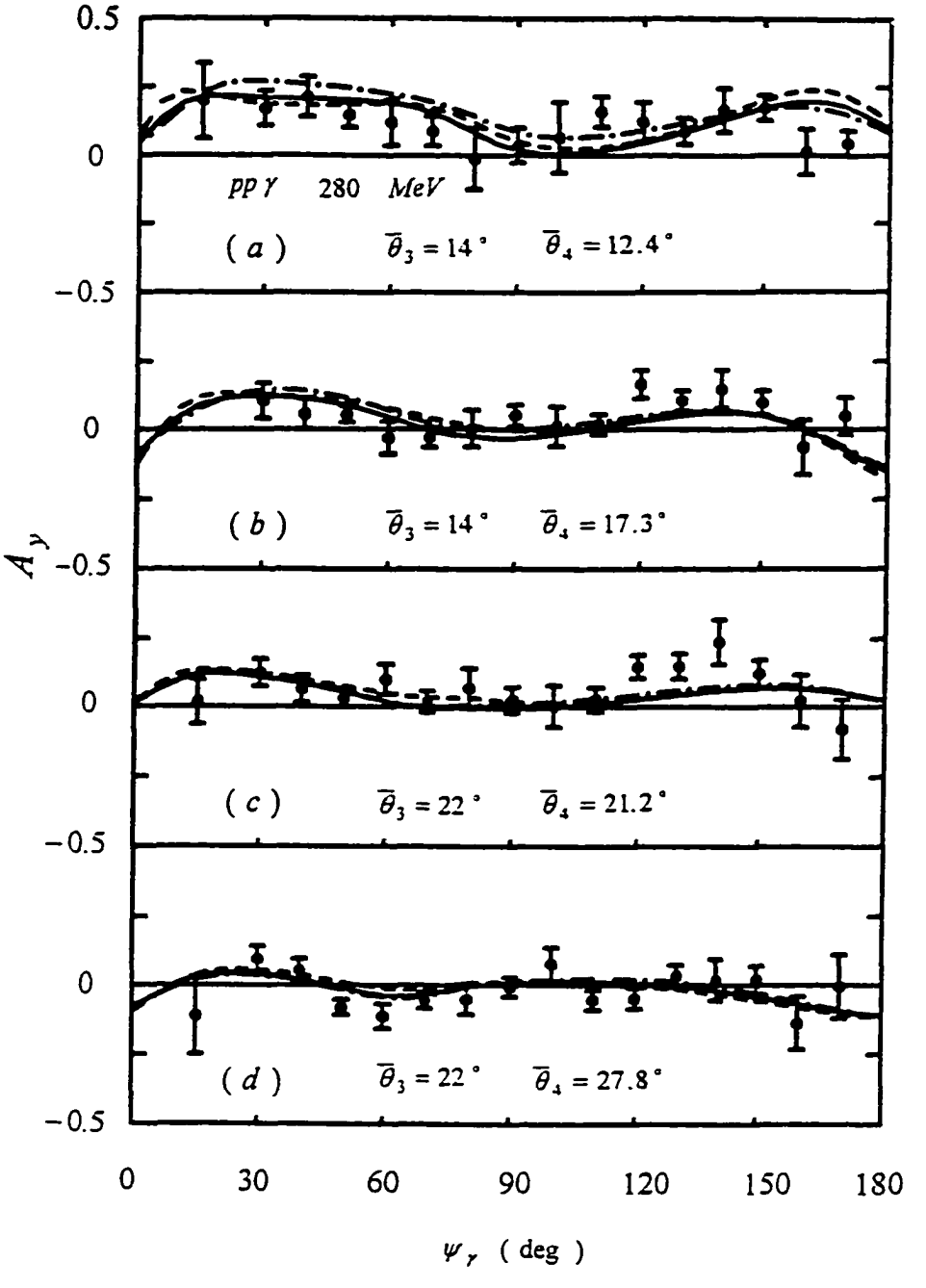

Fig.11. Analyzing powers A_y as functions of ψ_γ at 280 MeV for four sets of proton scattering angles ($\bar{\theta}_3$, $\bar{\theta}_4$). All curves represent analyzing powers for $\bar{A}_y^{pv}$ but they are calculated using three different sets of parameters, I_a (dashed curve), I_b (solid curve), and I_d (dash-dotted curve). The data are from Ref. [7].

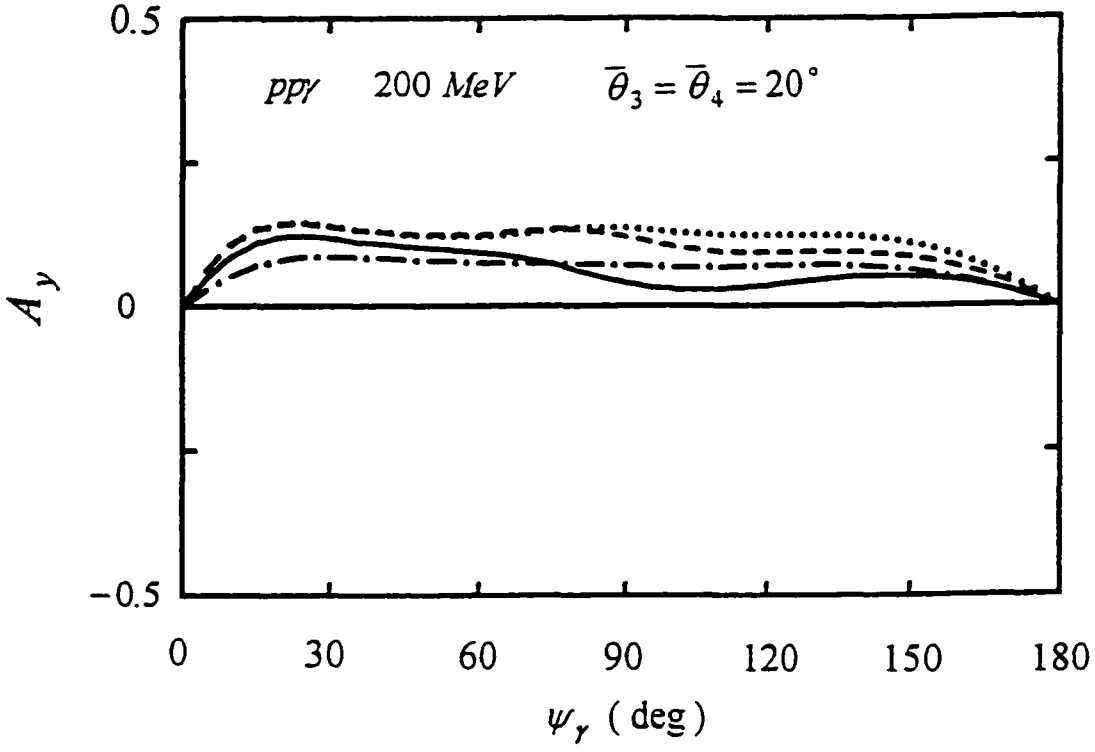

Fig.12. Analyzing powers A_y as functions of ψ_γ at 200 MeV for $\bar{\theta}_3 = \bar{\theta}_4 = 20^\circ$. The solid curve (calculated using the set I_b parameters), dash-dotted curve (calculated using the set II_a parameters), dashed curve, and dotted curve represent the results for $\bar{A}_y^{pv}$, $\bar{A}_y^{ps}$, A_y^{pv} and A_y^{ps}, respectively.

II.6 Discussion

Since the measured analyzing powers at 280 MeV in the region $60° \leq \psi_\gamma \leq 120°$ cannot be described by the calculated A_y^{pv} and A_y^{ps}, all calculations based upon the on-shell $p_\gamma p$ vertex can be ruled out by the data in this region. Moreover, Figs. 7(a) and 8 clearly show that the cross sections $\bar{\sigma}^{ps}_{pp\gamma}$, which are calculated using ps coupling and the off-shell $p_\gamma p$ vertices, fail to fit the data at 200 MeV and 280 MeV (with the $\frac{2}{3}$-normalization factor). Thus, the combined experimental data including both cross sections and analyzing powers in the energy region from 157 MeV to 280 MeV strongly indicate that only those calculations which use the pv coupling and the off-shell $p_\gamma p$ vertices consistently describe the data.

The above conclusion is based on the use of the off-shell $p_\gamma p$ vertices Γ^1_μ and Γ^2_μ given by Eqs. (II-40a) and (II-40b), respectively, which depend on two form factors $F_2^+(\omega^2)$ and $F_2^-(\omega^2)$. In order to study the contribution from $F_2^-(\omega^2)$, we have also calculated cross sections and analyzing powers using only the form factor $F_2^+(\omega^2)$. In other words, we have used two approximate vertices which are obtained from Eqs. (II-40a) and (II-40b) by dropping those terms involving $F_2^-(\omega^2)$,

$$\begin{aligned} \Gamma^1_\mu(p_i, p_i + K) &\approx \tilde{\Gamma}^1_\mu(p_i, p_i + K) \\ &= \gamma_\mu - \frac{i}{2m}\sigma_{\mu\nu}K^\nu F_2^+(\omega_i^2)\frac{\not{p}_i + \not{K} + m}{2m} \quad , \end{aligned} \tag{II-62a}$$

and

$$\begin{aligned} \Gamma^2_\mu(p_j - K, p_j) &\approx \tilde{\Gamma}^2_\mu(p_j - K, p_j) \\ &= \gamma_\mu - \frac{i}{2m}F_2^+(\omega_j^2)\frac{\not{p}_j - \not{K} + m}{2m}\sigma_{\mu\nu}K^\nu \, . \end{aligned} \tag{II-62b}$$

Some of the results obtained are shown in Figs. 13 and 14. Denoting the calculated

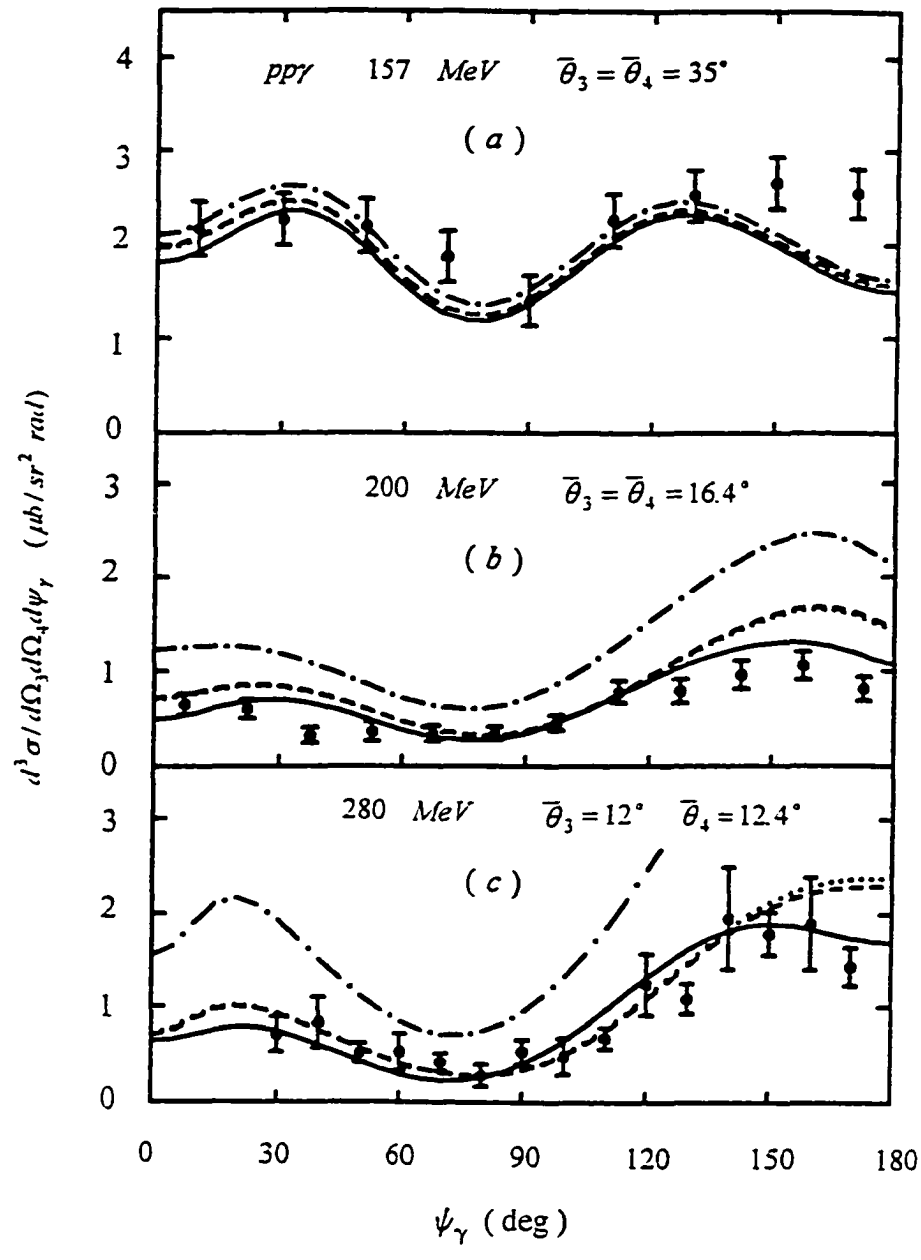

Fig.13. Coplanar ppγ cross sections $d^3\sigma/d\Omega_3 d\Omega_4 d\psi_\gamma$ as functions of ψ_γ at 157 MeV ($\bar{\theta}_3 = \bar{\theta}_4 = 35^\circ$), 200 MeV ($\bar{\theta}_3 = \bar{\theta}_4 = 16.4^\circ$), and 280 MeV ($\bar{\theta}_3 = 12^\circ$, $\bar{\theta}_4 = 12.4^\circ$). The solid curves, dash-dotted curves, dashed curves, and dotted curves represent the cross sections $\bar{\sigma}^{pv}_{pp\gamma}$, $\bar{\sigma}^{ps}_{pp\gamma}$, $\tilde{\sigma}^{pv}_{pp\gamma}$, and $\tilde{\sigma}^{ps}_{pp\gamma}$, respectively. The full off-shell pγp vertices (Γ^1_μ and Γ^2_μ) have been used to calculated $\bar{\sigma}^{pv}_{pp\gamma}$ (using the set I_b parameters) and $\bar{\sigma}^{ps}_{pp\gamma}$ (using the set II_a parameters). On the other hand, $\tilde{\sigma}^{pv}_{pp\gamma}$ and $\tilde{\sigma}^{ps}_{pp\gamma}$ are calculated using the two approximate vertices ($\tilde{\Gamma}^1_\mu$ and $\tilde{\Gamma}^2_\mu$), which depend only on the form factor $F_2^+(\omega^2)$. The data at 157, 200 and 280 MeV are from Refs. [37], [5] and [7], respectively.

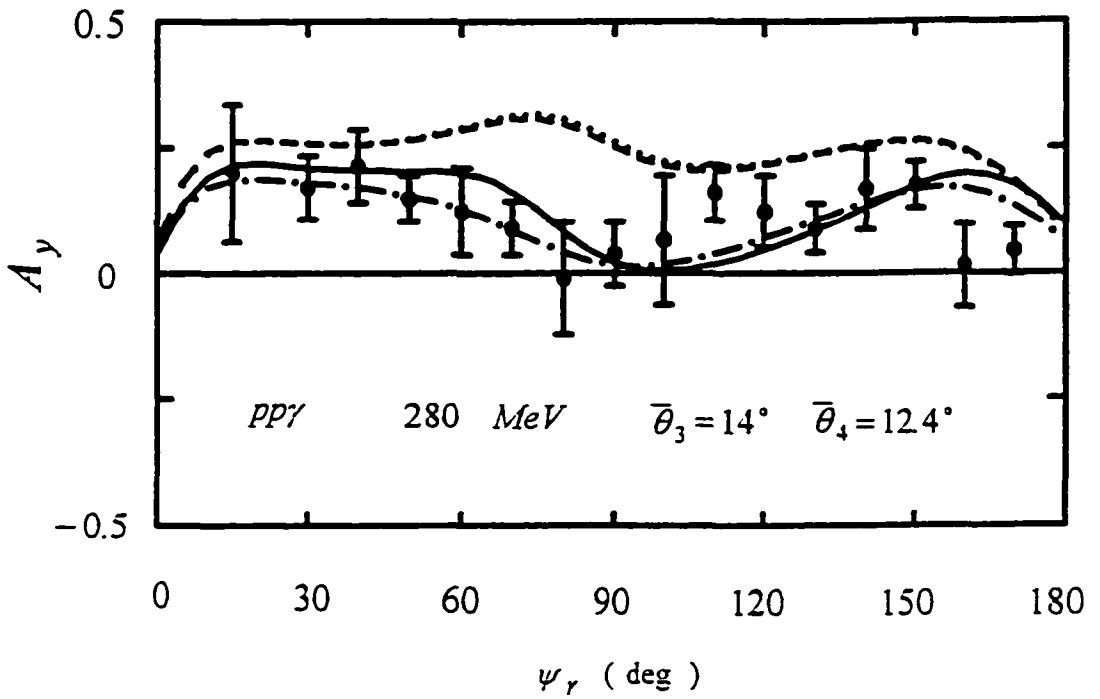

Fig.14. Analyzing powers A_y as functions of ψ_γ at 280 MeV for ($\bar{\theta}_3$, $\bar{\theta}_4$) = (14°, 12.4°). The solid curves, dash-dotted curves, dashed curves, and dotted curves represent the analyzing powers $\bar{A}_y^{pv}$, $\bar{A}_y^{ps}$, $\tilde{A}_y^{pv}$, and $\tilde{A}_y^{ps}$, respectively. The full off-shell $p\gamma p$ vertices (Γ_μ^1 and Γ_μ^2) have been used to calculated $\bar{A}_y^{pv}$ (using the set I_b parameters) and $\bar{A}_y^{ps}$ (using the set II_a parameters), but the two approximate vertices ($\tilde{\Gamma}_\mu^1$ and $\tilde{\Gamma}_\mu^2$) have been used to calculated $\tilde{A}_y^{pv}$ and $\tilde{A}_y^{ps}$. The data are from Ref. [7].

cross sections and analyzing powers respectively as $\tilde{\sigma}^{ps}_{pp\gamma}$ and $\tilde{A}^{ps}_{y}$ for ps coupling and $\tilde{\sigma}^{pv}_{pp\gamma}$ and $\tilde{A}^{pv}_{y}$ for pv coupling, our results can be summarized as follows: (i) Generally speaking, the cross sections ($\tilde{\sigma}^{ps(pv)}_{pp\gamma}$) and analyzing powers ($\tilde{A}^{ps(pv)}_{y}$) calculated using the vertices $\tilde{\Gamma}^{1}_{\mu}$ and $\tilde{\Gamma}^{2}_{\mu}$ are similar to those cross sections ($\sigma^{ps(pv)}_{pp\gamma}$) and analyzing powers ($A^{ps(pv)}_{y}$) calculated using the on-shell vertex Γ^{p}_{μ} (Eq. (II-13)). This can be seen if we compare Fig. 13(a) with Fig. 5, Fig. 13(b) with Fig. 7, Fig. 13(c) with Fig. 8(a), and Fig. 14 with Fig. 10(a). This is not surprising. For small K, we have $F_2^{+}(\omega_i^2) \approx F_2^{+}(\omega_j^2) \approx \kappa_p = 1.79$ (see Fig. 2) and $\tilde{\Gamma}^{1}_{\mu} \approx \tilde{\Gamma}^{2}_{\mu} \approx \Gamma_{\mu}$. Therefore, we expect $\tilde{\sigma}^{ps(pv)}_{pp\gamma}$ and $\tilde{A}^{ps(pv)}_{y}$ to be similar to $\sigma^{ps(pv)}_{pp\gamma}$ and $A^{ps(pv)}_{y}$, respectively. (ii) Deviations in cross section ($\tilde{\sigma}^{ps}_{pp\gamma} - \tilde{\sigma}^{pv}_{pp\gamma}$) and analyzing power ($\tilde{A}^{ps}_{y} - \tilde{A}^{pv}_{y}$) are extremely small. (iii) The agreement between the calculated cross sections ($\tilde{\sigma}^{ps}_{pp\gamma}$ or $\tilde{\sigma}^{pv}_{pp\gamma}$) and the experimental data is in general good. However, this is not the case for the analyzing powers. The calculated analyzing powers ($\tilde{A}^{ps}_{y}$ or $\tilde{A}^{pv}_{y}$) are in very poor agreement with the experimental data at 280 MeV in the region $60° \leq \psi_\gamma \leq 120°$ for most cases. (iv) Good agreement between the calculated analyzing powers and the TRIUMF data (especially in the region $60° \leq \psi_\gamma \leq 120°$) can be achieved if the form factor $F_2^{-}(\omega^2)$ is taken into account (see Figs. 14 and 10). Our results represent the first clear evidence for the need of the form factor $F_2^{-}(\omega^2)$ to describe the measured analyzing powers.

Our findings may have a significant implication. In the abstract of Ref. [7], the authors state " The experiment shows the first unambiguous evidence for off-shell effects in the free nucleon-nucleon interaction, in that the analyzing powers disagree strongly with the predictions of the soft-photon approximation (which incorporates only

on-shell information) but are consistent with the results of calculations using the Bonn and Paris potentials. " The soft-photon approximation used to predict the analyzing powers in Ref. [7] is Low's conventional amplitude. Since the on-shell $p\gamma p$ vertex has been used in Low's amplitude, this vertex might cause the same problem in describing the data (analyzing powers) in the region $60° < \psi_\gamma < 120°$. Therefore, the large discrepancy found in the predictions calculated between the potential model and the soft-photon approximation could be mainly due to the electromagnetic vertex, rather than the hadronic off-shell effects.

As shown in Section II.3, our $pp\gamma$ amplitudes are generated from Horowitz's OBE diagrams with OBE parameters, which involve masses, coupling constants and cut-off parameters for ten "mesons". Our calculations are based on three sets of parameters developed by Horowitz at 135, 200 and 300 MeV. In these sets, masses are fixed, while the coupling constants and cut-off parameters vary with energy. However, our study shows that the calculated $pp\gamma$ cross sections are not sensitive to the variation of parameters with energy. For example, using the on-shell $p\gamma p$ vertex and three different sets of Horowitz parameters, the calculated $pp\gamma$ cross sections at 280 MeV for $(\bar{\theta}_3, \bar{\theta}_4) = (12°, 12.4°)$ give very similar results, which are in good agreement with the TRIUMF data and most of the results obtained in the potential model. A comparison between the TRIUMF data and the theoretical predictions calculated using the parameters at 300 MeV is shown in Fig. 8a. Moreover, we have also found that the calculated analyzing powers using the three sets of parameters (and the on-shell $p\gamma p$ vertex) yield almost the same results at forward ($\psi_\gamma < 10°$) and backward ($\psi_\gamma > 170°$) photon angles. Thus, even though the $pp\gamma$ reaction samples the NN

interaction down to rather low energy at forward and backward photon angles, we believe that our results should still be quite accurate. Specifically, our predicted photon angular distribution successfully describes the rising of the cross sections at forward and backward photon angles even for the case of small proton angles. Note that the existence of some cancellation in the charge contribution (due to two identical protons) leads to the dominance of the magnetic moment contribution in the $pp\gamma$ process at 280 MeV. This is why the typical quadruple shapes are not observed in most of the observed $pp\gamma$ spectra. The controlling factor for the rising cross sections at forward and backward angles is the magnetic moment of the proton, not the energy dependence of the Horowitz's parameters.

The TRIUMF data at 200 MeV have played an important role in our investigation of the ps-pv problem. This is because TRIUMF's recent cross sections at 280 MeV involve an ambiguity due to the use of a $\frac{2}{3}$-normalization factor. One should not only compare the theoretical predictions with the data at 280 MeV but should also investigate the implications for the other data at 157 and 200 MeV. Obviously, new measurements in pp_γ cross sections and analyzing powers in the energy region between 200 and 300 MeV could help to resolve this ambiguity. Moreover, the new data could also be used to determine the parameters C_1 and C_2. It would certainly be of interest to know if these new parameters are consistent with the set of parameters obtained from the TRIUMF data, and if the combined data could be used to select the best set of parameters.

A mixture of ps coupling and pv coupling is a possibility. This however requires the introduction of another free parameter. More data would allow one to investigate

this problem.

In conclusion, the off-shell $p_\gamma p$ vertex must be used in our pp_γ calculations. The experimental data, which include cross sections and analyzing powers at 157, 200 and 280 MeV, can only be consistently described by the calculations using pseudovector coupling and the off-shell $p_\gamma p$ vertex. More accurate measurements of cross sections and/or analyzing powers for small proton scattering angles in the energy region between 200 and 300 MeV could be used to resolve the $\frac{2}{3}$-ambiguity, to check our results , and to provide more precise data for further investigation of the off-shell proton electromagnetic vertex and the ps-pv problem. More complete theoretical calculations which take into account the rescattering term and other contributions are needed in order to confirm our findings.

Chapter III

RESCATTERING CONTRIBUTION

The existence of a serious discrepancy between the measured analyzing powers and the calculated A_y^{pv} or A_y^{ps} at 280 MeV in the region $60° \leq \psi_\gamma \leq 120°$ (for those cases with small proton scattering angles) is significant and unusual. In this region, the data show a minimum around $\psi_\gamma = 90°$ for many cases, yet each of the calculated curves shows a large maximum peaked near $\psi_\gamma = 90°$ for the same cases. To resolve this discrepancy, we have focused our investigation on an important contribution from the form factor F_2^-. However one might raise the question as to whether the rescattering term, which has heretofore not been included in our model, may possibly be the cause of the discrepancy. To answer this question, we proceed with an investigation of the rescattering contribution.

III.1 Rescattering Diagrams And Amplitudes

As we have mentioned in Section II.1, Horowitz's model is not a simple OBE model, i.e., this model is realistic and presumably incorporates iteration effects. The full iteration scheme for $pp\gamma$ process may be represented diagramationally as

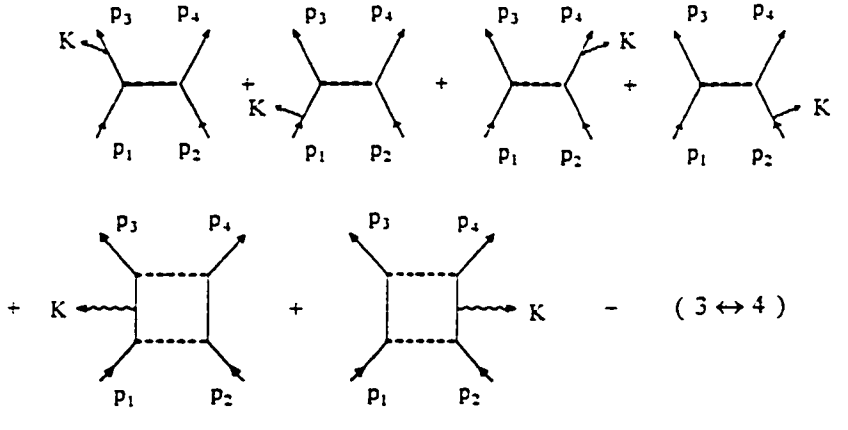

Fig.15. The full iteration scheme for $pp\gamma$ process in Horowitz OBE model.

where the heavy dashed line denotes iteration. The first four of the above diagrams correspond to the tree diagrams, while the later two correspond to the rescattering diagrams which we will presently consider. Hence, the rescattering contribution in Horowitz's model comes from four diagrams as shown in Fig.16.

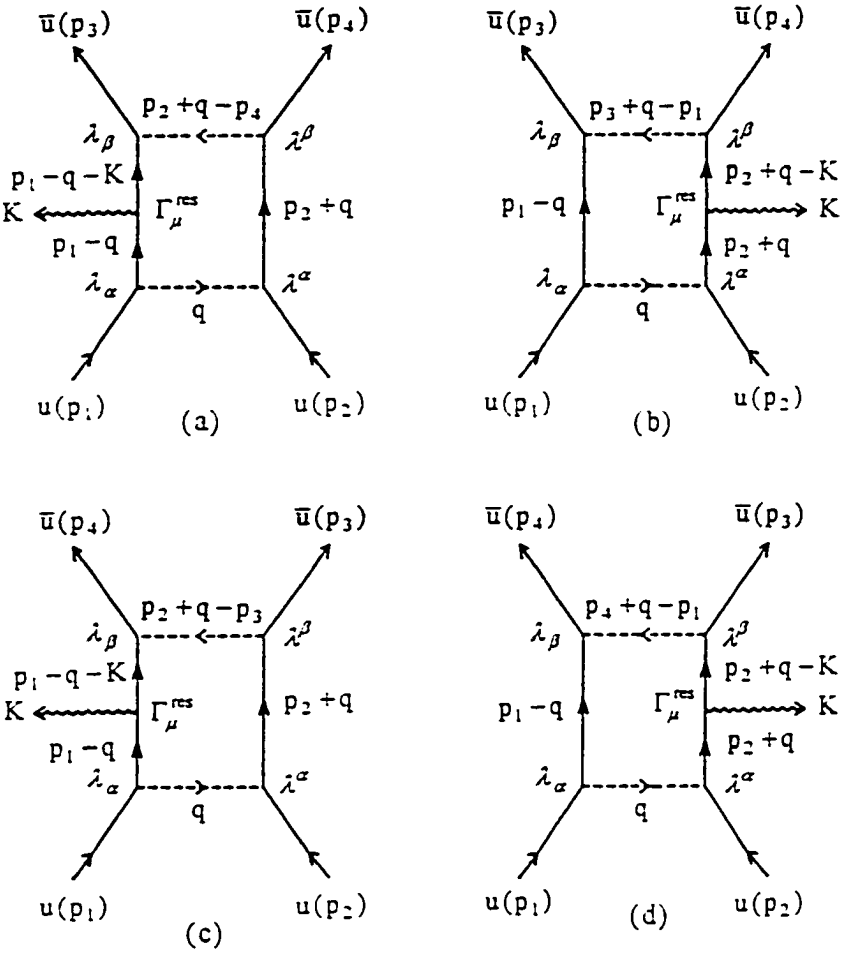

Fig.16. Feynman diagrams for the $pp\gamma$ rescattering process in Horowitz OBE model.

Using the Feynman rules, we can express the rescattering amplitude for ps coupling as

$$M_{\mu}^{res(ps)} = M_{a\mu}^{ps} + M_{b\mu}^{ps} + M_{c\mu}^{ps} + M_{d\mu}^{ps} , \qquad \text{(III-1)}$$

where

$$M^{ps}_{a\mu} = \sum_{\alpha,\beta=1}^{5}\sum_{\gamma,\tau=1}^{4}\int\frac{d^4q}{(2\pi)^4}\left\{\left[\bar{u}(p_3,\nu_3)\lambda_\beta iS_F(p_1-q-K)\Gamma^{res}_\mu iS_F(p_1-q)\lambda_\alpha u(p_1,\nu_1)\right]\right.$$

$$\left.\cdot\left[\bar{u}(p_4,\nu_4)\lambda^\beta iS_F(p_2+q)\lambda^\alpha u(p_2,\nu_2)\right]\left[f^2_{\beta\gamma}(p_2+q-p_4)G_{\beta\gamma}(p_2+q-p_4)f^2_{\alpha\tau}(q)G_{\alpha\tau}(q)\right]\right\}$$

$$= i\sum_{\alpha,\beta=1}^{5}\sum_{\gamma,\tau=1}^{4}\int\frac{d^4q}{(2\pi)^4}\left\{\left[\bar{u}(p_3,\nu_3)\lambda_\beta(\not{p}_1-\not{q}-\not{K}+m)\Gamma^{res}_\mu(\not{p}_1-\not{q}+m)\lambda_\alpha u(p_1,\nu_1)\right]\right.$$

$$\cdot\left[\bar{u}(p_4,\nu_4)\lambda^\beta(\not{p}_2+\not{q}+m)\lambda^\alpha u(p_2,\nu_2)\right]\left[\frac{1}{(p_1-q-K)^2-m^2+i\epsilon}\frac{1}{(p_1-q)^2-m^2+i\epsilon}\right.$$

$$\left.\left.\frac{1}{(p_2+q)^2-m^2+i\epsilon}\frac{4\pi g^2_{\beta\gamma}f^2_{\beta\gamma}(p_2+q-p_4)}{(p_2+q-p_4)^2-m^2_{\beta\gamma}+i\epsilon_{\beta\gamma}}\frac{4\pi g^2_{\alpha\tau}f^2_{\alpha\tau}(q)}{q^2-m^2_{\alpha\tau}+i\epsilon_{\alpha\tau}}\right]\right\}, \qquad \text{(III-2)}$$

$$M^{ps}_{b\mu} = \sum_{\alpha,\beta=1}^{5}\sum_{\gamma,\tau=1}^{4}\int\frac{d^4q}{(2\pi)^4}\left\{\left[\bar{u}(p_4,\nu_4)\lambda^\beta iS_F(p_2+q-K)\Gamma^{res}_\mu iS_F(p_2+q)\lambda^\alpha u(p_2,\nu_2)\right]\right.$$

$$\left.\cdot\left[\bar{u}(p_3,\nu_3)\lambda_\beta iS_F(p_1-q)\lambda_\alpha u(p_1,\nu_1)\right]\left[f^2_{\beta\gamma}(p_3+q-p_1)G_{\beta\gamma}(p_3+q-p_1)f^2_{\alpha\tau}(q)G_{\alpha\tau}(q)\right]\right\}$$

$$= i\sum_{\alpha,\beta=1}^{5}\sum_{\gamma,\tau=1}^{4}\int\frac{d^4q}{(2\pi)^4}\left\{\left[\bar{u}(p_4,\nu_4)\lambda^\beta(\not{p}_2+\not{q}-\not{K}+m)\Gamma^{res}_\mu(\not{p}_2+\not{q}+m)\lambda^\alpha u(p_2,\nu_2)\right]\right.$$

$$\cdot\left[\bar{u}(p_3,\nu_3)\lambda_\beta(\not{p}_1-\not{q}+m)\lambda_\alpha u(p_1,\nu_1)\right]\left[\frac{1}{(p_1-q)^2-m^2+i\epsilon}\frac{1}{(p_2+q-K)^2-m^2+i\epsilon}\right.$$

$$\left.\left.\frac{1}{(p_2+q)^2-m^2+i\epsilon}\frac{4\pi g^2_{\beta\gamma}f^2_{\beta\gamma}(p_3+q-p_1)}{(p_3+q-p_1)^2-m^2_{\beta\gamma}+i\epsilon_{\beta\gamma}}\frac{4\pi g^2_{\alpha\tau}f^2_{\alpha\tau}(q)}{q^2-m^2_{\alpha\tau}+i\epsilon_{\alpha\tau}}\right]\right\}, \qquad \text{(III-3)}$$

$$M^{ps}_{c\mu} = -M^{ps}_{a\mu}(3\leftrightarrow4), \qquad \text{(III-4)}$$

$$M^{ps}_{d\mu} = -M^{ps}_{b\mu}(3\leftrightarrow4), \qquad \text{(III-5)}$$

In the above expressions, ϵ, $\epsilon_{\alpha\tau}$, and $\epsilon_{\beta\gamma}$ are all positive, infinitesimal, and in general be distinct. Correspondingly, the total bremsstrahlung amplitude for ps coupling is

$$M^{ps}_{i\mu} = M^{ps}_{\mu} + M^{res(ps)}_{\mu} = M^{ps}_{\mu} + M^{ps}_{a\mu} + M^{ps}_{b\mu} + M^{ps}_{c\mu} + M^{ps}_{d\mu}, \qquad \text{(III-6)}$$

The amplitude $M_{t\mu}^{ps}$ must satisfy both the Pauli principle and the gauge invariance condition. Obviously, $M_{t\mu}^{ps}$ obeys the Pauli principle. As for gauge invariance, since the single scattering term M_{μ}^{ps} is gauge invariant already (see Part A of Section II.3), imposing the gauge invariance condition to $M_{t\mu}^{ps}$ gives

$$(M_{a\mu}^{ps} + M_{b\mu}^{ps} + M_{c\mu}^{ps} + M_{d\mu}^{ps}) \cdot K^{\mu} = 0 \ . \tag{III-7}$$

This equation tells us that we can choose the $p\gamma p$ vertex in Eqs. (III-2)-(III-5) as

$$\Gamma_{\mu}^{res} = - \frac{i \kappa_p}{2m} \sigma_{\mu\nu} K^{\nu} \ . \tag{III-8}$$

For simplicity, let

$$\Xi_1^{ps}(q) = (4\pi)^2 g_{\beta\gamma}^2 g_{\alpha\tau}^2 \left[\bar{u}(p_3,\nu_3) \lambda_{\beta} (\not{p}_1 - \not{q} + \not{K} + m) \Gamma_{\mu}^{res} (\not{p}_1 - \not{q} + m) \lambda_{\alpha} u(p_1,\nu_1) \right]$$
$$\cdot \left[\bar{u}(p_4,\nu_4) \lambda^{\beta} (\not{p}_2 + \not{q} + m) \lambda^{\alpha} u(p_2,\nu_2) \right] \tag{III-9}$$

$$\Xi_2^{ps}(q) = (4\pi)^2 g_{\beta\gamma}^2 g_{\alpha\tau}^2 \left[\bar{u}(p_3,\nu_3) \lambda_{\beta} (\not{p}_1 - \not{q} + m) \lambda_{\alpha} u(p_1,\nu_1) \right]$$
$$\cdot \left[\bar{u}(p_4,\nu_4) \lambda^{\beta} (\not{p}_2 + \not{q} - \not{K} + m) \Gamma_{\mu}^{res} (\not{p}_2 + \not{q} + m) \lambda^{\alpha} u(p_2,\nu_2) \right] \tag{III-10}$$

and then equations (III-2) and (III-3) become

$$M_{a\mu}^{ps} = i \sum_{\alpha,\beta=1}^{5} \sum_{\gamma,\tau=1}^{4} \int \frac{d^4q}{(2\pi)^4} \Xi_1^{ps}(q) \, f_{\beta\gamma}^2 (p_2+q-p_4) \, f_{\alpha\tau}^2(q) \cdot \left[\frac{1}{[(p_1-q-K)^2 - m^2 + i\epsilon]} \right.$$
$$\left. \frac{1}{[(p_1-q)^2 - m^2 + i\epsilon]} \frac{1}{[(p_2+q)^2 - m^2 + i\epsilon]} \frac{1}{[(p_2+q-p_4)^2 - m_{\beta\gamma}^2 + i\epsilon_{\beta\gamma}]} \frac{1}{[q^2 - m_{\alpha\tau}^2 + i\epsilon_{\alpha\tau}]} \right]$$
$$= \frac{i}{(2\pi)^4} \sum_{\alpha,\beta=1}^{5} \sum_{\gamma,\tau=1}^{4} \int_{-\infty}^{\infty} dq^o \left\{ \int_{-\infty}^{\infty} d^3\bar{q} \ \Xi_1^{ps}(q) \ f_{\beta\gamma}^2 (p_2+q-p_4) \ f_{\alpha\tau}^2(q) \cdot \right.$$
$$\left[\frac{1}{[q^o + K^o - p_1^o - \sqrt{(\bar{\vec{q}} + \bar{\vec{K}} - \bar{\vec{p}}_1)^2 + m^2} + i\epsilon]} \frac{1}{[q^o + K^o - p_1^o + \sqrt{(\bar{\vec{q}} + \bar{\vec{K}} - \bar{\vec{p}}_1)^2 + m^2} - i\epsilon]} \right.$$
$$\left. \frac{1}{[q^o - p_1^o - \sqrt{(\bar{\vec{q}} - \bar{\vec{p}}_1)^2 + m^2} + i\epsilon]} \frac{1}{[q^o - p_1^o + \sqrt{(\bar{\vec{q}} - \bar{\vec{p}}_1)^2 + m^2} - i\epsilon]} \right.$$

$$\frac{1}{[q^o+p_2^o-\sqrt{(\vec{q}+\vec{p}_2)^2+m^2}+i\epsilon]}\,\frac{1}{[q^o+p_2^o+\sqrt{(\vec{q}+\vec{p}_2)^2+m^2}-i\epsilon]}$$

$$\frac{1}{[q^o+p_2^o-p_4^o-\sqrt{(\vec{q}+\vec{p}_2-\vec{p}_4)^2+m_{\beta\gamma}^2}+i\epsilon_{\beta\gamma}]}\,\frac{1}{[q^o+p_2^o-p_4^o+\sqrt{(\vec{q}+\vec{p}_2-\vec{p}_4)^2+m_{\beta\gamma}^2}-i\epsilon_{\beta\gamma}]}$$

$$\left.\frac{1}{[q^o-\sqrt{\vec{q}^2+m_{\alpha\tau}^2}+i\epsilon_{\alpha\tau}]}\,\frac{1}{[q^o+\sqrt{\vec{q}^2+m_{\alpha\tau}^2}-i\epsilon_{\alpha\tau}]}\right]\Bigg\}\,, \qquad \text{(III-11)}$$

$$M_{b\mu}^{ps}=\frac{i}{(2\pi)^4}\sum_{\alpha,\beta=1}^{5}\sum_{\gamma,\tau=1}^{4}\int_{-\infty}^{\infty}dq^o\left\{\int_{-\infty}^{\infty}d^3\vec{q}\;\Xi_2^{ps}(q)\;f_{\beta\gamma}^2(p_3+q-p_1)\;f_{\alpha\tau}^2(q)\cdot\right.$$

$$\left[\frac{1}{[q^o-p_1^o-\sqrt{(\vec{q}-\vec{p}_1)^2+m^2}+i\epsilon]}\,\frac{1}{[q^o-p_1^o+\sqrt{(\vec{q}-\vec{p}_1)^2+m^2}-i\epsilon]}\right.$$

$$\frac{1}{[q^o-K^o+p_2^o-\sqrt{(\vec{q}-\vec{K}+\vec{p}_2)^2+m^2}+i\epsilon]}\,\frac{1}{[q^o-K^o+p_2^o+\sqrt{(\vec{q}-\vec{K}+\vec{p}_2)^2+m^2}-i\epsilon]}$$

$$\frac{1}{[q^o+p_2^o-\sqrt{(\vec{q}+\vec{p}_2)^2+m^2}+i\epsilon]}\,\frac{1}{[q^o+p_2^o+\sqrt{(\vec{q}+\vec{p}_2)^2+m^2}-i\epsilon]}$$

$$\frac{1}{[q^o+p_3^o-p_1^o-\sqrt{(\vec{q}+\vec{p}_3-\vec{p}_1)^2+m_{\beta\gamma}^2}+i\epsilon_{\beta\gamma}]}\,\frac{1}{[q^o+p_3^o-p_1^o+\sqrt{(\vec{q}+\vec{p}_3-\vec{p}_1)^2+m_{\beta\gamma}^2}-i\epsilon_{\beta\gamma}]}$$

$$\left.\left.\frac{1}{[q^o-\sqrt{\vec{q}^2+m_{\alpha\tau}^2}+i\epsilon_{\alpha\tau}]}\,\frac{1}{[q^o+\sqrt{\vec{q}^2+m_{\alpha\tau}^2}-i\epsilon_{\alpha\tau}]}\right]\right\}\,, \qquad \text{(III-12)}$$

For pv coupling, the total bremsstrahlung amplitude has the form of

$$M_{t\mu}^{pv}=M_{\mu}^{pv}+M_{\mu}^{res(pv)}=M_{\mu}^{pv}+M_{a\mu}^{pv}+M_{b\mu}^{pv}+M_{c\mu}^{pv}+M_{d\mu}^{pv}\,, \qquad \text{(III-13)}$$

where $M_{a\mu}^{pv}$, $M_{b\mu}^{pv}$, $M_{c\mu}^{pv}$, and $M_{d\mu}^{pv}$ have the same expressions as $M_{a\mu}^{ps}$, $M_{b\mu}^{ps}$, $M_{c\mu}^{ps}$, and $M_{d\mu}^{ps}$, respectively, but with $\Xi_1^{ps}(q)$ and $\Xi_2^{ps}(q)$ replaced by $\Xi_1^{pv}(q)$ and $\Xi_2^{pv}(q)$, respectively. $\Xi_1^{pv}(q)$ and $\Xi_2^{pv}(q)$ are defined as

$$\Xi_1^{pv}(q)=(4\pi)^2 g_{\beta\gamma}^2\,g_{\alpha\tau}^2\left[\bar{u}(p_3,\nu_3)\lambda'_{\beta}(\not{p}_1-\not{q}+\not{K}+m)\Gamma_{\mu}^{res}(\not{p}_1-\not{q}+m)\lambda'_{\alpha}u(p_1,\nu_1)\right]$$

$$\cdot\left[\bar{u}(p_4,\nu_4)\lambda'^{\beta}(\not p_2+\not q+m)\lambda'^{\alpha}u(p_2,\nu_2)\right] \qquad \text{(III-14)}$$

$$\Xi_2^{pv}(q)=(4\pi)^2 g_{\beta\gamma}^2 g_{\alpha\tau}^2\left[\bar{u}(p_3,\nu_3)\lambda'_{\beta}(\not p_1-\not q+m)\lambda'_{\alpha}u(p_1,\nu_1)\right]$$

$$\cdot\left[\bar{u}(p_4,\nu_4)\lambda'^{\beta}(\not p_2+\not q-\not K+m)\Gamma_{\mu}^{res}(\not p_2+\not q+m)\lambda'^{\alpha}u(p_2,\nu_2)\right] \qquad \text{(III-15)}$$

where $\lambda'_{\alpha}(\lambda'_{\beta})$ are the same as $\lambda_{\alpha}(\lambda_{\beta})$ except $\lambda'_5=\lambda_5\frac{\not q}{(2m)}$ ($\lambda'_5=\lambda_5\frac{\not p_4-\not p_2-\not q}{(2m)}$ or $\lambda_5\frac{\not p_1-\not q-\not p_3}{(2m)}$).

Theoretically, we can now calculate the total bremsstrahlung amplitudes for both ps coupling and pv coupling by computing Eqs. (III-11), (III-12), (III-4), (III-5), (III-6), and (III-13), and thus obtain the total cross sections and total analyzing powers which include the rescattering contribution. Unfortunately, difficulties arise when one evaluates Eqs. (III-11), (III-12), (III-4), and (III-5) directly, since the integrands of these equations have singularities and the integrations will diverge. In the following sections, we discuss these problems and present a method for the calculation of these integrals.

III.2 q^0 Component Integration

The q^0 component integration is carried out analytically using contour integration. In the complex q^0 plane there are a total of 14 poles, among which 10 poles are from the five propagators while the other 4 are from the meson form factors $f_{\alpha\tau}^2$ and $f_{\beta\gamma}^2$. Unlike the poles from the propagators which correspond to the proton or meson being on the mass-shell, the poles from the meson form factors do not have any physical meaning. Therefore, these poles generated from the meson form factors should

make no contribution and they are ignored in our calculations. The physical poles in Eqs.(III-11)-(III-12) completely come from the five propagators. These physical poles are exhibited in Fig.17.

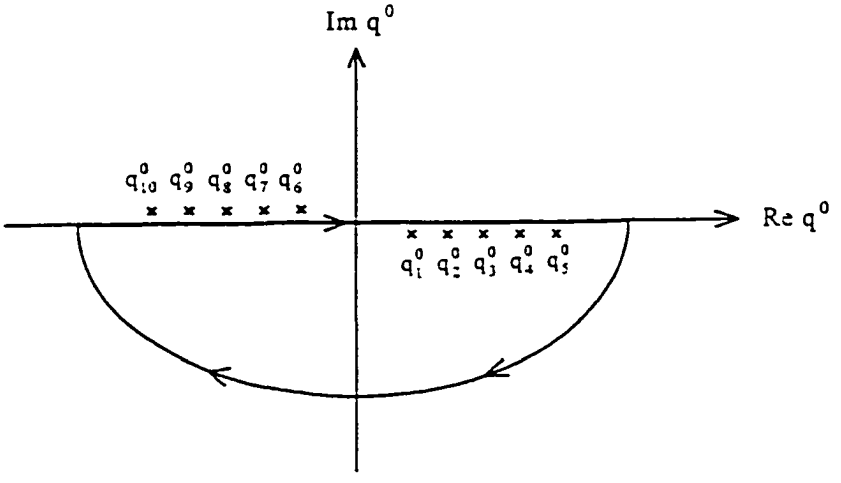

Fig.17. Location of the ten physical poles of Eq.(III-11) in the complex q^o plane.

For the integration of Eq.(III-11)

$$q_1^o = p_1^o - K^o + \sqrt{(\vec{q}+\vec{K}-\vec{p}_1)^2+m^2} - i\epsilon, \qquad q_6^o = p_1^o - K^o - \sqrt{(\vec{q}+\vec{K}-\vec{p}_1)^2+m^2} + i\epsilon,$$

$$q_2^o = p_1^o + \sqrt{(\vec{q}-\vec{p}_1)^2+m^2} - i\epsilon, \qquad q_7^o = p_1^o - \sqrt{(\vec{q}-\vec{p}_1)^2+m^2} + i\epsilon,$$

$$q_3^o = -p_2^o + \sqrt{(\vec{q}+\vec{p}_2)^2+m^2} - i\epsilon, \qquad q_8^o = -p_2^o - \sqrt{(\vec{q}+\vec{p}_2)^2+m^2} + i\epsilon, \quad \text{(III-16)}$$

$$q_4^o = p_4^o - p_2^o + \sqrt{(\vec{q}+\vec{p}_2-\vec{p}_4)^2+m_{\beta\gamma}^2} - i\epsilon_{\beta\gamma}, \qquad q_9^o = p_4^o - p_2^o - \sqrt{(\vec{q}+\vec{p}_2-\vec{p}_4)^2+m_{\beta\gamma}^2} + i\epsilon_{\beta\gamma},$$

$$q_5^o = \sqrt{\vec{q}^2+m_{\alpha\tau}^2} - i\epsilon_{\alpha\tau}, \qquad q_{10}^o = -\sqrt{\vec{q}^2+m_{\alpha\tau}^2} + i\epsilon_{\alpha\tau}.$$

Similarly, for the integration of Eq. (III-12), one has

$$
\begin{aligned}
q_1'^{o} &= p_1^o + \sqrt{(\vec{q}-\vec{p}_1)^2+m^2} - i\epsilon, & q_6'^{o} &= p_1^o - \sqrt{(\vec{q}-\vec{p}_1)^2+m^2} + i\epsilon, \\
q_2'^{o} &= K^o - p_2^o + \sqrt{(\vec{q}-\vec{K}+\vec{p}_2)^2+m^2} - i\epsilon, & q_7'^{o} &= K^o - p_2^o - \sqrt{(\vec{q}-\vec{K}+\vec{p}_2)^2+m^2} + i\epsilon, \\
q_3'^{o} &= -p_2^o + \sqrt{(\vec{q}+\vec{p}_2)^2+m^2} - i\epsilon, & q_8'^{o} &= -p_2^o - \sqrt{(\vec{q}+\vec{p}_2)^2+m^2} + i\epsilon, \quad \text{(III-17)} \\
q_4'^{o} &= p_1^o - p_3^o + \sqrt{(\vec{q}+\vec{p}_3-\vec{p}_1)^2+m_{\beta\gamma}^2} - i\epsilon_{\beta\gamma}, & q_9'^{o} &= p_1^o - p_3^o - \sqrt{(\vec{q}+\vec{p}_3-\vec{p}_1)^2+m_{\beta\gamma}^2} + i\epsilon_{\beta\gamma}, \\
q_5'^{o} &= \sqrt{\vec{q}^2+m_{\alpha\tau}^2} - i\epsilon_{\alpha\tau}, & q_{10}'^{o} &= -\sqrt{\vec{q}^2+m_{\alpha\tau}^2} + i\epsilon_{\alpha\tau}.
\end{aligned}
$$

Choosing the contour around the lower half plane, Cauchy's theorem gives

$$
\begin{aligned}
M_{a\mu}^{ps} = \frac{i}{(2\pi)^4} \sum_{\alpha,\beta=1}^{5} \sum_{\gamma,\tau=1}^{4} (-2\pi i) \int_{-\infty}^{\infty} d^3\vec{q} \\
\Bigg\{ \Big(\Xi_1^{ps}(q)\ f_{\beta\gamma}^2(p_2+q-p_4)\ f_{\alpha\tau}^2(q) \Big)_{q^o = q_1^o} \\
\Bigg[\frac{1}{2\left[\sqrt{(\vec{q}+\vec{K}-\vec{p}_1)^2+m^2} - i\epsilon\right]} \frac{1}{\left[-K^o + \sqrt{(\vec{q}+\vec{k}-\vec{p}_1)^2+m^2} - \sqrt{(\vec{q}-\vec{p}_1)^2+m^2}\right]} \\
\frac{1}{\left[-K^o + \sqrt{(\vec{q}+\vec{k}-\vec{p}_1)^2+m^2} + \sqrt{(\vec{q}-\vec{p}_1)^2+m^2} - i\epsilon\right]} \\
\frac{1}{\left[p_1^o + p_2^o - K^o + \sqrt{(\vec{q}+\vec{k}-\vec{p}_1)^2+m^2} - \sqrt{(\vec{q}+\vec{p}_2)^2+m^2}\right]} \\
\frac{1}{\left[p_1^o + p_2^o - K^o + \sqrt{(\vec{q}+\vec{k}-\vec{p}_1)^2+m^2} + \sqrt{(\vec{q}+\vec{p}_2)^2+m^2} - i\epsilon\right]} \\
\frac{1}{\left[p_1^o + p_2^o - p_4^o - K^o + \sqrt{(\vec{q}+\vec{k}-\vec{p}_1)^2+m^2} - \sqrt{(\vec{q}+\vec{p}_2-\vec{p}_4)^2+m_{\beta\gamma}^2} + i(\epsilon_{\beta\gamma}-\epsilon)\right]} \\
\frac{1}{\left[p_1^o + p_2^o - p_4^o - K^o + \sqrt{(\vec{q}+\vec{k}-\vec{p}_1)^2+m^2} + \sqrt{(\vec{q}+\vec{p}_2-\vec{p}_4)^2+m_{\beta\gamma}^2} - i(\epsilon_{\beta\gamma}-\epsilon)\right]} \\
\frac{1}{\left[p_1^o - K^o + \sqrt{(\vec{q}+\vec{k}-\vec{p}_1)^2+m^2} - \sqrt{\vec{q}^2+m_{\alpha\tau}^2} + i(\epsilon_{\alpha\tau}-\epsilon)\right]}
\end{aligned}
$$

$$\left.\frac{1}{[p_1^o - K^o + \sqrt{(\vec{q}+\vec{k}-\vec{p}_1)^2+m^2} + \sqrt{\vec{q}^2+m_{\alpha\tau}^2} - i(\epsilon_{\alpha\tau}+\epsilon)]}\right]$$

$$+ \left(\Xi_1^{ps}(q)\, f_{\beta\gamma}^2(p_2+q-p_4)\, f_{\alpha\tau}^2(q)\right)_{q^o=q_2^o}$$

$$\left[\frac{1}{[K^o + \sqrt{(\vec{q}-\vec{p}_1)^2+m^2} - \sqrt{(\vec{q}+\vec{K}-\vec{p}_1)^2+m^2}]}\right.$$

$$\frac{1}{[K^o + \sqrt{(\vec{q}-\vec{p}_1)^2+m^2} + \sqrt{(\vec{q}+\vec{K}-\vec{p}_1)^2+m^2} - i\epsilon]}\,\frac{1}{2[\sqrt{(\vec{q}-\vec{p}_1)^2+m^2} - i\epsilon]}$$

$$\frac{1}{[p_1^o + p_2^o + \sqrt{(\vec{q}-\vec{p}_1)^2+m^2} - \sqrt{(\vec{q}+\vec{p}_2)^2+m^2}]}$$

$$\frac{1}{[p_1^o + p_2^o + \sqrt{(\vec{q}-\vec{p}_1)^2+m^2} + \sqrt{(\vec{q}+\vec{p}_2)^2+m^2} - i\epsilon]}$$

$$\frac{1}{[p_1^o + p_2^o - p_4^o + \sqrt{(\vec{q}-\vec{p}_1)^2+m^2} - \sqrt{(\vec{q}+\vec{p}_2-\vec{p}_4)^2+m_{\beta\gamma}^2} + i(\epsilon_{\beta\gamma}-\epsilon)]}$$

$$\frac{1}{[p_1^o + p_2^o - p_4^o + \sqrt{(\vec{q}-\vec{p}_1)^2+m^2} + \sqrt{(\vec{q}+\vec{p}_2-\vec{p}_4)^2+m_{\beta\gamma}^2} - i(\epsilon_{\beta\gamma}+\epsilon)]}$$

$$\frac{1}{[p_1^o + \sqrt{(\vec{q}-\vec{p}_1)^2+m^2} - \sqrt{\vec{q}^2+m_{\alpha\tau}^2} + i(\epsilon_{\alpha\tau}-\epsilon)]}$$

$$\left.\frac{1}{[p_1^o + \sqrt{(\vec{q}-\vec{p}_1)^2+m^2} + \sqrt{\vec{q}^2+m_{\alpha\tau}^2} - i(\epsilon_{\alpha\tau}+\epsilon)]}\right]$$

$$+ \left(\Xi_1^{ps}(q)\, f_{\beta\gamma}^2(p_2+q-p_4)\, f_{\alpha\tau}^2(q)\right)_{q^o=q_3^o}$$

$$\left[\frac{1}{[K^o - p_1^o - p_2^o + \sqrt{(\vec{q}+\vec{p}_2)^2+m^2} - \sqrt{(\vec{q}+\vec{K}-\vec{p}_1)^2+m^2}]}\right.$$

$$\frac{1}{[K^o - p_1^o - p_2^o + \sqrt{(\vec{q}+\vec{p}_2)^2+m^2} + \sqrt{(\vec{q}+\vec{K}-\vec{p}_1)^2+m^2} - i\epsilon]}$$

$$\frac{1}{[-p_1^o - p_2^o + \sqrt{(\vec{q}+\vec{p}_2)^2+m^2} - \sqrt{(\vec{q}-\vec{p}_1)^2+m^2}]}$$

$$\frac{1}{[-p_1^o-p_2^o+\sqrt{(\vec{q}+\vec{p}_2)^2+m^2}+\sqrt{(\vec{q}-\vec{p}_1)^2+m^2}-i\epsilon]}\,\frac{1}{2[\sqrt{(\vec{q}+\vec{p}_2)^2+m^2}-i\epsilon]}$$

$$\frac{1}{[-p_4^o+\sqrt{(\vec{q}+\vec{p}_2)^2+m^2}-\sqrt{(\vec{q}+\vec{p}_2-\vec{p}_4)^2+m_{\beta\gamma}^2}+i(\epsilon_{\beta\gamma}-\epsilon)]}$$

$$\frac{1}{[-p_4^o+\sqrt{(\vec{q}+\vec{p}_2)^2+m^2}+\sqrt{(\vec{q}+\vec{p}_2-\vec{p}_4)^2+m_{\beta\gamma}^2}-i(\epsilon_{\beta\gamma}+\epsilon)]}$$

$$\frac{1}{[-p_2^o+\sqrt{(\vec{q}+\vec{p}_2)^2+m^2}-\sqrt{\vec{q}^2+m_{\alpha\tau}^2}+i(\epsilon_{\alpha\tau}-\epsilon)]}$$

$$\left.\frac{1}{[-p_2^o+\sqrt{(\vec{q}+\vec{p}_2)^2+m^2}+\sqrt{\vec{q}^2+m_{\alpha\tau}^2}-i(\epsilon_{\alpha\tau}+\epsilon)]}\right]$$

$$+\left(\Xi_1^{ps}(q)\; f_{\beta\gamma}^2(p_2+q-p_4)\; f_{\alpha\tau}^2(q)\right)_{q^o=q_4^o}$$

$$\left[\frac{1}{[K^o-p_1^o-p_2^o+p_4^o+\sqrt{(\vec{q}+\vec{p}_2-\vec{p}_4)^2+m_{\beta\gamma}^2}-\sqrt{(\vec{q}+\vec{K}-\vec{p}_1)^2+m^2}+i(\epsilon-\epsilon_{\beta\gamma})]}\right.$$

$$\frac{1}{[K^o-p_1^o-p_2^o+p_4^o+\sqrt{(\vec{q}+\vec{p}_2-\vec{p}_4)^2+m_{\beta\gamma}^2}+\sqrt{(\vec{q}+\vec{K}-\vec{p}_1)^2+m^2}-i(\epsilon-\epsilon_{\beta\gamma})]}$$

$$\frac{1}{[-p_1^o-p_2^o+p_4^o+\sqrt{(\vec{q}+\vec{p}_2-\vec{p}_4)^2+m_{\beta\gamma}^2}-\sqrt{(\vec{q}-\vec{p}_1)^2+m^2}+i(\epsilon-\epsilon_{\beta\gamma})]}$$

$$\frac{1}{[-p_1^o-p_2^o+p_4^o+\sqrt{(\vec{q}+\vec{p}_2-\vec{p}_4)^2+m_{\beta\gamma}^2}+\sqrt{(\vec{q}-\vec{p}_1)^2+m^2}-i(\epsilon+\epsilon_{\beta\gamma})]}$$

$$\frac{1}{[p_4^o+\sqrt{(\vec{q}+\vec{p}_2-\vec{p}_4)^2+m_{\beta\gamma}^2}-\sqrt{(\vec{q}+\vec{p}_2)^2+m^2}+i(\epsilon-\epsilon_{\beta\gamma})]}$$

$$\frac{1}{[p_4^o+\sqrt{(\vec{q}+\vec{p}_2-\vec{p}_4)^2+m_{\beta\gamma}^2}+\sqrt{(\vec{q}+\vec{p}_2)^2+m^2}-i(\epsilon+\epsilon_{\beta\gamma})]}$$

$$\frac{1}{2[\sqrt{(\vec{q}+\vec{p}_2-\vec{p}_4)^2+m_{\beta\gamma}^2}-i\epsilon_{\beta\gamma}]}$$

$$\frac{1}{[-p_2^o+p_4^o+\sqrt{(\vec{q}+\vec{p}_2-\vec{p}_4)^2+m_{\beta\gamma}^2}+\sqrt{\vec{q}^2+m_{\alpha\tau}^2}-i(\epsilon_{\alpha\tau}+\epsilon_{\beta\gamma})]}$$

$$\left.\frac{1}{[-p_2^o+p_4^o+\sqrt{(\vec{q}+\vec{p}_2-\vec{p}_4)^2+m_{\beta\gamma}^2}-\sqrt{\vec{q}^2+m_{\alpha\tau}^2}+i(\epsilon_{\alpha\tau}-\epsilon_{\beta\gamma})]}\right]$$

$$+\left(\Xi_1^{ps}(q)\ f_{\beta\gamma}^2(p_2+q-p_4)\ f_{\alpha\tau}^2(q)\right)_{q^o=q_5^o}$$

$$\left[\frac{1}{[K^o-p_1^o+\sqrt{\vec{q}^2+m_{\alpha\tau}^2}-\sqrt{(\vec{q}+\vec{K}-\vec{p}_1)^2+m^2}+i(\epsilon-\epsilon_{\alpha\tau})]}\right.$$

$$\frac{1}{[K^o-p_1^o+\sqrt{\vec{q}^2+m_{\alpha\tau}^2}+\sqrt{(\vec{q}+\vec{K}-\vec{p}_1)^2+m^2}-i(\epsilon+\epsilon_{\alpha\tau})]}$$

$$\frac{1}{[-p_1^o+\sqrt{\vec{q}^2+m_{\alpha\tau}^2}-\sqrt{(\vec{q}-\vec{p}_1)^2+m^2}+i(\epsilon-\epsilon_{\alpha\tau})]}$$

$$\frac{1}{[-p_1^o+\sqrt{\vec{q}^2+m_{\alpha\tau}^2}+\sqrt{(\vec{q}-\vec{p}_1)^2+m^2}-i(\epsilon+\epsilon_{\alpha\tau})]}$$

$$\frac{1}{[p_2^o+\sqrt{\vec{q}^2+m_{\alpha\tau}^2}-\sqrt{(\vec{q}+\vec{p}_2)^2+m^2}+i(\epsilon-\epsilon_{\alpha\tau})]}$$

$$\frac{1}{[p_2^o+\sqrt{\vec{q}^2+m_{\alpha\tau}^2}+\sqrt{(\vec{q}+\vec{p}_2)^2+m^2}-i(\epsilon+\epsilon_{\alpha\tau})]}$$

$$\frac{1}{[p_2^o-p_4^o+\sqrt{\vec{q}^2+m_{\alpha\tau}^2}-\sqrt{(\vec{q}+\vec{p}_2-\vec{p}_4)^2+m_{\beta\gamma}^2}+i(\epsilon_{\beta\gamma}-\epsilon_{\alpha\tau})]}$$

$$\frac{1}{[p_2^o-p_4^o+\sqrt{\vec{q}^2+m_{\alpha\tau}^2}+\sqrt{(\vec{q}+\vec{p}_2-\vec{p}_4)^2+m_{\beta\gamma}^2}-i(\epsilon_{\beta\gamma}+\epsilon_{\alpha\tau})]}$$

$$\left.\left.\frac{1}{2[\sqrt{\vec{q}^2+m_{\alpha\tau}^2}-i\epsilon_{\alpha\tau}]}\right]\right\} \qquad \text{(III-18)}$$

$$M_{b\mu}^{ps}=\frac{i}{(2\pi)^4}\sum_{\alpha,\beta=1}^{5}\sum_{\gamma,\tau=1}^{4}(-2\pi i)\int_{-\infty}^{\infty}d^3\vec{q}$$

$$
\left\{ \left(\Xi_2^{ps}(q)\; f^2_{\beta\gamma}(p_3+q-p_1)\; f^2_{\alpha\tau}(q) \right)_{q^o = q'^o_1} \right.
$$

$$
\left[\frac{1}{2[\sqrt{(\vec{q}-\vec{p}_1)^2+m^2}-i\epsilon]} \frac{1}{[p_1^o+p_2^o-K^o+\sqrt{(\vec{q}-\vec{p}_1)^2+m^2}-\sqrt{(\vec{q}-\vec{K}+\vec{p}_2)^2+m^2}]} \right.
$$

$$
\frac{1}{[p_1^o+p_2^o-K^o+\sqrt{(\vec{q}-\vec{p}_1)^2+m^2}+\sqrt{(\vec{q}-\vec{K}+\vec{p}_2)^2+m^2}-i\epsilon]}
$$

$$
\frac{1}{[p_1^o+p_2^o+\sqrt{(\vec{q}-\vec{p}_1)^2+m^2}-\sqrt{(\vec{q}+\vec{p}_2)^2+m^2}]}
$$

$$
\frac{1}{[p_1^o+p_2^o+\sqrt{(\vec{q}-\vec{p}_1)^2+m^2}+\sqrt{(\vec{q}+\vec{p}_2)^2+m^2}-i\epsilon]}
$$

$$
\frac{1}{[p_3^o+\sqrt{(\vec{q}-\vec{p}_1)^2+m^2}-\sqrt{(\vec{q}+\vec{p}_3-\vec{p}_1)^2+m^2_{\beta\gamma}}+i(\epsilon_{\beta\gamma}-\epsilon)]}
$$

$$
\frac{1}{[p_3^o+\sqrt{(\vec{q}-\vec{p}_1)^2+m^2}+\sqrt{(\vec{q}+\vec{p}_3-\vec{p}_1)^2+m^2_{\beta\gamma}}-i(\epsilon_{\beta\gamma}+\epsilon)]}
$$

$$
\frac{1}{[p_1^o+\sqrt{(\vec{q}-\vec{p}_1)^2+m^2}-\sqrt{\vec{q}^2+m^2_{\alpha\tau}}+i(\epsilon_{\alpha\tau}-\epsilon)]}
$$

$$
\left. \frac{1}{[p_1^o+\sqrt{(\vec{q}-\vec{p}_1)^2+m^2}+\sqrt{\vec{q}^2+m^2_{\alpha\tau}}-i(\epsilon_{\alpha\tau}+\epsilon)]} \right]
$$

$$
+ \left(\Xi_2^{ps}(q)\; f^2_{\beta\gamma}(p_3+q-p_1)\; f^2_{\alpha\tau}(q) \right)_{q^o = q'^o_2}
$$

$$
\left[\frac{1}{[K^o-p_1^o-p_2^o+\sqrt{(\vec{q}-\vec{K}+\vec{p}_2)^2+m^2}-\sqrt{(\vec{q}-\vec{p}_1)^2+m^2}]} \right.
$$

$$
\frac{1}{[K^o-p_1^o-p_2^o+\sqrt{(\vec{q}-\vec{K}+\vec{p}_2)^2+m^2}+\sqrt{(\vec{q}-\vec{p}_1)^2+m^2}-i\epsilon]}
$$

$$
\frac{1}{2[\sqrt{(\vec{q}-\vec{K}+\vec{p}_2)^2+m^2}-i\epsilon]} \frac{1}{[K^o+\sqrt{(\vec{q}-\vec{K}+\vec{p}_2)^2+m^2}-\sqrt{(\vec{q}+\vec{p}_2)^2+m^2}]}
$$

$$
\frac{1}{[K^o+\sqrt{(\vec{q}-\vec{K}+\vec{p}_2)^2+m^2}+\sqrt{(\vec{q}+\vec{p}_2)^2+m^2}-i\epsilon]}
$$

$$
\frac{1}{[K^o-p_1^o-p_2^o+p_3^o+\sqrt{(\vec{q}-\vec{K}+\vec{p}_2)^2+m^2}-\sqrt{(\vec{q}+\vec{p}_3-\vec{p}_1)^2+m^2_{\beta\gamma}}+i(\epsilon_{\beta\gamma}-\epsilon)]}
$$

$$\frac{1}{[K^o-p_1^o-p_2^o+p_3^o+\sqrt{(\vec{q}-\vec{K}+\vec{p}_2)^2+m^2}+\sqrt{(\vec{q}+\vec{p}_3-\vec{p}_1)^2+m_{\beta\gamma}^2}-i(\epsilon_{\beta\gamma}-\epsilon)]}$$

$$\left[\frac{1}{[K^o-p_2^o+\sqrt{(\vec{q}-\vec{K}+\vec{p}_2)^2+m^2}-\sqrt{\vec{q}^2+m_{\alpha\tau}^2}+i(\epsilon_{\alpha\tau}-\epsilon)]}\right.$$

$$\left.\frac{1}{[K^o-p_2^o+\sqrt{(\vec{q}-\vec{K}+\vec{p}_2)^2+m^2}+\sqrt{\vec{q}^2+m_{\alpha\tau}^2}-i(\epsilon_{\alpha\tau}+\epsilon)]}\right]$$

$$+\left(\Xi_2^{ps}(q)\ f_{\beta\gamma}^2(p_3+q-p_1)\ f_{\alpha\tau}^2(q)\right)_{q^o=q'^o_3}$$

$$\left[\frac{1}{[-p_1^o-p_2^o+\sqrt{(\vec{q}+\vec{p}_2)^2+m^2}-\sqrt{(\vec{q}-\vec{p}_1)^2+m^2}]}\right.$$

$$\frac{1}{[-p_1^o-p_2^o+\sqrt{(\vec{q}+\vec{p}_2)^2+m^2}+\sqrt{(\vec{q}-\vec{p}_1)^2+m^2}-i\epsilon]}$$

$$\frac{1}{[-K^o+\sqrt{(\vec{q}+\vec{p}_2)^2+m^2}-\sqrt{(\vec{q}-\vec{K}+\vec{p}_2)^2+m^2}]}$$

$$\frac{1}{[-K^o+\sqrt{(\vec{q}+\vec{p}_2)^2+m^2}+\sqrt{(\vec{q}-\vec{K}+\vec{p}_2)^2+m^2}-i\epsilon]}\frac{1}{2[\sqrt{(\vec{q}+\vec{p}_2)^2+m^2}-i\epsilon]}$$

$$\frac{1}{[p_3^o-p_1^o-p_2^o+\sqrt{(\vec{q}+\vec{p}_2)^2+m^2}-\sqrt{(\vec{q}+\vec{p}_3-\vec{p}_1)^2+m_{\beta\gamma}^2}+i(\epsilon_{\beta\gamma}-\epsilon)]}$$

$$\frac{1}{[p_3^o-p_1^o-p_2^o+\sqrt{(\vec{q}+\vec{p}_2)^2+m^2}+\sqrt{(\vec{q}+\vec{p}_3-\vec{p}_1)^2+m_{\beta\gamma}^2}-i(\epsilon_{\beta\gamma}+\epsilon)]}$$

$$\frac{1}{[-p_2^o+\sqrt{(\vec{q}+\vec{p}_2)^2+m^2}-\sqrt{\vec{q}^2+m_{\alpha\tau}^2}+i(\epsilon_{\alpha\tau}-\epsilon)]}$$

$$\left.\frac{1}{[-p_2^o+\sqrt{(\vec{q}+\vec{p}_2)^2+m^2}+\sqrt{\vec{q}^2+m_{\alpha\tau}^2}-i(\epsilon_{\alpha\tau}+\epsilon)]}\right]$$

$$+\left(\Xi_2^{ps}(q)\ f_{\beta\gamma}^2(p_3+q-p_1)\ f_{\alpha\tau}^2(q)\right)_{q^o=q'^o_4}$$

$$\left[\frac{1}{[-p_3^o+\sqrt{(\vec{q}+\vec{p}_3-\vec{p}_1)^2+m_{\beta\gamma}^2}-\sqrt{(\vec{q}-\vec{p}_1)^2+m^2}+i(\epsilon-\epsilon_{\beta\gamma})]}\right.$$

$$\frac{1}{[-p_3^o+\sqrt{(\vec{q}+\vec{p}_3-\vec{p}_1)^2+m_{\beta\gamma}^2}+\sqrt{(\vec{q}-\vec{p}_1)^2+m^2}\ -i(\epsilon+\epsilon_{\beta\gamma})]}$$

$$\frac{1}{[p_1^o+p_2^o-p_3^o-K^o+\sqrt{(\vec{q}+\vec{p}_3-\vec{p}_1)^2+m_{\beta\gamma}^2}\ -\sqrt{(\vec{q}-\vec{K}+\vec{p}_2)^2+m^2}+i(\epsilon-\epsilon_{\beta\gamma})]}$$

$$\frac{1}{[p_1^o+p_2^o-p_3^o-K^o+\sqrt{(\vec{q}+\vec{p}_3-\vec{p}_1)^2+m_{\beta\gamma}^2}\ +\sqrt{(\vec{q}-\vec{K}+\vec{p}_2)^2+m^2}-i(\epsilon-\epsilon_{\beta\gamma})]}$$

$$\frac{1}{[p_1^o+p_2^o-p_3^o+\sqrt{(\vec{q}+\vec{p}_3-\vec{p}_1)^2+m_{\beta\gamma}^2}\ -\sqrt{(\vec{q}+\vec{p}_2)^2+m^2}\ +i(\epsilon-\epsilon_{\beta\gamma})]}$$

$$\frac{1}{[p_1^o+p_2^o-p_3^o+\sqrt{(\vec{q}+\vec{p}_3-\vec{p}_1)^2+m_{\beta\gamma}^2}\ +\sqrt{(\vec{q}+\vec{p}_2)^2+m^2}\ -i(\epsilon+\epsilon_{\beta\gamma})]}$$

$$\frac{1}{2\,[\sqrt{(\vec{q}+\vec{p}_3-\vec{p}_1)^2+m_{\beta\gamma}^2}\ -i\epsilon_{\beta\gamma}]}$$

$$\frac{1}{[p_1^o-p_3^o+\sqrt{(\vec{q}+\vec{p}_3-\vec{p}_1)^2+m_{\beta\gamma}^2}-\sqrt{\vec{q}^2+m_{\alpha\tau}^2}+i(\epsilon_{\alpha\tau}-\epsilon_{\beta\gamma})]}$$

$$\left.\frac{1}{[p_1^o-p_3^o+\sqrt{(\vec{q}+\vec{p}_3-\vec{p}_1)^2+m_{\beta\gamma}^2}+\sqrt{\vec{q}^2+m_{\alpha\tau}^2}-i(\epsilon_{\alpha\tau}+\epsilon_{\beta\gamma})]}\right]$$

$$+\ \left(\Xi_2^{ps}(q)\ f_{\beta\gamma}^2(p_3+q-p_1)\ f_{\alpha\tau}^2(q)\right)_{q^o=q'^o_5}$$

$$\left[\frac{1}{[-p_1^o+\sqrt{\vec{q}^2+m_{\alpha\tau}^2}-\sqrt{(\vec{q}-\vec{p}_1)^2+m^2}+i(\epsilon-\epsilon_{\alpha\tau})]}\right.$$

$$\frac{1}{[-p_1^o+\sqrt{\vec{q}^2+m_{\alpha\tau}^2}+\sqrt{(\vec{q}-\vec{p}_1)^2+m^2}-i(\epsilon+\epsilon_{\alpha\tau})]}$$

$$\frac{1}{[p_2^o-K^o+\sqrt{\vec{q}^2+m_{\alpha\tau}^2}-\sqrt{(\vec{q}-\vec{K}+\vec{p}_2)^2+m^2}+i(\epsilon-\epsilon_{\alpha\tau})]}$$

$$\frac{1}{[p_2^o-K^o+\sqrt{\vec{q}^2+m_{\alpha\tau}^2}+\sqrt{(\vec{q}-\vec{K}+\vec{p}_2)^2+m^2}-i(\epsilon+\epsilon_{\alpha\tau})]}$$

$$\frac{1}{[p_2^o+\sqrt{\vec{q}^2+m_{\alpha\tau}^2}-\sqrt{(\vec{q}+\vec{p}_2)^2+m^2}+i(\epsilon-\epsilon_{\alpha\tau})]}$$

$$\frac{1}{[p_2^o+\sqrt{\vec{q}^2+m_{\alpha\tau}^2}+\sqrt{(\vec{q}+\vec{p}_2)^2+m^2}-i(\epsilon+\epsilon_{\alpha\tau})]}$$

$$\frac{1}{[p_3^o-p_1^o+\sqrt{\vec{q}^2+m_{\alpha\tau}^2}-\sqrt{(\vec{q}+\vec{p}_3-\vec{p}_1)^2+m_{\beta\gamma}^2}+i(\epsilon_{\beta\gamma}-\epsilon_{\alpha\tau})]}$$

$$\frac{1}{[p_3^o-p_1^o+\sqrt{\vec{q}^2+m_{\alpha\tau}^2}+\sqrt{(\vec{q}+\vec{p}_3-\vec{p}_1)^2+m_{\beta\gamma}^2}-i(\epsilon_{\beta\gamma}+\epsilon_{\alpha\tau})]}$$

$$\left.\left.\frac{1}{2[\sqrt{\vec{q}^2+m_{\alpha\tau}^2}-i\epsilon_{\alpha\tau}]}\right]\right\} \qquad \text{(III-19)}$$

For pv coupling, the corresponding equations have the same expressions but with $\Xi_1^{ps}(q)$ ($\Xi_2^{ps}(q)$) replaced by $\Xi_1^{pv}(q)$ ($\Xi_2^{pv}(q)$).

We evaluate the above integrals in the center-of-mass frame. By making the transformation $\vec{q}\rightarrow(\vec{q}+\vec{p}_1)$ and noting that $p_1^o = p_2^o$ and $\vec{p}_2 = -\vec{p}_1$, equations (III-16)-(III-19) become

$$\bar{q}_1^o = p_1^o - K^o + \sqrt{(\vec{q}+\vec{K})^2+m^2} - i\epsilon \qquad \bar{q}_6^o = p_1^o - K^o - \sqrt{(\vec{q}+\vec{K})^2+m^2} + i\epsilon$$

$$\bar{q}_2^o = p_1^o + \sqrt{\vec{q}^2+m^2} - i\epsilon \qquad \bar{q}_7^o = p_1^o - \sqrt{\vec{q}_1^{\,2}+m^2} + i\epsilon$$

$$\bar{q}_3^o = -p_1^o + \sqrt{\vec{q}^2+m^2} - i\epsilon \qquad \bar{q}_8^o = -p_1^o - \sqrt{\vec{q}^2+m^2} + i\epsilon \qquad \text{(III-20)}$$

$$\bar{q}_4^o = p_4^o - p_1^o + \sqrt{(\vec{q}-\vec{p}_4)^2+m_{\beta\gamma}^2} - i\epsilon_{\beta\gamma} \qquad \bar{q}_9^o = p_4^o - p_1^o - \sqrt{(\vec{q}-\vec{p}_4)^2+m_{\beta\gamma}^2} + i\epsilon_{\beta\gamma}$$

$$\bar{q}_5^o = \sqrt{(\vec{q}+\vec{p}_1)^2+m_{\alpha\tau}^2} - i\epsilon_{\alpha\tau} \qquad \bar{q}_{10}^o = -\sqrt{(\vec{q}+\vec{p}_1)^2+m_{\alpha\tau}^2} + i\epsilon_{\alpha\tau},$$

$$\bar{q}_1^{/o} = p_1^o + \sqrt{\vec{q}^2 + m^2} - i\epsilon \qquad \bar{q}_6^{/o} = p_1^o - \sqrt{\vec{q}^2 + m^2} + i\epsilon$$

$$\bar{q}_2^{/o} = K^o - p_1^o + \sqrt{(\vec{q}-\vec{K})^2 + m^2} - i\epsilon \qquad \bar{q}_7^{/o} = K^o - p_1^o - \sqrt{(\vec{q}-\vec{K})^2 + m^2} + i\epsilon$$

$$\bar{q}_3^{/o} = -p_1^o + \sqrt{\vec{q}^2 + m^2} - i\epsilon \qquad \bar{q}_8^{/o} = -p_1^o - \sqrt{\vec{q}^2 + m^2} + i\epsilon \qquad \text{(III-21)}$$

$$\bar{q}_4^{/o} = p_1^o - p_3^o + \sqrt{(\vec{q}+\vec{p}_3)^2 + m_{\beta\gamma}^2} - i\epsilon_{\beta\gamma} \qquad \bar{q}_9^{/o} = p_1^o - p_3^o - \sqrt{(\vec{q}+\vec{p}_3)^2 + m_{\beta\gamma}^2} + i\epsilon_{\beta\gamma}$$

$$\bar{q}_5^{/o} = \sqrt{(\vec{q}+\vec{p}_1)^2 + m_{\alpha\tau}^2} - i\epsilon_{\alpha\tau} \qquad \bar{q}_{10}^{/o} = -\sqrt{(\vec{q}+\vec{p}_1)^2 + m_{\alpha\tau}^2} + i\epsilon_{\alpha\tau},$$

$$M_{a\mu}^{ps} = \frac{1}{(2\pi)^3} \sum_{\alpha,\beta=1}^{5} \sum_{\gamma,\tau=1}^{4} \int_{-\infty}^{\infty} d^3\vec{q}$$

$$\left\{ \left(\Xi_1^{ps}(q)\ f_{\beta\gamma}^2(p_2+q-p_4)\ f_{\alpha\tau}^2(q) \right)_{q^o=\bar{q}_1^o,\ \vec{q}\to\vec{q}+\vec{p}_1} \right.$$

$$\left[\frac{1}{2[\sqrt{(\vec{q}+\vec{K})^2+m^2} - i\epsilon]} \frac{1}{[-K^o + \sqrt{(\vec{q}+\vec{K})^2+m^2} - \sqrt{\vec{q}^2+m^2}\ ]} \right.$$

$$\frac{1}{[-K^o + \sqrt{(\vec{q}+\vec{k})^2+m^2} + \sqrt{\vec{q}^2+m^2} - i\epsilon]}$$

$$\frac{1}{[2p_1^o - K^o + \sqrt{(\vec{q}+\vec{K})^2+m^2} - \sqrt{\vec{q}^2+m^2}\ ]}$$

$$\frac{1}{[2p_1^o - K^o + \sqrt{(\vec{q}+\vec{K})^2+m^2} + \sqrt{\vec{q}^2+m^2} - i\epsilon]}$$

$$\frac{1}{[p_3^o + \sqrt{(\vec{q}+\vec{K})^2+m^2} - \sqrt{(\vec{q}-\vec{p}_4)^2+m_{\beta\gamma}^2} + i(\epsilon_{\beta\gamma}-\epsilon)]}$$

$$\frac{1}{[p_3^o + \sqrt{(\vec{q}+\vec{K})^2+m^2} + \sqrt{(\vec{q}-\vec{p}_4)^2+m_{\beta\gamma}^2} - i(\epsilon_{\beta\gamma}+\epsilon)]}$$

$$\frac{1}{[p_1^o - K^o + \sqrt{(\vec{q}+\vec{K})^2+m^2} - \sqrt{(\vec{q}+\vec{p}_1)^2+m_{\alpha\tau}^2} + i(\epsilon_{\alpha\tau}-\epsilon)]}$$

$$\left. \left. \frac{1}{[p_1^o - K^o + \sqrt{(\vec{q}+\vec{K})^2+m^2} + \sqrt{(\vec{q}+\vec{p}_1)^2+m_{\alpha\tau}^2} - i(\epsilon_{\alpha\tau}+\epsilon)]} \right] \right.$$

$$
+ \left(\Xi_1^{ps}(q)\; f_{\beta\gamma}^2(p_2+q-p_4)\; f_{\alpha\tau}^2(q) \right)_{q^o=\bar{q}_2^o,\ \vec{q}\to\vec{q}+\vec{p}_1}
$$

$$
\left[\frac{1}{[K^o+\sqrt{\vec{q}^2+m^2}\ -\sqrt{(\vec{q}+\vec{K})^2+m^2}\ ]} \right.
$$

$$
\frac{1}{[K^o+\sqrt{\vec{q}^2+m^2}\ +\sqrt{(\vec{q}+\vec{K})^2+m^2}\ -i\epsilon\,]}\ \frac{1}{2\,[\sqrt{\vec{q}^2+m^2}\ -i\epsilon\,]}
$$

$$
\frac{1}{2\,[p_1^o\,]}\ \frac{1}{2\,[p_1^o+\sqrt{\vec{q}^2+m^2}\ -i\epsilon]}
$$

$$
\frac{1}{[2\,p_1^o-p_4^o+\sqrt{\vec{q}^2+m^2}\ -\sqrt{(\vec{q}-\vec{p}_4)^2+m_{\beta\gamma}^2}\ +i(\epsilon_{\beta\gamma}-\epsilon)]}
$$

$$
\frac{1}{[2\,p_1^o-p_4^o+\sqrt{\vec{q}^2+m^2}\ +\sqrt{(\vec{q}-\vec{p}_4)^2+m_{\beta\gamma}^2}\ -i(\epsilon_{\beta\gamma}+\epsilon)]}
$$

$$
\frac{1}{[p_1^o+\sqrt{\vec{q}^2+m^2}\ -\sqrt{(\vec{q}+\vec{p}_1)^2+m_{\alpha\tau}^2}\ +i(\epsilon_{\alpha\tau}-\epsilon)]}
$$

$$
\left. \frac{1}{[p_1^o+\sqrt{\vec{q}^2+m^2}\ +\sqrt{(\vec{q}+\vec{p}_1)^2+m_{\alpha\tau}^2}\ -i(\epsilon_{\alpha\tau}+\epsilon)]} \right]
$$

$$
+ \left(\Xi_1^{ps}(q)\; f_{\beta\gamma}^2(p_2+q-p_4)\; f_{\alpha\tau}^2(q) \right)_{q^o=\bar{q}_3^o,\ \vec{q}\to\vec{q}+\vec{p}_1}
$$

$$
\left[\frac{1}{[K^o-2\,p_1^o+\sqrt{\vec{q}^2+m^2}\ -\sqrt{(\vec{q}+\vec{K})^2+m^2}\ ]} \right.
$$

$$
\frac{1}{[K^o-2\,p_1^o+\sqrt{\vec{q}^2+m^2}\ +\sqrt{(\vec{q}+\vec{K})^2+m^2}\ -i\epsilon\,]}
$$

$$
\frac{1}{2\,[-p_1^o\,]}\ \frac{1}{2\,[-p_1^o+\sqrt{\vec{q}^2+m^2}\ -i\epsilon]}\ \frac{1}{2\,[\sqrt{\vec{q}^2+m^2}\ -i\epsilon\,]}
$$

$$
\frac{1}{[-p_4^o+\sqrt{\vec{q}^2+m^2}\ -\sqrt{(\vec{q}-\vec{p}_4)^2+m_{\beta\gamma}^2}\ +i(\epsilon_{\beta\gamma}-\epsilon)]}
$$

$$
\frac{1}{[-p_4^o+\sqrt{\vec{q}^2+m^2}\ +\sqrt{(\vec{q}-\vec{p}_4)^2+m_{\beta\gamma}^2}\ -i(\epsilon_{\beta\gamma}+\epsilon)]}
$$

$$\frac{1}{[-p_1^{\circ}+\sqrt{\vec{q}^2+m^2}-\sqrt{(\vec{q}+\vec{p}_1)^2+m_{\alpha\tau}^2}+i(\epsilon_{\alpha\tau}-\epsilon)]}$$

$$\left.\frac{1}{[-p_1^{\circ}+\sqrt{\vec{q}^2+m^2}+\sqrt{(\vec{q}+\vec{p}_1)^2+m_{\alpha\tau}^2}-i(\epsilon_{\alpha\tau}+\epsilon)]}\right]$$

$$+\left(\Xi_1^{ps}(q)\, f_{\beta\gamma}^2(p_2+q-p_4)\, f_{\alpha\tau}^2(q)\right)_{q^{\circ}=\bar{q}_4^{\circ},\ \vec{q}\to\vec{q}+\vec{p}_1}$$

$$\left[\frac{1}{[-p_3^{\circ}+\sqrt{(\vec{q}-\vec{p}_4)^2+m_{\beta\gamma}^2}-\sqrt{(\vec{q}+\vec{K})^2+m^2}+i(\epsilon-\epsilon_{\beta\gamma})]}\right.$$

$$\frac{1}{[-p_3^{\circ}+\sqrt{(\vec{q}-\vec{p}_4)^2+m_{\beta\gamma}^2}+\sqrt{(\vec{q}+\vec{K})^2+m^2}-i(\epsilon+\epsilon_{\beta\gamma})]}$$

$$\frac{1}{[-2\,p_1^{\circ}+p_4^{\circ}+\sqrt{(\vec{q}-\vec{p}_4)^2+m_{\beta\gamma}^2}-\sqrt{\vec{q}^2+m^2}+i(\epsilon-\epsilon_{\beta\gamma})]}$$

$$\frac{1}{[-2\,p_1^{\circ}+p_4^{\circ}+\sqrt{(\vec{q}-\vec{p}_4)^2+m_{\beta\gamma}^2}+\sqrt{\vec{q}^2+m^2}-i(\epsilon+\epsilon_{\beta\gamma})]}$$

$$\frac{1}{[p_4^{\circ}+\sqrt{(\vec{q}-\vec{p}_4)^2+m_{\beta\gamma}^2}-\sqrt{\vec{q}^2+m^2}+i(\epsilon-\epsilon_{\beta\gamma})]}$$

$$\frac{1}{[p_4^{\circ}+\sqrt{(\vec{q}-\vec{p}_4)^2+m_{\beta\gamma}^2}+\sqrt{\vec{q}^2+m^2}-i(\epsilon+\epsilon_{\beta\gamma})]}$$

$$\frac{1}{2\,[\sqrt{(\vec{q}-\vec{p}_4)^2+m_{\beta\gamma}^2}-i\epsilon_{\beta\gamma}]}$$

$$\frac{1}{[-p_1^{\circ}+p_4^{\circ}+\sqrt{(\vec{q}-\vec{p}_4)^2+m_{\beta\gamma}^2}+\sqrt{(\vec{q}+\vec{p}_1)^2+m_{\alpha\tau}^2}-i(\epsilon_{\alpha\tau}+\epsilon_{\beta\gamma})]}$$

$$\left.\frac{1}{[-p_1^{\circ}+p_4^{\circ}+\sqrt{(\vec{q}-\vec{p}_4)^2+m_{\beta\gamma}^2}-\sqrt{(\vec{q}+\vec{p}_1)^2+m_{\alpha\tau}^2}+i(\epsilon_{\alpha\tau}-\epsilon_{\beta\gamma})]}\right]$$

$$+\left(\Xi_1^{ps}(q)\, f_{\beta\gamma}^2(p_2+q-p_4)\, f_{\alpha\tau}^2(q)\right)_{q^{\circ}=\bar{q}_5^{\circ},\ \vec{q}\to\vec{q}+\vec{p}_1}$$

$$\left[\frac{1}{[K^{o}-p_1^{o}+\sqrt{(\vec{q}+\vec{p}_1)^2+m_{\alpha\tau}^2}\ -\sqrt{(\vec{q}+\vec{K})^2+m^2}\ +i(\epsilon-\epsilon_{\alpha\tau})]}\right.$$

$$\frac{1}{[K^{o}-p_1^{o}+\sqrt{(\vec{q}+\vec{p}_1)^2+m_{\alpha\tau}^2}\ +\sqrt{(\vec{q}+\vec{K})^2+m^2}\ -i(\epsilon+\epsilon_{\alpha\tau})]}$$

$$\frac{1}{[-p_1^{o}+\sqrt{(\vec{q}+\vec{p}_1)^2+m_{\alpha\tau}^2}\ -\sqrt{\vec{q}^2+m^2}\ +i(\epsilon-\epsilon_{\alpha\tau})]}$$

$$\frac{1}{[-p_1^{o}+\sqrt{(\vec{q}+\vec{p}_1)^2+m_{\alpha\tau}^2}\ +\sqrt{\vec{q}^2+m^2}\ -i(\epsilon+\epsilon_{\alpha\tau})]}$$

$$\frac{1}{[p_1^{o}+\sqrt{(\vec{q}+\vec{p}_1)^2+m_{\alpha\tau}^2}\ -\sqrt{\vec{q}^2+m^2}\ +i(\epsilon-\epsilon_{\alpha\tau})]}$$

$$\frac{1}{[p_1^{o}+\sqrt{(\vec{q}+\vec{p}_1)^2+m_{\alpha\tau}^2}\ +\sqrt{\vec{q}^2+m^2}\ -i(\epsilon+\epsilon_{\alpha\tau})]}$$

$$\frac{1}{[p_1^{o}-p_4^{o}+\sqrt{(\vec{q}+\vec{p}_1)^2+m_{\alpha\tau}^2}\ -\sqrt{(\vec{q}-\vec{p}_4)^2+m_{\beta\gamma}^2}\ +i(\epsilon_{\beta\gamma}-\epsilon_{\alpha\tau})]}$$

$$\frac{1}{[p_1^{o}-p_4^{o}+\sqrt{(\vec{q}+\vec{p}_1)^2+m_{\alpha\tau}^2}\ +\sqrt{(\vec{q}-\vec{p}_4)^2+m_{\beta\gamma}^2}\ -i(\epsilon_{\beta\gamma}+\epsilon_{\alpha\tau})]}$$

$$\left.\left.\frac{1}{2\,[\sqrt{(\vec{q}+\vec{p}_1)^2+m_{\alpha\tau}^2}\ -i\epsilon_{\alpha\tau}]}\right]\right\} \qquad \text{(III-22)}$$

$$M_{b\mu}^{ps}=\frac{1}{(2\pi)^3}\sum_{\alpha,\beta=1}^{5}\sum_{\gamma,\tau=1}^{4}\int_{-\infty}^{\infty}d^3\vec{q}$$

$$\left\{\left(\Xi_2^{ps}(q)\ f_{\beta\gamma}^2(p_3+q-p_1)\ f_{\alpha\tau}^2(q)\right)_{q^{o}=\bar{q}'^{o}_{1},\ \vec{q}\to\vec{q}+\vec{p}_1}\right.$$

$$\left[\frac{1}{2\,[\sqrt{\vec{q}^2+m^2}\ -i\epsilon]}\ \frac{1}{[2\,p_1^{o}-K^{o}+\sqrt{\vec{q}^2+m^2}\ -\sqrt{(\vec{q}-\vec{K})^2+m^2}\,]}\right.$$

$$\frac{1}{[2\,p_1^{o}-K^{o}+\sqrt{\vec{q}^2+m^2}\ +\sqrt{(\vec{q}-\vec{K})^2+m^2}-i\epsilon\,]}$$

$$\left.\frac{1}{2\,[p_1^{o}]}\ \frac{1}{2\,[p_1^{o}+\sqrt{\vec{q}^2+m^2}\ -i\epsilon\,]}\right]$$

$$\frac{1}{[p_3^o+\sqrt{\vec{q}^2+m^2}-\sqrt{(\vec{q}+\vec{p}_3)^2+m_{\beta\gamma}^2}+i(\epsilon_{\beta\gamma}-\epsilon)]}$$

$$\frac{1}{[p_3^o+\sqrt{\vec{q}^2+m^2}+\sqrt{(\vec{q}+\vec{p}_3)^2+m_{\beta\gamma}^2}-i(\epsilon_{\beta\gamma}+\epsilon)]}$$

$$\frac{1}{[p_1^o+\sqrt{\vec{q}^2+m^2}-\sqrt{(\vec{q}+\vec{p}_1)^2+m_{\alpha\tau}^2}+i(\epsilon_{\alpha\tau}-\epsilon)]}$$

$$\left.\frac{1}{[p_1^o+\sqrt{\vec{q}^2+m^2}+\sqrt{(\vec{q}+\vec{p}_1)^2+m_{\alpha\tau}^2}-i(\epsilon_{\alpha\tau}+\epsilon)]}\right]$$

$$+\left(\Xi_2^{ps}(q)\, f_{\beta\gamma}^2(p_3+q-p_1)\, f_{\alpha\tau}^2(q)\right)_{q^o=\bar{q}'^o_2,\ \vec{q}\to\vec{q}+\vec{p}_1}$$

$$\left[\frac{1}{[K^o-2p_1^o+\sqrt{(\vec{q}-\vec{K})^2+m^2}-\sqrt{\vec{q}^2+m^2}]}\right.$$

$$\frac{1}{[K^o-2p_1^o+\sqrt{(\vec{q}-\vec{K})^2+m^2}+\sqrt{\vec{q}^2+m^2}-i\epsilon]}$$

$$\frac{1}{2[\sqrt{(\vec{q}-\vec{K})^2+m^2}-i\epsilon]}\,\frac{1}{[K^o+\sqrt{(\vec{q}-\vec{K})^2+m^2}-\sqrt{\vec{q}^2+m^2}]}$$

$$\frac{1}{[K^o+\sqrt{(\vec{q}-\vec{K})^2+m^2}+\sqrt{\vec{q}^2+m^2}-i\epsilon]}$$

$$\frac{1}{[-p_4^o+\sqrt{(\vec{q}-\vec{K})^2+m^2}-\sqrt{(\vec{q}+\vec{p}_3)^2+m_{\beta\gamma}^2}+i(\epsilon_{\beta\gamma}-\epsilon)]}$$

$$\frac{1}{[-p_4^o+\sqrt{(\vec{q}-\vec{K})^2+m^2}+\sqrt{(\vec{q}+\vec{p}_3)^2+m_{\beta\gamma}^2}-i(\epsilon_{\beta\gamma}+\epsilon)]}$$

$$\frac{1}{[K^o-p_1^o+\sqrt{(\vec{q}-\vec{K})^2+m^2}-\sqrt{(\vec{q}+\vec{p}_1)^2+m_{\alpha\tau}^2}+i(\epsilon_{\alpha\tau}-\epsilon)]}$$

$$\left.\frac{1}{[K^o-p_1^o+\sqrt{(\vec{q}-\vec{K})^2+m^2}+\sqrt{(\vec{q}+\vec{p}_1)^2+m_{\alpha\tau}^2}-i(\epsilon_{\alpha\tau}+\epsilon)]}\right]$$

$$+\left(\Xi_2^{ps}(q)\, f_{\beta\gamma}^2(p_3+q-p_1)\, f_{\alpha\tau}^2(q)\right)_{q^o=\bar{q}'^o_3,\ \vec{q}\to\vec{q}+\vec{p}_1}$$

$$\left[\frac{1}{2[-p_1^o]}\frac{1}{2[-p_1^o+\sqrt{\vec{q}^2+m^2}-i\epsilon]}\right.$$

$$\frac{1}{[-K^o+\sqrt{\vec{q}^2+m^2}-\sqrt{(\vec{q}-\vec{K})^2+m^2}]}$$

$$\frac{1}{[-K^o+\sqrt{\vec{q}^2+m^2}+\sqrt{(\vec{q}-\vec{K})^2+m^2}-i\epsilon]}\frac{1}{2[\sqrt{\vec{q}^2+m^2}-i\epsilon]}$$

$$\frac{1}{[p_3^o-2p_1^o+\sqrt{\vec{q}^2+m^2}-\sqrt{(\vec{q}+\vec{p}_3)^2+m_{\beta\gamma}^2}+i(\epsilon_{\beta\gamma}-\epsilon)]}$$

$$\frac{1}{[p_3^o-2p_1^o+\sqrt{\vec{q}^2+m^2}+\sqrt{(\vec{q}+\vec{p}_3)^2+m_{\beta\gamma}^2}-i(\epsilon_{\beta\gamma}+\epsilon)]}$$

$$\frac{1}{[-p_1^o+\sqrt{\vec{q}^2+m^2}-\sqrt{(\vec{q}+\vec{p}_1)^2+m_{\alpha\tau}^2}+i(\epsilon_{\alpha\tau}-\epsilon)]}$$

$$\left.\frac{1}{[-p_1^o+\sqrt{\vec{q}^2+m^2}+\sqrt{(\vec{q}+\vec{p}_1)^2+m_{\alpha\tau}^2}-i(\epsilon_{\alpha\tau}+\epsilon)]}\right]$$

$$+\left(\Xi_2^{ps}(q)\, f_{\beta\gamma}^2(p_3+q-p_1)\, f_{\alpha\tau}^2(q)\right)_{q^o=\bar{q}'^o_4,\ \vec{q}\to\vec{q}+\vec{p}_1}$$

$$\left[\frac{1}{[-p_3^o+\sqrt{(\vec{q}+\vec{p}_3)^2+m_{\beta\gamma}^2}-\sqrt{\vec{q}^2+m^2}+i(\epsilon-\epsilon_{\beta\gamma})]}\right.$$

$$\frac{1}{[-p_3^o+\sqrt{(\vec{q}+\vec{p}_3)^2+m_{\beta\gamma}^2}+\sqrt{\vec{q}^2+m^2}-i(\epsilon+\epsilon_{\beta\gamma})]}$$

$$\frac{1}{[p_4^o+\sqrt{(\vec{q}+\vec{p}_3)^2+m_{\beta\gamma}^2}-\sqrt{(\vec{q}-\vec{K})^2+m^2}+i(\epsilon-\epsilon_{\beta\gamma})]}$$

$$\frac{1}{[p_4^o+\sqrt{(\vec{q}+\vec{p}_3)^2+m_{\beta\gamma}^2}+\sqrt{(\vec{q}-\vec{K})^2+m^2}-i(\epsilon+\epsilon_{\beta\gamma})]}$$

$$\frac{1}{[2p_1^o-p_3^o+\sqrt{(\vec{q}+\vec{p}_3)^2+m_{\beta\gamma}^2}-\sqrt{\vec{q}^2+m^2}+i(\epsilon-\epsilon_{\beta\gamma})]}$$

$$\left.\frac{1}{[2p_1^o-p_3^o+\sqrt{(\vec{q}+\vec{p}_3)^2+m_{\beta\gamma}^2}+\sqrt{\vec{q}^2+m^2}-i(\epsilon+\epsilon_{\beta\gamma})]}\right.$$

$$\frac{1}{2\left[\sqrt{(\vec{q}+\vec{p}_3)^2+m_{\beta\gamma}^2}\ -i\epsilon_{\beta\gamma}\right]}$$

$$\frac{1}{\left[p_1^{\,o}-p_3^{\,o}+\sqrt{(\vec{q}+\vec{p}_3)^2+m_{\beta\gamma}^2}+\sqrt{(\vec{q}+\vec{p}_1)^2+m_{\alpha\tau}^2}\ -i(\epsilon_{\alpha\tau}+\epsilon_{\beta\gamma})\right]}$$

$$\left.\frac{1}{\left[p_1^{\,o}-p_3^{\,o}+\sqrt{(\vec{q}+\vec{p}_3)^2+m_{\beta\gamma}^2}-\sqrt{(\vec{q}+\vec{p}_1)^2+m_{\alpha\tau}^2}\ +i(\epsilon_{\alpha\tau}-\epsilon_{\beta\gamma})\right]}\right]$$

$$+\ \left(\Xi_2^{ps}(q)\ f_{\beta\gamma}^2(p_3+q-p_1)\ f_{\alpha\tau}^2(q)\right)_{q^o=\bar{q}'^o_5,\ \vec{q}\to\vec{q}+\vec{p}_1}$$

$$\left[\frac{1}{\left[-p_1^{\,o}+\sqrt{(\vec{q}+\vec{p}_1)^2+m_{\alpha\tau}^2}\ -\sqrt{\vec{q}^2+m^2}\ +i(\epsilon-\epsilon_{\alpha\tau})\right]}\right.$$

$$\frac{1}{\left[-p_1^{\,o}+\sqrt{(\vec{q}+\vec{p}_1)^2+m_{\alpha\tau}^2}\ +\sqrt{\vec{q}^2+m^2}\ -i(\epsilon+\epsilon_{\alpha\tau})\right]}$$

$$\frac{1}{\left[p_1^{\,o}-K^{\,o}+\sqrt{(\vec{q}+\vec{p}_1)^2+m_{\alpha\tau}^2}\ -\sqrt{(\vec{q}-\vec{K})^2+m^2}\ +i(\epsilon-\epsilon_{\alpha\tau})\right]}$$

$$\frac{1}{\left[p_1^{\,o}-K^{\,o}+\sqrt{(\vec{q}+\vec{p}_1)^2+m_{\alpha\tau}^2}\ +\sqrt{(\vec{q}-\vec{K})^2+m^2}\ -i(\epsilon+\epsilon_{\alpha\tau})\right]}$$

$$\frac{1}{\left[p_1^{\,o}+\sqrt{(\vec{q}+\vec{p}_1)^2+m_{\alpha\tau}^2}\ -\sqrt{\vec{q}^2+m^2}\ +i(\epsilon-\epsilon_{\alpha\tau})\right]}$$

$$\frac{1}{\left[p_1^{\,o}+\sqrt{(\vec{q}+\vec{p}_1)^2+m_{\alpha\tau}^2}\ +\sqrt{\vec{q}^2+m^2}\ -i(\epsilon+\epsilon_{\alpha\tau})\right]}$$

$$\frac{1}{\left[p_3^{\,o}-p_1^{\,o}+\sqrt{(\vec{q}+\vec{p}_1)^2+m_{\alpha\tau}^2}\ -\sqrt{(\vec{q}+\vec{p}_3)^2+m_{\beta\gamma}^2}\ +i(\epsilon_{\beta\gamma}-\epsilon_{\alpha\tau})\right]}$$

$$\frac{1}{\left[p_3^{\,o}-p_1^{\,o}+\sqrt{(\vec{q}+\vec{p}_1)^2+m_{\alpha\tau}^2}\ +\sqrt{(\vec{q}+\vec{p}_3)^2+m_{\beta\gamma}^2}\ -i(\epsilon_{\beta\gamma}+\epsilon_{\alpha\tau})\right]}$$

$$\left.\left.\frac{1}{2\left[\sqrt{(\vec{q}+\vec{p}_1)^2+m_{\alpha\tau}^2}\ -i\epsilon_{\alpha\tau}\right]}\right]\right\}\ . \qquad \text{(III-23)}$$

For pv coupling, the corresponding equations have the same expressions but with $\Xi_1^{ps}(q)$ ($\Xi_2^{ps}(q)$) replaced by $\Xi_1^{pv}(q)$ ($\Xi_2^{pv}(q)$).

III.3 Convergence And The Meson Form Factor

Before performing the integrations in (III-22) and (III-23), we examine the convergence of the above equations using power counting.

From equations (III-22)-(III-23) one can see that the denominators all have the form of either $(\zeta_o+\sqrt{(\bar{q}-\bar{v}_1)^2+\zeta_1^2}+\sqrt{(\bar{q}-\bar{v}_2)^2+\zeta_2^2})$ or $(\zeta_o+\sqrt{(\bar{q}-\bar{v}_1)^2+\zeta_1^2}-\sqrt{(\bar{q}-\bar{v}_2)^2+\zeta_2^2})$, where ζ_i (i = 0, 1, 2) and $\bar{v}_j$ (j = 1, 2) are constants and constant vectors, respectively. When $|\bar{q}|$ becomes very large they act like $|\bar{q}|$ or $|\bar{q}|^0$. Therefore, for large $|\bar{q}|$ the behavior of the five propagators is $\frac{1}{|\bar{q}|^5}$, while the quantities $\Xi_1^{ps}(q)$ and $\Xi_2^{ps}(q)$ are of the order of $|\bar{q}|^3$, and $\Xi_1^{pv}(q)$ and $\Xi_2^{pv}(q)$ are of the order of $|\bar{q}|^7$.

From the definition of the meson form factor (II-8c) and using a similar analysis, one obtains the following large $|\bar{q}|$ asymptotic behavior for $f_{\alpha\tau}(q)$, $f_{\beta\gamma}(p_2+q-p_4)$, and $f_{\beta\gamma}(p_3+q-p_1)$:

$$f_{\alpha\tau}(q) \approx \begin{cases} \frac{1}{|\bar{q}|}, & \text{for } q^o \neq \bar{q}_5^o \text{ or } \bar{q}'^o_5 \\ \frac{1}{|\bar{q}|^o}, & \text{for } q^o = \bar{q}_5^o \text{ or } \bar{q}'^o_5 \end{cases} \qquad \text{(III-24a)}$$

$$f_{\beta\gamma}(p_2+q-p_4) \approx \begin{cases} \frac{1}{|\bar{q}|}, & \text{for } q^o \neq \bar{q}_4^o \\ \frac{1}{|\bar{q}|^o}, & \text{for } q^o = \bar{q}_4^o \end{cases} \qquad \text{(III-24b)}$$

$$f_{\beta\gamma}(p_3+q-p_1) \approx \begin{cases} \dfrac{1}{|\vec{q}|}, & \text{for } q^o \neq \bar{q}'^o_4 \\ \dfrac{1}{|\vec{q}|^o}, & \text{for } q^o = \bar{q}'^o_4 \end{cases} \qquad \text{(III-24c)}$$

As we shall see in the next section, the two form factors $f^2_{\alpha\tau}$ and $f^2_{\beta\gamma}$ will become constants ($|\vec{q}|^o$) on the hyperbolic surfaces $\bar{q}^o_4 - \bar{q}^o_5 = 0$ and $\bar{q}'^o_4 - \bar{q}'^o_5 = 0$. So for large $|\vec{q}|$, the integrations (III-22) and (III-23) behave like $|\vec{q}|^3 \cdot |\vec{q}|^3 \cdot \frac{1}{|\vec{q}|^0} \cdot \frac{1}{|\vec{q}|^5} = |\vec{q}|$ and therefore the rescattering amplitude for ps coupling will diverge. Similarly, the rescattering amplitude for pv coupling will also diverge in the form of $|\vec{q}|^3 \cdot |\vec{q}|^7 \cdot \frac{1}{|\vec{q}|^0} \cdot \frac{1}{|\vec{q}|^5} = |\vec{q}|^5$. In fact, our numerical calculations verify these conclusions. This divergence problem comes from the unbalanced behavior of the five propagators, i.e., only the two meson propagators have the form factor in Horowitz's model, and this situation makes the contribution of the meson form factors in the five terms of equations (III-22) and (III-23) quite different: $\frac{1}{|\vec{q}|^4}$ in the first three terms and $\frac{1}{|\vec{q}|^2}$ (or $\frac{1}{|\vec{q}|^0}$ on the above two hyperbolic surfaces) in the last two terms. In order to circumvent this divergence problem, we need to modify the meson form factor. The most convenient way to modify the meson form factor is to use the conventional nonrelativistic one which removes the unbalanced behavior and becomes the relativistic one for elastic cases in the c.m. frame. In fact, Horowitz used the form of the nonrelativistic form factor in his original paper [35]. The nonrelativistic meson form factor has the form

$$\bar{f}(\vec{q}) = \frac{\Lambda^2}{\vec{q}^2 + \Lambda^2} . \qquad \text{(III-25)}$$

Correspondingly,

$$f_{\alpha\tau}(q) \simeq \bar{f}_{\alpha\tau}(\vec{q}) = \frac{\Lambda^2_{\alpha\tau}}{\vec{q}^2 + \Lambda^2_{\alpha\tau}} , \qquad \text{(III-26a)}$$

$$f_{\beta\gamma}(p_2+q-p_4) \simeq \bar{f}_{\beta\gamma}(\vec{p}_2+\vec{q}-\vec{p}_4) = \frac{\Lambda_{\alpha\tau}^2}{(\vec{p}_2+\vec{q}-\vec{p}_4)^2+\Lambda_{\alpha\tau}^2}\ , \qquad \text{(III-26b)}$$

$$f_{\beta\gamma}(p_3+q-p_1) \simeq \bar{f}_{\beta\gamma}(\vec{p}_3+\vec{q}-\vec{p}_1) = \frac{\Lambda_{\alpha\tau}^2}{(\vec{p}_3+\vec{q}-\vec{p}_1)^2+\Lambda_{\alpha\tau}^2}\ . \qquad \text{(III-26c)}$$

For large $|\vec{q}|$, all are of the order of $\frac{1}{|\vec{q}|^2}$.

Using the modified form factor, the rescattering amplitude for ps coupling behaves like $|\vec{q}|^3 \cdot |\vec{q}|^3 \cdot \frac{1}{|\vec{q}|^8} \cdot \frac{1}{|\vec{q}|^5} = \frac{1}{|\vec{q}|^7}$, and for pv coupling like $|\vec{q}|^3 \cdot |\vec{q}|^7 \cdot \frac{1}{|\vec{q}|^8} \cdot \frac{1}{|\vec{q}|^5} = \frac{1}{|\vec{q}|^3}$. Therefore, they are all convergent. In the following discussion, we will use the modified meson form factor.

III.4 $\vec{q}$ Component Integration

The evaluation of equations (III-22)-(III-23) is not so straight forward due to the singularities. We first analyze the singularities and then use an identity to derive an expressions for these equations which can be evaluated.

A. Singularities of the Integrands

Upon examination of the denominators in all five terms of Eq. (III-22), one finds that the factor $[K^o-2p_1^o+\sqrt{\vec{q}^2+m^2}+\sqrt{(\vec{q}+\vec{K})^2+m^2}\,]$ and $[-p_1^o+\sqrt{\vec{q}^2+m^2}]$ in the third term, $[-p_1^o+p_4^o+\sqrt{(\vec{q}-\vec{p}_4)^2+m_{\beta\gamma}^2}-\sqrt{(\vec{q}+\vec{p}_1)^2+m_{\alpha\tau}^2}\,]$ in the fourth term, and $[p_1^o-p_4^o+\sqrt{(\vec{q}+\vec{p}_1)^2+m_{\alpha\tau}^2}-\sqrt{(\vec{q}-\vec{p}_4)^2+m_{\beta\gamma}^2}\,]$ in the fifth term can be zero. So the third term has singularities on the elliptical surface $[K^o-2p_1^o+\sqrt{\vec{q}^2+m^2}+\sqrt{(\vec{q}+\vec{K})^2+m^2}\,]=0$ and on the spherical surface $[-p_1^o+\sqrt{\vec{q}^2+m^2}]=0$, and the fourth and fifth terms on the hyperbolic surface $[-p_1^o+p_4^o+\sqrt{(\vec{q}-\vec{p}_4)^2+m_{\beta\gamma}^2}-\sqrt{(\vec{q}+\vec{p}_1)^2+m_{\alpha\tau}^2}\,]=0$. Similarly, for

equation (III-23), the second term has singularities on the elliptical surfaces $[K^o-2p_1^o+\sqrt{(\vec{q}-\vec{K})^2+m^2}+\sqrt{\vec{q}^2+m^2}\,]=0$ and $[K^o-p_1^o+\sqrt{(\vec{q}-\vec{K})^2+m^2}-\sqrt{(\vec{q}+\vec{p}_1)^2+m_{\alpha\tau}^2}\,]=0$, the third term on the spherical surface $[-p_1^o+\sqrt{\vec{q}^2+m^2}\,]=0$, the fourth term on the hyperbolic surface $[p_1^o-p_3^o+\sqrt{(\vec{q}+\vec{p}_3)^2+m_{\beta\gamma}^2}-\sqrt{(\vec{q}+\vec{p}_1)^2+m_{\alpha\tau}^2}\,]=0$, and the fifth term on the elliptical surface $[p_1^o-K^o+\sqrt{(\vec{q}+\vec{p}_1)^2+m_{\alpha\tau}^2}-\sqrt{(\vec{q}-\vec{K})^2+m^2}\,]=0$ and the hyperbolic surface $[p_3^o-p_1^o+\sqrt{(\vec{q}+\vec{p}_1)^2+m_{\alpha\tau}^2}-\sqrt{(\vec{q}+\vec{p}_3)^2+m_{\beta\gamma}^2}\,]=0$.

We do not need to consider all of the singularities in calculating the integrations since the singularities which occur on the surfaces $\vec{q}_i-\vec{q}_j=0$ or $\vec{q}'_i-\vec{q}'_j=0$ are removable [47]; i.e. the respective pole contributions are of opposite sign and cancel. We refer to these kind of singularities as spurious singularities [48].

B. Resulting Expressions

For a real function F(x)

$$\frac{1}{F(x)\pm i\epsilon}=\begin{cases}\dfrac{1}{F(x)}, & \text{if there is no real root for } F(x)\\ P\left(\dfrac{1}{F(x)}\right)\mp i\pi\dfrac{\delta(x-x_o)}{|F'(x_o)|}, & \text{if there is a real root } x_o \text{ for } F(x)\end{cases} \qquad \text{(III-27)}$$

where P denotes the principal value.

Using the above identity, we have the following equations

$$\frac{1}{[K^o-2p_1^o+\sqrt{\vec{q}^2+m^2}+\sqrt{(\vec{q}+\vec{K})^2+m^2}-i\epsilon\,]}$$

$$=P\left[\frac{1}{K^o-2p_1^o+\sqrt{\vec{q}^2+m^2}+\sqrt{(\vec{q}+\vec{K})^2+m^2}}\right]+i\pi\delta(|\vec{q}'|-Q)\frac{1}{|D_1|} \qquad \text{(III-28)}$$

$$\frac{1}{[-p_1^o+\sqrt{\vec{q}^2+m^2}-i\epsilon]} = P\left[\frac{1}{-p_1^o+\sqrt{\vec{q}^2+m^2}}\right] + i\pi\frac{p_1^o}{|\vec{p}_1|}\delta(|\vec{q}|-|\vec{p}_1|) \qquad \text{(III-29)}$$

$$\frac{1}{[-p_1^o+p_4^o+\sqrt{(\vec{q}-\vec{p}_4)^2+m_{\beta\gamma}^2}-\sqrt{(\vec{q}+\vec{p}_1)^2+m_{\alpha\tau}^2}+i(\epsilon_{\alpha\tau}-\epsilon_{\beta\gamma})]}$$

$$= P\left[\frac{1}{p_4^o-p_1^o+\sqrt{(\vec{q}-\vec{p}_4)^2+m_{\beta\gamma}^2}-\sqrt{(\vec{q}+\vec{p}_1)^2+m_{\alpha\tau}^2}}\right]$$

$$-i\pi\delta\left[p_4^o-p_1^o+\sqrt{(\vec{q}-\vec{p}_4)^2+m_{\beta\gamma}^2}-\sqrt{(\vec{q}+\vec{p}_1)^2+m_{\alpha\tau}^2}\right] \qquad \text{(III-30)}$$

$$\frac{1}{[p_1^o-p_4^o+\sqrt{(\vec{q}+\vec{p}_1)^2+m_{\alpha\tau}^2}-\sqrt{(\vec{q}-\vec{p}_4)^2+m_{\beta\gamma}^2}+i(\epsilon_{\beta\gamma}-\epsilon_{\alpha\tau})]}$$

$$= -\frac{1}{[-p_1^o+p_4^o+\sqrt{(\vec{q}-\vec{p}_4)^2+m_{\beta\gamma}^2}-\sqrt{(\vec{q}+\vec{p}_1)^2+m_{\alpha\tau}^2}+i(\epsilon_{\alpha\tau}-\epsilon_{\beta\gamma})]}$$

$$= -P\left[\frac{1}{-p_1^o+p_4^o+\sqrt{(\vec{q}-\vec{p}_4)^2+m_{\beta\gamma}^2}-\sqrt{(\vec{q}+\vec{p}_1)^2+m_{\alpha\tau}^2}}\right]$$

$$+i\pi\delta\left[-p_1^o+p_4^o+\sqrt{(\vec{q}-\vec{p}_4)^2+m_{\beta\gamma}^2}-\sqrt{(\vec{q}+\vec{p}_1)^2+m_{\alpha\tau}^2}\right] \qquad \text{(III-31)}$$

and

$$\frac{1}{[K^o-2p_1^o+\sqrt{(\vec{q}-\vec{K})^2+m^2}+\sqrt{\vec{q}^2+m^2}-i\epsilon]}$$

$$= P\left[\frac{1}{K^o-2p_1^o+\sqrt{(\vec{q}-\vec{K})^2+m^2}+\sqrt{\vec{q}^2+m^2}}\right] + i\pi\delta(|\vec{q}''|-Q)\frac{1}{|D_2|} \qquad \text{(III-32)}$$

$$\frac{1}{[K^o-p_1^o+\sqrt{(\vec{q}-\vec{K})^2+m^2}-\sqrt{(\vec{q}+\vec{p}_1)^2+m_{\alpha\tau}^2}-i(\epsilon_{\alpha\tau}-\epsilon)]}$$

$$= P\left[\frac{1}{K^o - p_1^o + \sqrt{(\vec{q}-\vec{K})^2+m^2} - \sqrt{(\vec{q}+\vec{p}_1)^2+m_{\alpha\tau}^2}}\right]$$

$$+ i\pi\delta\left[K^o - p_1^o + \sqrt{(\vec{q}-\vec{K})^2+m^2} - \sqrt{(\vec{q}+\vec{p}_1)^2+m_{\alpha\tau}^2}\right] \quad \text{(III-33)}$$

$$\frac{1}{[-p_1^o + \sqrt{\vec{q}^2+m^2} - i\epsilon]} = P\left[\frac{1}{-p_1^o + \sqrt{\vec{q}^2+m^2}}\right] + i\pi\frac{p_1^o}{|\vec{p}_1|}\delta(|\vec{q}| - |\vec{p}_1|) \quad \text{(III-34)}$$

$$\frac{1}{[p_1^o - p_3^o + \sqrt{(\vec{q}+\vec{p}_3)^2+m_{\beta\gamma}^2} - \sqrt{(\vec{q}+\vec{p}_1)^2+m_{\alpha\tau}^2} + i(\epsilon_{\alpha\tau} - \epsilon_{\beta\gamma})]}$$

$$= P\left[\frac{1}{p_1^o - p_3^o + \sqrt{(\vec{q}+\vec{p}_3)^2+m_{\beta\gamma}^2} - \sqrt{(\vec{q}+\vec{p}_1)^2+m_{\alpha\tau}^2}}\right]$$

$$- i\pi\delta\left[p_1^o - p_3^o + \sqrt{(\vec{q}+\vec{p}_3)^2+m_{\beta\gamma}^2} - \sqrt{(\vec{q}+\vec{p}_1)^2+m_{\alpha\tau}^2}\right] \quad \text{(III-35)}$$

$$\frac{1}{[p_1^o - K^o + \sqrt{(\vec{q}+\vec{p}_1)^2+m_{\alpha\tau}^2} - \sqrt{(\vec{q}-\vec{K})^2+m^2} + i(\epsilon - \epsilon_{\alpha\tau})]}$$

$$= -\frac{1}{[K^o - p_1^o + \sqrt{(\vec{q}-\vec{K})^2+m^2} - \sqrt{(\vec{q}+\vec{p}_1)^2+m_{\alpha\tau}^2} - i(\epsilon_{\alpha\tau} - \epsilon)]}$$

$$= -P\left[\frac{1}{K^o - p_1^o + \sqrt{(\vec{q}-\vec{K})^2+m^2} - \sqrt{(\vec{q}+\vec{p}_1)^2+m_{\alpha\tau}^2}}\right]$$

$$- i\pi\delta\left[K^o - p_1^o + \sqrt{(\vec{q}-\vec{K})^2+m^2} - \sqrt{(\vec{q}+\vec{p}_1)^2+m_{\alpha\tau}^2}\right] \quad \text{(III-36)}$$

$$\frac{1}{[p_3^o - p_1^o + \sqrt{(\vec{q}+\vec{p}_1)^2+m_{\alpha\tau}^2} - \sqrt{(\vec{q}+\vec{p}_3)^2+m_{\beta\gamma}^2} + i(\epsilon_{\beta\gamma} - \epsilon_{\alpha\tau})]}$$

$$= -\frac{1}{[p_1^o - p_3^o + \sqrt{(\vec{q}+\vec{p}_3)^2+m_{\beta\gamma}^2} - \sqrt{(\vec{q}+\vec{p}_1)^2+m_{\alpha\tau}^2} + i(\epsilon_{\alpha\tau} - \epsilon_{\beta\gamma})]}$$

$$= -P\left[\frac{1}{p_1^o - p_3^o + \sqrt{(\vec{q}+\vec{p}_3)^2+m_{\beta\gamma}^2} - \sqrt{(\vec{q}+\vec{p}_1)^2+m_{\alpha\tau}^2}}\right]$$

$$+ i\pi\delta\left[p_1^o - p_3^o + \sqrt{(\vec{q}+\vec{p}_3)^2+m_{\beta\gamma}^2} - \sqrt{(\vec{q}+\vec{p}_1)^2+m_{\alpha\tau}^2}\right] \qquad \text{(III-37)}$$

where

$$\begin{cases} q_x = \frac{1}{K^o}\left[K_z q_x' + K_x\left(q_z' - \frac{1}{2}K^o\right)\right], & q_x' = |\vec{q}'|\sin\theta\cos\phi \\ q_y = q_y', & q_y' = |\vec{q}'|\sin\theta\sin\phi \\ q_z = \frac{1}{K^o}\left[-K_x q_x' + K_z\left(q_z' - \frac{1}{2}K^o\right)\right], & q_z' = |\vec{q}'|\cos\theta \end{cases} \qquad \text{(III-38)}$$

$$\begin{cases} q_x = \frac{1}{K^o}\left[-K_z q_x'' - K_x\left(q_z'' - \frac{1}{2}K^o\right)\right], & q_x'' = |\vec{q}''|\sin\theta\cos\phi \\ q_y = q_y'', & q_y'' = |\vec{q}''|\sin\theta\sin\phi \\ q_z = \frac{1}{K^o}\left[K_x q_x'' - K_z\left(q_z'' - \frac{1}{2}K^o\right)\right], & q_z'' = |\vec{q}''|\cos\theta \end{cases} \qquad \text{(III-39)}$$

$$Q = \frac{(2p_1^o - K^o)\sqrt{p_1^o(p_1^o - K^o) - m^2)}}{\sqrt{(2p_1^o - K^o)^2 - K^{o2}\cos^2\theta}}, \qquad \text{(III-40)}$$

$$D_1 = \frac{(2p_1^o - K^o)(|\vec{q}'| - \frac{1}{2}K^o\cos\theta) + K^o\cos\theta\sqrt{|\vec{q}'|^2\sin^2\theta + (|\vec{q}'|\cos\theta - \frac{1}{2}K^o)^2 + m^2}}{\sqrt{(|\vec{q}'|^2\sin^2\theta + (|\vec{q}'|\cos\theta + \frac{1}{2}K^o)^2 + m^2)(|\vec{q}'|^2\sin^2\theta + (|\vec{q}'|\cos\theta - \frac{1}{2}K^o)^2 + m^2)}} \qquad \text{(III-41)}$$

$$D_2 = \frac{(2p_1^o - K^o)(|\vec{q}''| - \frac{1}{2}K^o\cos\theta) + K^o\cos\theta\sqrt{|\vec{q}''|^2\sin^2\theta + (|\vec{q}''|\cos\theta - \frac{1}{2}K^o)^2 + m^2}}{\sqrt{(|\vec{q}''|^2\sin^2\theta + (|\vec{q}''|\cos\theta + \frac{1}{2}K^o)^2 + m^2)(|\vec{q}''|^2\sin^2\theta + (|\vec{q}''|\cos\theta - \frac{1}{2}K^o)^2 + m^2)}} \qquad \text{(III-42)}$$

Substituting equations (III-28)-(III-31), (III-38), (III-40), and (III-41) into equation (III-22), and noting that the part in the fourth term with the factor $-i\pi\delta\left[-p_1^o+p_4^o+\sqrt{(\vec{q}-\vec{p}_4)^2+m_{\beta\gamma}^2}\ -\sqrt{(\vec{q}+\vec{p}_1)^2+m_{\alpha\tau}^2}\right]$ cancels the part in the fifth term with the factor $i\pi\delta\left[-p_1^o+p_4^o+\sqrt{(\vec{q}-\vec{p}_4)^2+m_{\beta\gamma}^2}-\sqrt{(\vec{q}+\vec{p}_1)^2+m_{\alpha\tau}^2}\right]$, and furthermore that the sum of the respective principal value part of the fourth term and the fifth term yields a smooth function (the singularity on hyperbolic surface $\bar{q}_4-\bar{q}_5=0$ is a spurious singularity), we have

$$
\begin{aligned}
M_{a\mu}^{ps} = \frac{1}{(2\pi)^3}\sum_{\alpha,\beta=1}^{5}\sum_{\gamma,\tau=1}^{4}\int_{-\infty}^{\infty} d^3\vec{q}\,\Bigg\{\Big(\Xi_1^{ps}(q)\,\bar{f}_{\beta\gamma}^2(\vec{p}_2+\vec{q}-\vec{p}_4)\,\bar{f}_{\alpha\tau}^2(\vec{q})\Big)_{q^o=\bar{q}_1^o,\ \vec{q}\to\vec{q}+\vec{p}_1}\\
\Bigg[\frac{1}{2[\sqrt{(\vec{q}+\vec{K})^2+m^2}\,]}\,\frac{1}{[-K^o+\sqrt{(\vec{q}+\vec{K})^2+m^2}-\sqrt{\vec{q}^2+m^2}\,]}\\
\frac{1}{[-K^o+\sqrt{(\vec{q}+\vec{k})^2+m^2}+\sqrt{\vec{q}^2+m^2}\,]}\\
\frac{1}{[2p_1^o-K^o+\sqrt{(\vec{q}+\vec{K})^2+m^2}-\sqrt{\vec{q}^2+m^2}\,]}\\
\frac{1}{[2p_1^o-K^o+\sqrt{(\vec{q}+\vec{K})^2+m^2}+\sqrt{\vec{q}^2+m^2}\,]}\\
\frac{1}{[2p_1^o-p_4^o-K^o+\sqrt{(\vec{q}+\vec{K})^2+m^2}-\sqrt{(\vec{q}-\vec{p}_4)^2+m_{\beta\gamma}^2}\,]}\\
\frac{1}{[2p_1^o-p_4^o-K^o+\sqrt{(\vec{q}+\vec{K})^2+m^2}+\sqrt{(\vec{q}-\vec{p}_4)^2+m_{\beta\gamma}^2}\,]}\\
\frac{1}{[p_1^o-K^o+\sqrt{(\vec{q}+\vec{K})^2+m^2}-\sqrt{(\vec{q}+\vec{p}_1)^2+m_{\alpha\tau}^2}\,]}\\
\frac{1}{[p_1^o-K^o+\sqrt{(\vec{q}+\vec{K})^2+m^2}+\sqrt{(\vec{q}+\vec{p}_1)^2+m_{\alpha\tau}^2}\,]}\Bigg]
\end{aligned}
$$

$$
+ \left\{ \left(\Xi_1^{ps}(q)\, \bar{f}^2_{\beta\gamma}(\vec{p}_2+\vec{q}-\vec{p}_4)\, \bar{f}^2_{\alpha\tau}(\vec{q}) \right)_{q^o=\bar{q}_2^o,\ \vec{q}\to\vec{q}+\vec{p}_1} \right.
$$

$$
\left[\frac{1}{[K^o+\sqrt{\vec{q}^2+m^2}\ -\sqrt{(\vec{q}+\vec{K})^2+m^2}\ ]} \right.
$$

$$
\frac{1}{[K^o+\sqrt{\vec{q}^2+m^2}\ +\sqrt{(\vec{q}+\vec{K})^2+m^2}\ ]}\ \frac{1}{2\,[\sqrt{\vec{q}^2+m^2}\ ]}
$$

$$
\frac{1}{2\,[p_1^o]}\ \frac{1}{2\,[p_1^o+\sqrt{\vec{q}^2+m^2}\ ]}
$$

$$
\frac{1}{[2p_1^o-p_4^o+\sqrt{\vec{q}^2+m^2}\ -\sqrt{(\vec{q}-\vec{p}_4)^2+m^2_{\beta\gamma}}\ ]}
$$

$$
\frac{1}{[2p_1^o-p_4^o+\sqrt{\vec{q}^2+m^2}\ +\sqrt{(\vec{q}-\vec{p}_4)^2+m^2_{\beta\gamma}}\ ]}
$$

$$
\frac{1}{[p_1^o+\sqrt{\vec{q}^2+m^2}\ -\sqrt{(\vec{q}+\vec{p}_1)^2+m^2_{\alpha\tau}}\ ]}
$$

$$
\left. \left. \frac{1}{[p_1^o+\sqrt{\vec{q}^2+m^2}\ +\sqrt{(\vec{q}+\vec{p}_1)^2+m^2_{\alpha\tau}}\ ]} \right] \right.
$$

$$
+ \left(\Xi_1^{ps}(q)\, \bar{f}^2_{\beta\gamma}(\vec{p}_2+\vec{q}-\vec{p}_4)\, \bar{f}^2_{\alpha\tau}(\vec{q}) \right)_{q^o=\bar{q}_3^o,\ \vec{q}\to\vec{q}+\vec{p}_1}
$$

$$
P \left[\frac{1}{[K^o-2p_1^o+\sqrt{\vec{q}^2+m^2}\ -\sqrt{(\vec{q}+\vec{K})^2+m^2}\ ]} \right.
$$

$$
\frac{1}{[K^o-2p_1^o+\sqrt{\vec{q}^2+m^2}\ +\sqrt{(\vec{q}+\vec{K})^2+m^2}\ ]}
$$

$$
\frac{1}{2\,[-p_1^o]}\ \frac{1}{2\,[-p_1^o+\sqrt{\vec{q}^2+m^2}-i\epsilon]}\ \frac{1}{2\,[\sqrt{\vec{q}^2+m^2}\ ]}
$$

$$
\frac{1}{[-p_4^o+\sqrt{\vec{q}^2+m^2}\ -\sqrt{(\vec{q}-\vec{p}_4)^2+m^2_{\beta\gamma}}\ ]}
$$

$$
\frac{1}{[-p_4^o+\sqrt{\vec{q}^2+m^2}\ +\sqrt{(\vec{q}-\vec{p}_4)^2+m^2_{\beta\gamma}}\ ]}
$$

$$
\frac{1}{[-p_1^o+\sqrt{\vec{q}^2+m^2}\ -\sqrt{(\vec{q}+\vec{p}_1)^2+m^2_{\alpha\tau}}\ ]}
$$

$$\left.\frac{1}{[-p_1^o+\sqrt{\vec{q}^2+m^2}+\sqrt{(\vec{q}+\vec{p}_1)^2+m_{\alpha\tau}^2}\,]}\right]_{\text{on } |\vec{q}|=|\vec{p}_1| \text{ and } |\vec{q}'|=Q}$$

$$+\left(\Xi_1^{ps}(q)\;\bar{f}^2_{\beta\gamma}(\vec{p}_2+\vec{q}-\vec{p}_4)\;\bar{f}^2_{\alpha\tau}(\vec{q})\right)_{q^o=\bar{q}_3^o,\;\vec{q}\to\vec{q}+\vec{p}_1}$$

$$\left[\frac{1}{[K^o-2p_1^o+\sqrt{\vec{q}^2+m^2}-\sqrt{(\vec{q}+\vec{K})^2+m^2}\,]}\right.$$

$$i\pi\delta(|\vec{q}'|-Q)\frac{1}{|D_1|}$$

$$\frac{1}{2[-p_1^o]}\;\frac{1}{2[-p_1^o+\sqrt{\vec{q}^2+m^2}-i\epsilon]}\;\frac{1}{2[\sqrt{\vec{q}^2+m^2}\,]}$$

$$\frac{1}{[-p_4^o+\sqrt{\vec{q}^2+m^2}-\sqrt{(\vec{q}-\vec{p}_4)^2+m_{\beta\gamma}^2}\,]}$$

$$\frac{1}{[-p_4^o+\sqrt{\vec{q}^2+m^2}+\sqrt{(\vec{q}-\vec{p}_4)^2+m_{\beta\gamma}^2}\,]}$$

$$\left.\frac{1}{[-p_1^o+\sqrt{\vec{q}^2+m^2}-\sqrt{(\vec{q}+\vec{p}_1)^2+m_{\alpha\tau}^2}\,]}\right]$$

$$\left.\frac{1}{[-p_1^o+\sqrt{\vec{q}^2+m^2}+\sqrt{(\vec{q}+\vec{p}_1)^2+m_{\alpha\tau}^2}\,]}\right]$$

$$+\left(\Xi_1^{ps}(q)\;\bar{f}^2_{\beta\gamma}(\vec{p}_2+\vec{q}-\vec{p}_4)\;\bar{f}^2_{\alpha\tau}(\vec{q})\right)_{q^o=\bar{q}_3^o,\;\vec{q}\to\vec{q}+\vec{p}_1}$$

$$\left[\frac{1}{[K^o-2p_1^o+\sqrt{\vec{q}^2+m^2}-\sqrt{(\vec{q}+\vec{K})^2+m^2}\,]}\right.$$

$$\frac{1}{[K^o-2p_1^o+\sqrt{\vec{q}^2+m^2}+\sqrt{(\vec{q}+\vec{K})^2+m^2}\,]}$$

$$\frac{1}{2[-p_1^o]}\left[i\pi\frac{p_1^o}{2|\vec{p}_1|}\,\delta(|\vec{q}|-|\vec{p}_1|)\right]\frac{1}{2[\sqrt{\vec{q}^2+m^2}\,]}$$

$$\frac{1}{[-p_4^o+\sqrt{\vec{q}^2+m^2}-\sqrt{(\vec{q}-\vec{p}_4)^2+m_{\beta\gamma}^2}\,]}$$

$$\frac{1}{[-p_4^o+\sqrt{\vec{q}^2+m^2}+\sqrt{(\vec{q}-\vec{p}_4)^2+m_{\beta\gamma}^2}\,]}\,\frac{1}{[-p_1^o+\sqrt{\vec{q}^2+m^2}-\sqrt{(\vec{q}+\vec{p}_1)^2+m_{\alpha\tau}^2}\,]}\left[\frac{1}{[-p_1^o+\sqrt{\vec{q}^2+m^2}+\sqrt{(\vec{q}+\vec{p}_1)^2+m_{\alpha\tau}^2}\,]}\right]$$

$$+\left(\bar{\Xi}_1^{ps}(q)\,\bar{f}_{\beta\gamma}^2(\vec{p}_2+\vec{q}-\vec{p}_4)\,\bar{f}_{\alpha\tau}^2(\vec{q})\right)_{q^o=\bar{q}_4^o,\ \vec{q}\to\vec{q}+\vec{p}_1}$$

$$\left[\frac{1}{[K^o-2p_1^o+p_4^o+\sqrt{(\vec{q}-\vec{p}_4)^2+m_{\beta\gamma}^2}-\sqrt{(\vec{q}+\vec{K})^2+m^2}+i(\epsilon-\epsilon_{\beta\gamma})]}\right.$$

$$\frac{1}{[K^o-2p_1^o+p_4^o+\sqrt{(\vec{q}-\vec{p}_4)^2+m_{\beta\gamma}^2}+\sqrt{(\vec{q}+\vec{K})^2+m^2}-i(\epsilon+\epsilon_{\beta\gamma})]}$$

$$\frac{1}{[-2p_1^o+p_4^o+\sqrt{(\vec{q}-\vec{p}_4)^2+m_{\beta\gamma}^2}-\sqrt{\vec{q}^2+m^2}+i(\epsilon-\epsilon_{\beta\gamma})]}$$

$$\frac{1}{[-2p_1^o+p_4^o+\sqrt{(\vec{q}-\vec{p}_4)^2+m_{\beta\gamma}^2}+\sqrt{\vec{q}^2+m^2}-i(\epsilon+\epsilon_{\beta\gamma})]}$$

$$\frac{1}{[p_4^o+\sqrt{(\vec{q}-\vec{p}_4)^2+m_{\beta\gamma}^2}-\sqrt{\vec{q}^2+m^2}+i(\epsilon-\epsilon_{\beta\gamma})]}$$

$$\frac{1}{[p_4^o+\sqrt{(\vec{q}-\vec{p}_4)^2+m_{\beta\gamma}^2}+\sqrt{\vec{q}^2+m^2}-i(\epsilon+\epsilon_{\beta\gamma})]}$$

$$\frac{1}{2[\sqrt{(\vec{q}-\vec{p}_4)^2+m_{\beta\gamma}^2}-i\epsilon_{\beta\gamma}]}$$

$$\frac{1}{[-p_1^o+p_4^o+\sqrt{(\vec{q}-\vec{p}_4)^2+m_{\beta\gamma}^2}+\sqrt{(\vec{q}+\vec{p}_1)^2+m_{\alpha\tau}^2}-i(\epsilon_{\alpha\tau}+\epsilon_{\beta\gamma})]}$$

$$\left.\frac{1}{[-p_1^o+p_4^o+\sqrt{(\vec{q}-\vec{p}_4)^2+m_{\beta\gamma}^2}-\sqrt{(\vec{q}+\vec{p}_1)^2+m_{\alpha\tau}^2}+i(\epsilon_{\alpha\tau}-\epsilon_{\beta\gamma})]}\right]$$

$$+ \left(\Xi_1^{ps}(q)\, \bar{f}^2_{\beta\gamma}(\vec{p}_2+\vec{q}-\vec{p}_4)\, \bar{f}^2_{\alpha\tau}(\vec{q}) \right)_{q^o=\bar{q}_5^o,\ \vec{q}\to\vec{q}+\vec{p}_1}$$

$$\left[\frac{1}{[K^o - p_1^o + \sqrt{(\vec{q}+\vec{p}_1)^2+m^2_{\alpha\tau}} - \sqrt{(\vec{q}+\vec{K})^2+m^2} + i(\epsilon-\epsilon_{\alpha\tau})]} \right.$$

$$\frac{1}{[K^o - p_1^o + \sqrt{(\vec{q}+\vec{p}_1)^2+m^2_{\alpha\tau}} + \sqrt{(\vec{q}+\vec{K})^2+m^2} - i(\epsilon+\epsilon_{\alpha\tau})]}$$

$$\frac{1}{[-p_1^o + \sqrt{(\vec{q}+\vec{p}_1)^2+m^2_{\alpha\tau}} - \sqrt{\vec{q}^2+m^2} + i(\epsilon-\epsilon_{\alpha\tau})]}$$

$$\frac{1}{[-p_1^o + \sqrt{(\vec{q}+\vec{p}_1)^2+m^2_{\alpha\tau}} + \sqrt{\vec{q}^2+m^2} - i(\epsilon+\epsilon_{\alpha\tau})]}$$

$$\frac{1}{[p_1^o + \sqrt{(\vec{q}+\vec{p}_1)^2+m^2_{\alpha\tau}} - \sqrt{\vec{q}^2+m^2} + i(\epsilon-\epsilon_{\alpha\tau})]}$$

$$\frac{1}{[p_1^o + \sqrt{(\vec{q}+\vec{p}_1)^2+m^2_{\alpha\tau}} + \sqrt{\vec{q}^2+m^2} - i(\epsilon+\epsilon_{\alpha\tau})]}$$

$$\frac{1}{[p_1^o - p_4^o + \sqrt{(\vec{q}+\vec{p}_1)^2+m^2_{\alpha\tau}} - \sqrt{(\vec{q}-\vec{p}_4)^2+m^2_{\beta\gamma}} + i(\epsilon_{\beta\gamma}-\epsilon_{\alpha\tau})]}$$

$$\frac{1}{[p_1^o - p_4^o + \sqrt{(\vec{q}+\vec{p}_1)^2+m^2_{\alpha\tau}} + \sqrt{(\vec{q}-\vec{p}_4)^2+m^2_{\beta\gamma}} - i(\epsilon_{\beta\gamma}+\epsilon_{\alpha\tau})]}$$

$$\left. \left. \frac{1}{2[\sqrt{(\vec{q}+\vec{p}_1)^2+m^2_{\alpha\tau}} - i\epsilon_{\alpha\tau}]} \right] \right\}$$

$$= \frac{1}{(2\pi)^3} \sum_{\alpha,\beta=1}^{5} \sum_{\gamma,\tau=1}^{4} \int_{-\infty}^{\infty} d^3\vec{q} \left\{ \left(\Xi_1^{ps}(q)\, \bar{f}^2_{\beta\gamma}(\vec{p}_2+\vec{q}-\vec{p}_4)\, \bar{f}^2_{\alpha\tau}(\vec{q}) \right)_{q^o=\bar{q}_1^o,\ \vec{q}\to\vec{q}+\vec{p}_1} \right.$$

$$\left[\frac{1}{2[\sqrt{(\vec{q}+\vec{K})^2+m^2}]} \frac{1}{[-K^o + \sqrt{(\vec{q}+\vec{K})^2+m^2} - \sqrt{\vec{q}^2+m^2}]} \right.$$

$$\frac{1}{[-K^o + \sqrt{(\vec{q}+\vec{k})^2+m^2} + \sqrt{\vec{q}^2+m^2}]}$$

$$\left. \left. \frac{1}{[2p_1^o - K^o + \sqrt{(\vec{q}+\vec{K})^2+m^2} - \sqrt{\vec{q}^2+m^2}]} \right] \right\}$$

$$\frac{1}{[2p_1^o - K^o + \sqrt{(\vec{q}+\vec{K})^2+m^2} + \sqrt{\vec{q}^2+m^2}\ ]}$$

$$\frac{1}{[2p_1^o - p_4^o - K^o + \sqrt{(\vec{q}+\vec{K})^2+m^2} - \sqrt{(\vec{q}-\vec{p}_4)^2+m_{\beta\gamma}^2}\ ]}$$

$$\frac{1}{[2p_1^o - p_4^o - K^o + \sqrt{(\vec{q}+\vec{K})^2+m^2} + \sqrt{(\vec{q}-\vec{p}_4)^2+m_{\beta\gamma}^2}\ ]}$$

$$\frac{1}{[p_1^o - K^o + \sqrt{(\vec{q}+\vec{K})^2+m^2} - \sqrt{(\vec{q}+\vec{p}_1)^2+m_{\alpha\tau}^2}\ ]}$$

$$\left.\frac{1}{[p_1^o - K^o + \sqrt{(\vec{q}+\vec{K})^2+m^2} + \sqrt{(\vec{q}+\vec{p}_1)^2+m_{\alpha\tau}^2}\ ]}\right]$$

$$+ \left(\Xi_1^{ps}(q)\ \bar{f}_{\beta\gamma}^2(\vec{p}_2+\vec{q}-\vec{p}_4)\ \bar{f}_{\alpha\tau}^2(\vec{q})\right)_{q^o=\bar{q}_2^o,\ \vec{q}\to\vec{q}+\vec{p}_1}$$

$$\left[\frac{1}{[K^o + \sqrt{\vec{q}^2+m^2} - \sqrt{(\vec{q}+\vec{K})^2+m^2}\ ]}\right.$$

$$\frac{1}{[K^o + \sqrt{\vec{q}^2+m^2} + \sqrt{(\vec{q}+\vec{K})^2+m^2}\ ]}\ \frac{1}{2[\sqrt{\vec{q}^2+m^2}\ ]}$$

$$\frac{1}{2[p_1^o]}\ \frac{1}{2[p_1^o + \sqrt{\vec{q}^2+m^2}\ ]}$$

$$\frac{1}{[2p_1^o - p_4^o + \sqrt{\vec{q}^2+m^2} - \sqrt{(\vec{q}-\vec{p}_4)^2+m_{\beta\gamma}^2}\ ]}$$

$$\frac{1}{[2p_1^o - p_4^o + \sqrt{\vec{q}^2+m^2} + \sqrt{(\vec{q}-\vec{p}_4)^2+m_{\beta\gamma}^2}\ ]}$$

$$\frac{1}{[p_1^o + \sqrt{\vec{q}^2+m^2} - \sqrt{(\vec{q}+\vec{p}_1)^2+m_{\alpha\tau}^2}\ ]}$$

$$\left.\frac{1}{[p_1^o + \sqrt{\vec{q}^2+m^2} + \sqrt{(\vec{q}+\vec{p}_1)^2+m_{\alpha\tau}^2}\ ]}\right]$$

$$+ \left(\Xi_1^{ps}(q)\ \bar{f}_{\beta\gamma}^2(\vec{p}_2+\vec{q}-\vec{p}_4)\ \bar{f}_{\alpha\tau}^2(\vec{q})\right)_{q^o=\bar{q}_4^o,\ \vec{q}\to\vec{q}+\vec{p}_1}$$

$$\left[\frac{1}{[K^o-2p_1^o+p_4^o+\sqrt{(\vec{q}-\vec{p}_4)^2+m_{\beta\gamma}^2}-\sqrt{(\vec{q}+\vec{K})^2+m^2}+i(\epsilon-\epsilon_{\beta\gamma})]}\right.$$

$$\frac{1}{[K^o-2p_1^o+p_4^o+\sqrt{(\vec{q}-\vec{p}_4)^2+m_{\beta\gamma}^2}+\sqrt{(\vec{q}+\vec{K})^2+m^2}-i(\epsilon+\epsilon_{\beta\gamma})]}$$

$$\frac{1}{[-2p_1^o+p_4^o+\sqrt{(\vec{q}-\vec{p}_4)^2+m_{\beta\gamma}^2}-\sqrt{\vec{q}^2+m^2}+i(\epsilon-\epsilon_{\beta\gamma})]}$$

$$\frac{1}{[-2p_1^o+p_4^o+\sqrt{(\vec{q}-\vec{p}_4)^2+m_{\beta\gamma}^2}+\sqrt{\vec{q}^2+m^2}-i(\epsilon+\epsilon_{\beta\gamma})]}$$

$$\frac{1}{[p_4^o+\sqrt{(\vec{q}-\vec{p}_4)^2+m_{\beta\gamma}^2}-\sqrt{\vec{q}^2+m^2}+i(\epsilon-\epsilon_{\beta\gamma})]}$$

$$\frac{1}{[p_4^o+\sqrt{(\vec{q}-\vec{p}_4)^2+m_{\beta\gamma}^2}+\sqrt{\vec{q}^2+m^2}-i(\epsilon+\epsilon_{\beta\gamma})]}$$

$$\frac{1}{2[\sqrt{(\vec{q}-\vec{p}_4)^2+m_{\beta\gamma}^2}-i\epsilon_{\beta\gamma}]}$$

$$\frac{1}{[-p_1^o+p_4^o+\sqrt{(\vec{q}-\vec{p}_4)^2+m_{\beta\gamma}^2}+\sqrt{(\vec{q}+\vec{p}_1)^2+m_{\alpha\tau}^2}-i(\epsilon_{\alpha\tau}+\epsilon_{\beta\gamma})]}$$

$$\left.\frac{1}{[-p_1^o+p_4^o+\sqrt{(\vec{q}-\vec{p}_4)^2+m_{\beta\gamma}^2}-\sqrt{(\vec{q}+\vec{p}_1)^2+m_{\alpha\tau}^2}+i(\epsilon_{\alpha\tau}-\epsilon_{\beta\gamma})]}\right]$$

$$+\left(\Xi_1^{ps}(q)\,\bar{f}_{\beta\gamma}^2(\vec{p}_2+\vec{q}-\vec{p}_4)\,\bar{f}_{\alpha\tau}^2(\vec{q})\right)_{q^o=\bar{q}_5^o,\ \vec{q}\to\vec{q}+\vec{p}_1}$$

$$\left[\frac{1}{[K^o-p_1^o+\sqrt{(\vec{q}+\vec{p}_1)^2+m_{\alpha\tau}^2}-\sqrt{(\vec{q}+\vec{K})^2+m^2}+i(\epsilon-\epsilon_{\alpha\tau})]}\right.$$

$$\frac{1}{[K^o-p_1^o+\sqrt{(\vec{q}+\vec{p}_1)^2+m_{\alpha\tau}^2}+\sqrt{(\vec{q}+\vec{K})^2+m^2}-i(\epsilon+\epsilon_{\alpha\tau})]}$$

$$\frac{1}{[-p_1^o+\sqrt{(\vec{q}+\vec{p}_1)^2+m_{\alpha\tau}^2}-\sqrt{\vec{q}^2+m^2}+i(\epsilon-\epsilon_{\alpha\tau})]}$$

$$\frac{1}{[-p_1^o+\sqrt{(\vec{q}+\vec{p}_1)^2+m_{\alpha\tau}^2}+\sqrt{\vec{q}^2+m^2}-i(\epsilon+\epsilon_{\alpha\tau})]}$$

$$\frac{1}{[p_1^o+\sqrt{(\vec{q}+\vec{p}_1)^2+m_{\alpha\tau}^2}-\sqrt{\vec{q}^2+m^2}+i(\epsilon-\epsilon_{\alpha\tau})]}$$

$$\frac{1}{[p_1^o+\sqrt{(\vec{q}+\vec{p}_1)^2+m_{\alpha\tau}^2}+\sqrt{\vec{q}^2+m^2}-i(\epsilon+\epsilon_{\alpha\tau})]}$$

$$\frac{1}{[p_1^o-p_4^o+\sqrt{(\vec{q}+\vec{p}_1)^2+m_{\alpha\tau}^2}-\sqrt{(\vec{q}-\vec{p}_4)^2+m_{\beta\gamma}^2}+i(\epsilon_{\beta\gamma}-\epsilon_{\alpha\tau})]}$$

$$\frac{1}{[p_1^o-p_4^o+\sqrt{(\vec{q}+\vec{p}_1)^2+m_{\alpha\tau}^2}+\sqrt{(\vec{q}-\vec{p}_4)^2+m_{\beta\gamma}^2}-i(\epsilon_{\beta\gamma}+\epsilon_{\alpha\tau})]}$$

$$\left.\left.\frac{1}{2[\sqrt{(\vec{q}+\vec{p}_1)^2+m_{\alpha\tau}^2}-i\epsilon_{\alpha\tau}]}\right]\right\}$$

$$+\frac{1}{(2\pi)^3}\sum_{\alpha,\beta=1}^{5}\sum_{\gamma,\tau=1}^{4}P\left[\int_{-\infty}^{\infty}d^3\vec{q}\left(\Xi_1^{ps}(q)\,\bar{f}_{\beta\gamma}^2(\vec{p}_2+\vec{q}-\vec{p}_4)\,\bar{f}_{\alpha\tau}^2(\vec{q})\right)_{q^o=\bar{q}_3^o,\ \vec{q}\to\vec{q}+\vec{p}_1}\right.$$

$$\frac{1}{[K^o-2p_1^o+\sqrt{\vec{q}^2+m^2}-\sqrt{(\vec{q}+\vec{K})^2+m^2}]}$$

$$\frac{1}{[K^o-2p_1^o+\sqrt{\vec{q}^2+m^2}+\sqrt{(\vec{q}+\vec{K})^2+m^2}]}$$

$$\frac{1}{2[-p_1^o]}\,\frac{1}{2[-p_1^o+\sqrt{\vec{q}^2+m^2}-i\epsilon]}\,\frac{1}{2[\sqrt{\vec{q}^2+m^2}]}$$

$$\frac{1}{[-p_4^o+\sqrt{\vec{q}^2+m^2}-\sqrt{(\vec{q}-\vec{p}_4)^2+m_{\beta\gamma}^2}]}$$

$$\frac{1}{[-p_4^o+\sqrt{\vec{q}^2+m^2}+\sqrt{(\vec{q}-\vec{p}_4)^2+m_{\beta\gamma}^2}]}$$

$$\frac{1}{[-p_1^o+\sqrt{\vec{q}^2+m^2}-\sqrt{(\vec{q}+\vec{p}_1)^2+m_{\alpha\tau}^2}]}$$

$$\left.\frac{1}{[-p_1^o+\sqrt{\vec{q}^2+m^2}+\sqrt{(\vec{q}+\vec{p}_1)^2+m_{\alpha\tau}^2}]}\right]_{\text{on } |\vec{q}|=|\vec{p}_1| \text{ and } |\vec{q}'|=Q}$$

$$+\frac{i\pi}{(2\pi)^3}\sum_{\alpha,\beta=1}^{5}\sum_{\gamma,\tau=1}^{4}\int_0^{\pi}d\theta\int_0^{2\pi}d\phi\left(\bar{\Xi}_1^{ps}(q)\,\bar{f}^2_{\beta\gamma}(\bar{p}_2+\bar{q}-\bar{p}_4)\,\bar{f}^2_{\alpha\tau}(\bar{q})\right)_{q^o=\bar{q}_3^o,\ \bar{q}\to\bar{q}+\bar{p}_1}$$

$$\left[\frac{1}{[K^o-2p_1^o+\sqrt{\bar{q}^2+m^2}-\sqrt{(\bar{q}+\bar{K})^2+m^2}\,]}\,\frac{|\bar{q}'|^2\sin\theta}{|D_1|}\right.$$

$$\frac{1}{2[-p_1^o]}\,\frac{1}{2[-p_1^o+\sqrt{\bar{q}^2+m^2}-i\epsilon]}\,\frac{1}{2[\sqrt{\bar{q}^2+m^2}\,]}$$

$$\frac{1}{[-p_4^o+\sqrt{\bar{q}^2+m^2}-\sqrt{(\bar{q}-\bar{p}_4)^2+m^2_{\beta\gamma}}\,]}$$

$$\frac{1}{[-p_4^o+\sqrt{\bar{q}^2+m^2}+\sqrt{(\bar{q}-\bar{p}_4)^2+m^2_{\beta\gamma}}\,]}$$

$$\left.\frac{1}{[-p_1^o+\sqrt{\bar{q}^2+m^2}-\sqrt{(\bar{q}+\bar{p}_1)^2+m^2_{\alpha\tau}}\,]}\right]_{|\bar{q}'|=Q}$$

$$+\frac{i\pi}{(2\pi)^3}\sum_{\alpha,\beta=1}^{5}\sum_{\gamma,\tau=1}^{4}\int_0^{\pi}d\theta\int_0^{2\pi}d\phi\left(\bar{\Xi}_1^{ps}(q)\,\bar{f}^2_{\beta\gamma}(\bar{p}_2+\bar{q}-\bar{p}_4)\,\bar{f}^2_{\alpha\tau}(\bar{q})\right)_{q^o=\bar{q}_3^o,\ \bar{q}\to\bar{q}+\bar{p}_1}$$

$$\left[\frac{1}{[K^o-2p_1^o+\sqrt{\bar{q}^2+m^2}-\sqrt{(\bar{q}+\bar{K})^2+m^2}\,]}\,\frac{|\bar{p}_1|^2 p_1^o\sin\theta}{2|\bar{p}_1|}\right.$$

$$\frac{1}{[K^o-2p_1^o+\sqrt{\bar{q}^2+m^2}+\sqrt{(\bar{q}+\bar{K})^2+m^2}\,]}$$

$$\frac{1}{2[-p_1^o]}\,\frac{1}{2[\sqrt{\bar{q}^2+m^2}\,]}$$

$$\frac{1}{[-p_4^o+\sqrt{\bar{q}^2+m^2}-\sqrt{(\bar{q}-\bar{p}_4)^2+m^2_{\beta\gamma}}\,]}$$

$$\frac{1}{[-p_4^o+\sqrt{\bar{q}^2+m^2}+\sqrt{(\bar{q}-\bar{p}_4)^2+m^2_{\beta\gamma}}\,]}$$

$$\left.\frac{1}{[-p_1^o+\sqrt{\bar{q}^2+m^2}-\sqrt{(\bar{q}+\bar{p}_1)^2+m^2_{\alpha\tau}}\,]}\right.$$

$$\left.\frac{1}{\left[-p_1^{\circ}+\sqrt{\vec{q}^2+m^2}+\sqrt{(\vec{q}+\vec{p}_1)^2+m_{\alpha\tau}^2}\right]}\right]_{|\vec{q}|=|\vec{p}_1|} \qquad \text{(III-43)}$$

Similarly, substituting equations (III-32)-(III-37), (III-39), (III-40), and (III-42) into equation (III-23), we have

$$M_{b\mu}^{ps}=\frac{1}{(2\pi)^3}\sum_{\alpha,\beta=1}^{5}\sum_{\gamma,\tau=1}^{4}\int_{-\infty}^{\infty}d^3\vec{q}\left\{\left(\Xi_2^{ps}(q)\,\bar{f}_{\beta\gamma}^2(\vec{p}_3+\vec{q}-\vec{p}_1)\,\bar{f}_{\alpha\tau}^2(\vec{q})\right)_{q^{\circ}=\bar{q}'^{\circ}_1,\ \vec{q}\to\vec{q}+\vec{p}_1}\right.$$

$$\left[\frac{1}{2\left[\sqrt{\vec{q}^2+m^2}\right]}\frac{1}{\left[2p_1^{\circ}-K^{\circ}+\sqrt{\vec{q}^2+m^2}-\sqrt{(\vec{q}-\vec{K})^2+m^2}\right]}\right.$$

$$\frac{1}{\left[2p_1^{\circ}-K^{\circ}+\sqrt{\vec{q}^2+m^2}+\sqrt{(\vec{q}-\vec{K})^2+m^2}\right]}$$

$$\frac{\frac{1}{2[p_1^{\circ}]}\frac{1}{2\left[p_1^{\circ}+\sqrt{\vec{q}^2+m^2}\right]}}{\left[p_3^{\circ}+\sqrt{\vec{q}^2+m^2}-\sqrt{(\vec{q}+\vec{p}_3)^2+m_{\beta\gamma}^2}\right]}$$

$$\frac{1}{\left[p_3^{\circ}+\sqrt{\vec{q}^2+m^2}+\sqrt{(\vec{q}+\vec{p}_3)^2+m_{\beta\gamma}^2}\right]}$$

$$\frac{1}{\left[p_1^{\circ}+\sqrt{\vec{q}^2+m^2}-\sqrt{(\vec{q}+\vec{p}_1)^2+m_{\alpha\tau}^2}\right]}$$

$$\left.\left.\frac{1}{\left[p_1^{\circ}+\sqrt{\vec{q}^2+m^2}+\sqrt{(\vec{q}+\vec{p}_1)^2+m_{\alpha\tau}^2}\right]}\right]\right.$$

$$+\left(\Xi_2^{ps}(q)\,\bar{f}_{\beta\gamma}^2(\vec{p}_3+\vec{q}-\vec{p}_1)\,\bar{f}_{\alpha\tau}^2(\vec{q})\right)_{q^{\circ}=\bar{q}'^{\circ}_3,\ \vec{q}\to\vec{q}+\vec{p}_1}$$

$$P\left[\frac{1}{2[-p_1^{\circ}]}\frac{1}{2\left[-p_1^{\circ}+\sqrt{\vec{q}^2+m^2}\right]}\right.$$

$$\frac{1}{[-K^o+\sqrt{\vec{q}^2+m^2}-\sqrt{(\vec{q}-\vec{K})^2+m^2}\,]}$$

$$\frac{1}{[-K^o+\sqrt{\vec{q}^2+m^2}+\sqrt{(\vec{q}-\vec{K})^2+m^2}\,]}\,\frac{1}{2[\sqrt{\vec{q}^2+m^2}\,]}$$

$$\frac{1}{[p_3^o-2p_1^o+\sqrt{\vec{q}^2+m^2}-\sqrt{(\vec{q}+\vec{p}_3)^2+m_{\beta\gamma}^2}\,]}$$

$$\frac{1}{[p_3^o-2p_1^o+\sqrt{\vec{q}^2+m^2}+\sqrt{(\vec{q}+\vec{p}_3)^2+m_{\beta\gamma}^2}\,]}$$

$$\left.\frac{1}{[-p_1^o+\sqrt{\vec{q}^2+m^2}-\sqrt{(\vec{q}+\vec{p}_1)^2+m_{\alpha\tau}^2}\,]}\,\frac{1}{[-p_1^o+\sqrt{\vec{q}^2+m^2}+\sqrt{(\vec{q}+\vec{p}_1)^2+m_{\alpha\tau}^2}\,]}\right]_{\text{on } |\vec{q}|=|\vec{p}_1|}\Bigg\}$$

$$+\frac{1}{(2\pi)^3}\sum_{\alpha,\beta=1}^{5}\sum_{\gamma,\tau=1}^{4}\int_{-\infty}^{\infty}d^3\vec{q}\,\Big\{\Big(\Xi_2^{ps}(q)\,\bar{f}_{\beta\gamma}^2(\vec{p}_3+\vec{q}-\vec{p}_1)\,\bar{f}_{\alpha\tau}^2(\vec{q})\Big)_{q^o=\bar{q}_2'^o,\ \vec{q}\to\vec{q}+\vec{p}_1}$$

$$P\left[\frac{1}{[K^o-2p_1^o+\sqrt{(\vec{q}-\vec{K})^2+m^2}-\sqrt{\vec{q}^2+m^2}\,]}\right.$$

$$\frac{1}{[K^o-2p_1^o+\sqrt{(\vec{q}-\vec{K})^2+m^2}+\sqrt{\vec{q}^2+m^2}\,]}$$

$$\frac{1}{2[\sqrt{(\vec{q}-\vec{K})^2+m^2}\,]}\,\frac{1}{[K^o+\sqrt{(\vec{q}-\vec{K})^2+m^2}-\sqrt{\vec{q}^2+m^2}\,]}$$

$$\frac{1}{[K^o+\sqrt{(\vec{q}-\vec{K})^2+m^2}+\sqrt{\vec{q}^2+m^2}\,]}$$

$$\frac{1}{[K^o-2p_1^o+p_3^o+\sqrt{(\vec{q}-\vec{K})^2+m^2}-\sqrt{(\vec{q}+\vec{p}_3)^2+m_{\beta\gamma}^2}\,]}$$

$$\frac{1}{[K^o-2p_1^o+p_3^o+\sqrt{(\vec{q}-\vec{K})^2+m^2}+\sqrt{(\vec{q}+\vec{p}_3)^2+m_{\beta\gamma}^2}\,]}$$

$$\left.\frac{1}{[K^o-p_1^o+\sqrt{(\vec{q}-\vec{K})^2+m^2}-\sqrt{(\vec{q}+\vec{p}_1)^2+m_{\alpha\tau}^2}\,]}\,\frac{1}{[K^o-p_1^o+\sqrt{(\vec{q}-\vec{K})^2+m^2}+\sqrt{(\vec{q}+\vec{p}_1)^2+m_{\alpha\tau}^2}\,]}\right]_{\text{on } |\vec{q}''|=Q}$$

$$+ \left(\Xi_2^{ps}(q)\ \bar{f}^2_{\beta\gamma}(\vec{p}_3+\vec{q}-\vec{p}_1)\ \bar{f}^2_{\alpha\tau}(\vec{q}) \right)_{q^o=\bar{q}'^o_4,\ \vec{q}\to\vec{q}+\vec{p}_1}$$

$$\left[\frac{1}{[-p_3^o+\sqrt{(\vec{q}+\vec{p}_3)^2+m^2_{\beta\gamma}}-\sqrt{\vec{q}^2+m^2}\ ]} \right.$$

$$\frac{1}{[-p_3^o+\sqrt{(\vec{q}+\vec{p}_3)^2+m^2_{\beta\gamma}}+\sqrt{\vec{q}^2+m^2}\ ]}$$

$$\frac{1}{[2\,p_1^o-p_3^o-K^o+\sqrt{(\vec{q}+\vec{p}_3)^2+m^2_{\beta\gamma}}-\sqrt{(\vec{q}-\vec{K})^2+m^2}\ ]}$$

$$\frac{1}{[2\,p_1^o-p_3^o-K^o+\sqrt{(\vec{q}+\vec{p}_3)^2+m^2_{\beta\gamma}}+\sqrt{(\vec{q}-\vec{K})^2+m^2}\ ]}$$

$$\frac{1}{[2\,p_1^o-p_3^o+\sqrt{(\vec{q}+\vec{p}_3)^2+m^2_{\beta\gamma}}-\sqrt{\vec{q}^2+m^2}\ ]}$$

$$\frac{1}{[2\,p_1^o-p_3^o+\sqrt{(\vec{q}+\vec{p}_3)^2+m^2_{\beta\gamma}}+\sqrt{\vec{q}^2+m^2}\ ]}$$

$$\frac{1}{2[\sqrt{(\vec{q}+\vec{p}_3)^2+m^2_{\beta\gamma}}\ ]}$$

$$\frac{1}{[p_1^o-p_3^o+\sqrt{(\vec{q}+\vec{p}_3)^2+m^2_{\beta\gamma}}+\sqrt{(\vec{q}+\vec{p}_1)^2+m^2_{\alpha\tau}}\ ]}$$

$$\left. \frac{1}{[p_1^o-p_3^o+\sqrt{(\vec{q}+\vec{p}_3)^2+m^2_{\beta\gamma}}-\sqrt{(\vec{q}+\vec{p}_1)^2+m^2_{\alpha\tau}}\ ]} \right]$$

$$+ \left(\Xi_2^{ps}(q)\ \bar{f}^2_{\beta\gamma}(\vec{p}_3+\vec{q}-\vec{p}_1)\ \bar{f}^2_{\alpha\tau}(\vec{q}) \right)_{q^o=\bar{q}'^o_5,\ \vec{q}\to\vec{q}+\vec{p}_1}$$

$$\left[\frac{1}{[-p_1^o+\sqrt{(\vec{q}+\vec{p}_1)^2+m^2_{\alpha\tau}}-\sqrt{\vec{q}^2+m^2}\ ]} \right.$$

$$\frac{1}{[-p_1^o+\sqrt{(\vec{q}+\vec{p}_1)^2+m^2_{\alpha\tau}}+\sqrt{\vec{q}^2+m^2}\ ]}$$

$$\left. \frac{1}{[p_1^o-K^o+\sqrt{(\vec{q}+\vec{p}_1)^2+m^2_{\alpha\tau}}-\sqrt{(\vec{q}-\vec{K})^2+m^2}\ ]} \right.$$

$$\frac{1}{[p_1^o - K^o + \sqrt{(\vec{q}+\vec{p}_1)^2 + m_{\alpha\tau}^2} + \sqrt{(\vec{q}-\vec{K})^2 + m^2}\,]}$$

$$\frac{1}{[p_1^o + \sqrt{(\vec{q}+\vec{p}_1)^2 + m_{\alpha\tau}^2} - \sqrt{\vec{q}^2 + m^2}\,]}$$

$$\frac{1}{[p_1^o + \sqrt{(\vec{q}+\vec{p}_1)^2 + m_{\alpha\tau}^2} + \sqrt{\vec{q}^2 + m^2}\,]}$$

$$\frac{1}{[p_3^o - p_1^o + \sqrt{(\vec{q}+\vec{p}_1)^2 + m_{\alpha\tau}^2} - \sqrt{(\vec{q}+\vec{p}_3)^2 + m_{\beta\gamma}^2}\,]}$$

$$\frac{1}{[p_3^o - p_1^o + \sqrt{(\vec{q}+\vec{p}_1)^2 + m_{\alpha\tau}^2} + \sqrt{(\vec{q}+\vec{p}_3)^2 + m_{\beta\gamma}^2}\,]}$$

$$\left.\left.\frac{1}{2\,[\sqrt{(\vec{q}+\vec{p}_1)^2 + m_{\alpha\tau}^2}\,]}\right]\right\}$$

$$+ \frac{i\pi}{(2\pi)^3} \sum_{\alpha,\beta=1\gamma,\tau=1}^{5} \sum^{4} \int_0^{\pi} d\theta \int_0^{2\pi} d\phi \left[\left(\bar{\Xi}_2^{ps}(q)\, \bar{f}_{\beta\gamma}^2(\vec{p}_3+\vec{q}-\vec{p}_1)\, \bar{f}_{\alpha\tau}^2(\vec{q}) \right)_{q^o = \bar{q}'^o_2,\ \vec{q}\to\vec{q}+\vec{p}_1} \right.$$

$$\frac{1}{[K^o - 2p_1^o + \sqrt{(\vec{q}-\vec{K})^2 + m^2} - \sqrt{\vec{q}^2 + m^2}\,]} \frac{|\vec{q}''|^2 \sin\theta}{|D_2|}$$

$$\frac{1}{2\,[\sqrt{(\vec{q}-\vec{K})^2 + m^2}\,]} \frac{1}{[K^o + \sqrt{(\vec{q}-\vec{K})^2 + m^2} - \sqrt{\vec{q}^2 + m^2}\,]}$$

$$\frac{1}{[K^o + \sqrt{(\vec{q}-\vec{K})^2 + m^2} + \sqrt{\vec{q}^2 + m^2}\,]}$$

$$\frac{1}{[K^o - 2p_1^o + p_3^o + \sqrt{(\vec{q}-\vec{K})^2 + m^2} - \sqrt{(\vec{q}+\vec{p}_3)^2 + m_{\beta\gamma}^2}\,]}$$

$$\frac{1}{[K^o - 2p_1^o + p_3^o + \sqrt{(\vec{q}-\vec{K})^2 + m^2} + \sqrt{(\vec{q}+\vec{p}_3)^2 + m_{\beta\gamma}^2}\,]}$$

$$\left.\left.\frac{1}{[K^o - p_1^o + \sqrt{(\vec{q}-\vec{K})^2 + m^2} - \sqrt{(\vec{q}+\vec{p}_1)^2 + m_{\alpha\tau}^2}\,]}\right.\right.$$

$$\left.\left.\frac{1}{[K^o - p_1^o + \sqrt{(\vec{q}-\vec{K})^2 + m^2} + \sqrt{(\vec{q}+\vec{p}_1)^2 + m_{\alpha\tau}^2}\,]}\right]\right]_{|\vec{q}''| = Q}$$

$$+\frac{i\pi}{(2\pi)^3}\sum_{\alpha,\beta=1}^{5}\sum_{\gamma,\tau=1}^{4}\int_0^{\pi}d\theta\int_0^{2\pi}d\phi\left[\left(\bar{Z}_2^{ps}(q)\,\bar{f}^2_{\beta\gamma}(\bar{p}_3+\bar{q}-\bar{p}_1)\,\bar{f}^2_{\alpha\tau}(\bar{q})\right)_{q^o=\bar{q}'^o_3,\ \bar{q}\to\bar{q}+\bar{p}_1}\right.$$

$$\frac{1}{2[-p_1^o]}\,\frac{|\bar{q}|^2\,p_1^o\sin\theta}{2\,|\bar{p}_1|}$$

$$\frac{1}{[-K^o+\sqrt{\bar{q}^2+m^2}\,-\sqrt{(\bar{q}-\bar{K})^2+m^2}\,]}$$

$$\frac{1}{[-K^o+\sqrt{\bar{q}^2+m^2}\,+\sqrt{(\bar{q}-\bar{K})^2+m^2}\,]}\,\frac{1}{2[\sqrt{\bar{q}^2+m^2}\,]}$$

$$\frac{1}{[p_3^o-2\,p_1^o+\sqrt{\bar{q}^2+m^2}\,-\sqrt{(\bar{q}+\bar{p}_3)^2+m^2_{\beta\gamma}}\,]}$$

$$\frac{1}{[p_3^o-2\,p_1^o+\sqrt{\bar{q}^2+m^2}\,+\sqrt{(\bar{q}+\bar{p}_3)^2+m^2_{\beta\gamma}}\,]}$$

$$\frac{1}{[-p_1^o+\sqrt{\bar{q}^2+m^2}\,-\sqrt{(\bar{q}+\bar{p}_1)^2+m^2_{\alpha\tau}}\,]}$$

$$\left.\frac{1}{[-p_1^o+\sqrt{\bar{q}^2+m^2}\,+\sqrt{(\bar{q}+\bar{p}_1)^2+m^2_{\alpha\tau}}\,]}\right]_{|\bar{q}|\,=\,|\bar{p}_1|}\qquad\text{(III-44)}$$

III.5 Bremsstrahlung Cross Sections And Analyzing Powers

The amplitudes $M_{t\mu}^{ps}$ and $M_{t\mu}^{pv}$ given by Eqs. (III-6) and (III-13) can be used to calculate (i) two different $pp\gamma$ differential cross sections, $\sigma^{ps}_{tpp\gamma}$ ($\equiv d^3\sigma_t^{ps}/d\Omega_3 d\Omega_4 d\psi_\gamma$) for ps coupling and $\sigma^{pv}_{tpp\gamma}$ ($\equiv d^3\sigma_t^{pv}/d\Omega_3 d\Omega_4 d\psi_\gamma$) for pv coupling, and (ii) two different analyzing powers, A_{ty}^{ps} for ps coupling and A_{ty}^{pv} for pv coupling. The expressions for these cross sections and analyzing powers are the same as Eqs. (II-52), (II-53), (II-55), (II-56), (II-59), and (II-60), respectively, but with $M_\mu^{ps(pv)}$ and $M_\nu^{ps(pv)}$ replaced by $M_{t\mu}^{ps(pv)}$ and $M_{t\nu}^{ps(pv)}$, respectively.

III.6 Results

The differential cross sections $\sigma^{ps}_{tpp\gamma}$ and $\sigma^{pv}_{tpp\gamma}$, and analyzing powers A^{ps}_{ty} and A^{pv}_{ty} have been calculated. Since the calculations of these cross sections and analyzing powers are much more complicated (it took about 1000 hours to get a single curve on a Pentium 200 PC) than that of the single scattering case, we just calculated $\sigma^{ps}_{tpp\gamma}$, $\sigma^{pv}_{tpp\gamma}$, A^{ps}_{ty}, and A^{pv}_{ty} for $(\bar{\theta}_3, \bar{\theta}_4) = (12°, 12.4°)$ at 280 Mev. As a demonstration of the rescattering contribution in the $pp\gamma$ process; however, one set of calculations is enough. The reason for choosing $(\bar{\theta}_3, \bar{\theta}_4) = (12°, 12.4°)$ is that the most significant discrepancies between the measured analyzing powers and the calculated ones at 280 MeV occur for small scattering angles.

In Fig. 18, we show four different cross sections ($\sigma^{ps}_{pp\gamma}$, $\sigma^{pv}_{pp\gamma}$, $\sigma^{ps}_{tpp\gamma}$, and $\sigma^{pv}_{tpp\gamma}$) as functions of ψ_γ at 280 MeV for $(\bar{\theta}_3, \bar{\theta}_4) = (12°, 12.4°)$. All these cross sections are calculated using the on-shell $p\gamma p$ vertex. The calculations with the rescattering term [$\sigma^{ps}_{tpp\gamma}$ (dotted curve) and $\sigma^{pv}_{tpp\gamma}$ (dash-dotted curve)] yield almost the same values as those without the rescattering term [$\sigma^{ps}_{pp\gamma}$ (dashed curve) and $\sigma^{pv}_{pp\gamma}$ (solid curve)], except for the forward and backward regions ($0 \leq \psi_\gamma \leq 30°$ and $150° \leq \psi_\gamma \leq 180°$). The contribution from the rescattering term enhances the cross section in these two regions and it slightly changes the overall agreement with the TRIUMF data [7], which include the $\frac{2}{3}$-normalization factor.

In Fig. 19, we present four different analyzing powers (A^{ps}_{y}, A^{pv}_{y}, A^{ps}_{ty} and A^{pv}_{ty}) as functions of ψ_γ at 280 MeV for $(\bar{\theta}_3, \bar{\theta}_4) = (12°, 12.4°)$. Again, all curves are calculated using the on-shell $p\gamma p$ vertex. The contribution from the rescattering

term [A_{ty}^{ps} (dotted curve) and A_{ty}^{pv} (dash-dotted curve)] does not improve the agreement with the TRIUMF data [7]. Like the calculated analyzing powers without the rescattering contribution [A_{y}^{ps} (dashed curve) and A_{y}^{pv} (solid curve)], A_{ty}^{ps} and A_{ty}^{pv} also give a large peak in the region $60° \leq \psi_\gamma \leq 120°$. This shows that the rescattering term is not the major cause of the existing large discrepancy between the calculated analyzing powers (A_{y}^{ps} and A_{y}^{pv}) and the data in the region $60° \leq \psi_\gamma \leq 120°$.

In order to demonstrate that the discrepancy can be resolved if we replace the on-shell $p\gamma p$ vertex by the off-shell $p\gamma p$ vertex, we have calculated both cross sections and analyzing powers using the set I_b parameters (off-shell $p\gamma p$ vertex, see Table II) and pv coupling and shown our results in Figs. 20 and 21. The calculated cross sections at 280 MeV for $(\bar{\theta}_3, \bar{\theta}_4) = (12°, 12.4°)$ are shown in Fig. 20. As expected, the rescattering term enhances the cross section in the forward and backward regions. In the region $30° \leq \psi_\gamma \leq 120°$, on the other hand, the dashed curve (with the rescattering term) and the solid curve (without the rescattering term) give almost identical results, which are in good agreement with the TRIUMF data. In Fig.21, we present the calculated analyzing powers at 280 MeV for $(\bar{\theta}_3, \bar{\theta}_4) = (12°, 12.4°)$. The dashed (solid) curve is the result calculated with (without) the rescattering contribution. Since the off-shell $p\gamma p$ vertex has been used in both calculations, the agreement with TRIUMF data is good for both cases. In other words, the large discrepancy between theory and experiment disappears in the region $30° \leq \psi_\gamma \leq 120°$. The rescattering term has a significant contribution. It enhances the second peak of the spectrum and changes the overall shape to be in better agreement with the data.

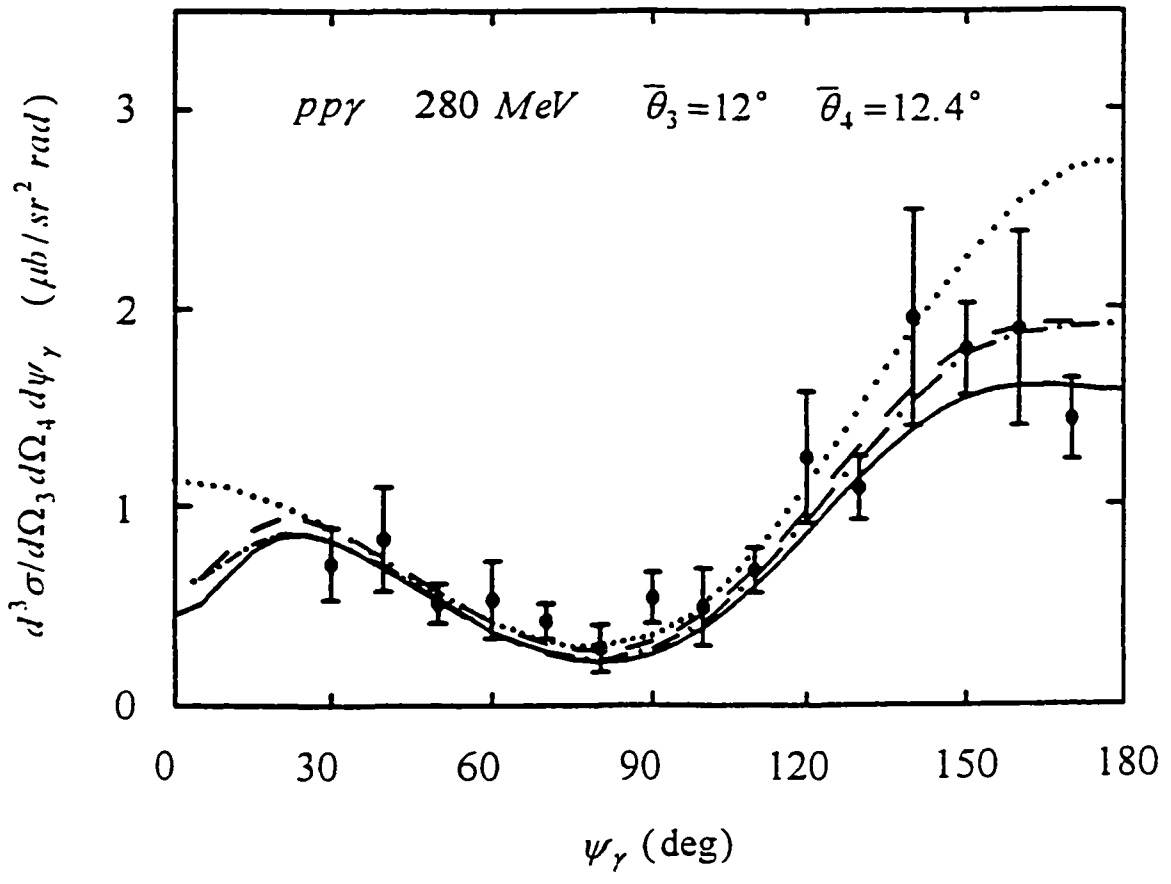

Fig. 18. Coplanar $pp\gamma$ cross sections $d^3\sigma/d\Omega_3 d\Omega_4 d\psi_\gamma$ as functions of ψ_γ at 280 MeV for $\bar{\theta}_3 = 12°$ and $\bar{\theta}_4 = 12.4°$. All curves are calculated using the on-shell $p\gamma p$ vertex. The dotted (dashed) curve represents calculation using ps coupling and with (without) the rescattering contribution, while the dash-dotted (solid) curve represents calculation using pv coupling and with (without) the rescattering contribution. The data, with a $\frac{2}{3}$-normalization factor, are from Ref. [7].

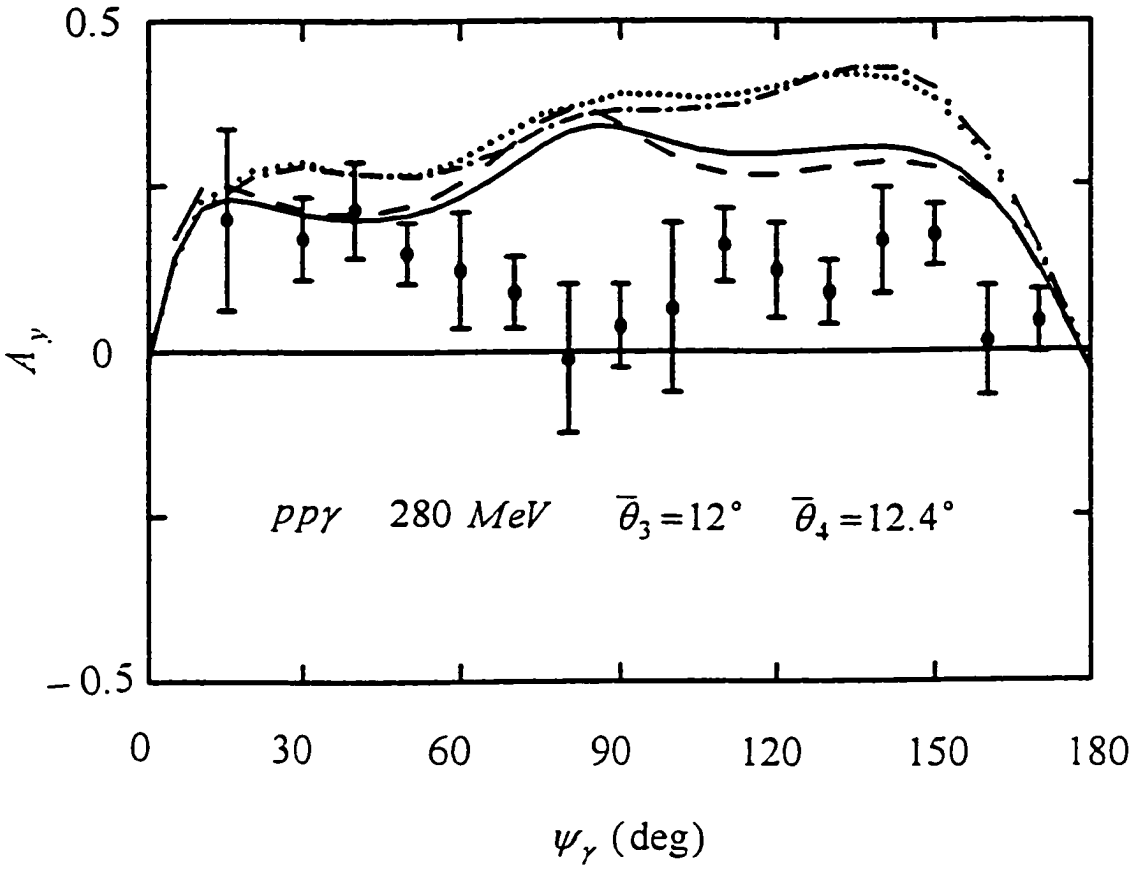

Fig.19. Coplanar $pp\gamma$ analyzing powers A_y as functions of ψ_γ at 280 MeV for $\bar{\theta}_3 = 12°$ and $\bar{\theta}_4 = 12.4°$. All curves are calculated using the on-shell $p\gamma p$ vertex. The dotted (dashed) curve represents calculation using ps coupling and with (without) the rescattering contribution, while the dash-dotted (solid) curve represents calculation using pv coupling and with (without) the rescattering contribution. The data, are from Ref.[7].

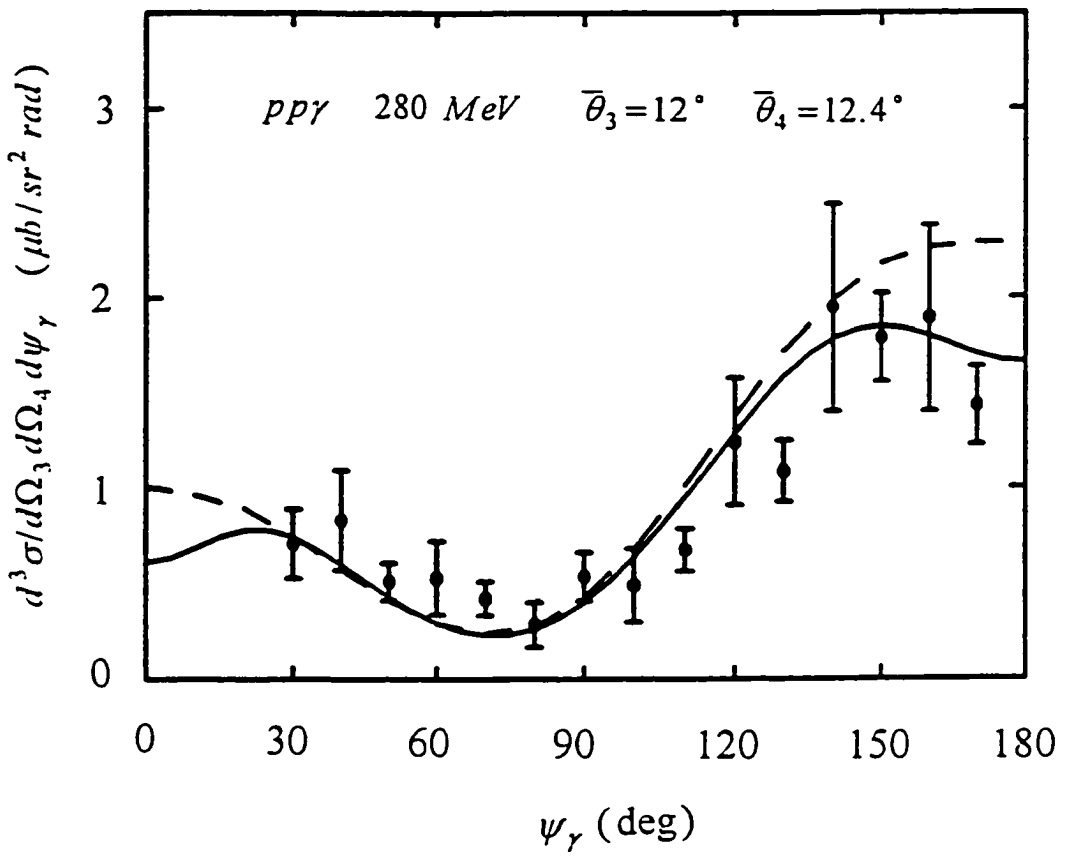

Fig.20. Coplanar $pp\gamma$ cross sections $d^3\sigma/d\Omega_3 d\Omega_4 d\psi_\gamma$ as functions of ψ_γ at 280 MeV for $\bar{\theta}_3 = 12°$ and $\bar{\theta}_4 = 12.4°$. Both curves are calculated using the pv coupling and the set I_b parameters (off-shell $p\gamma p$ vertex), but the dashed curve represents the calculation which includes the rescattering contribution while the solid curve has no such contribution. The results are compared with the TRIUMF data [7], which include a $\frac{2}{3}$-normalization factor.

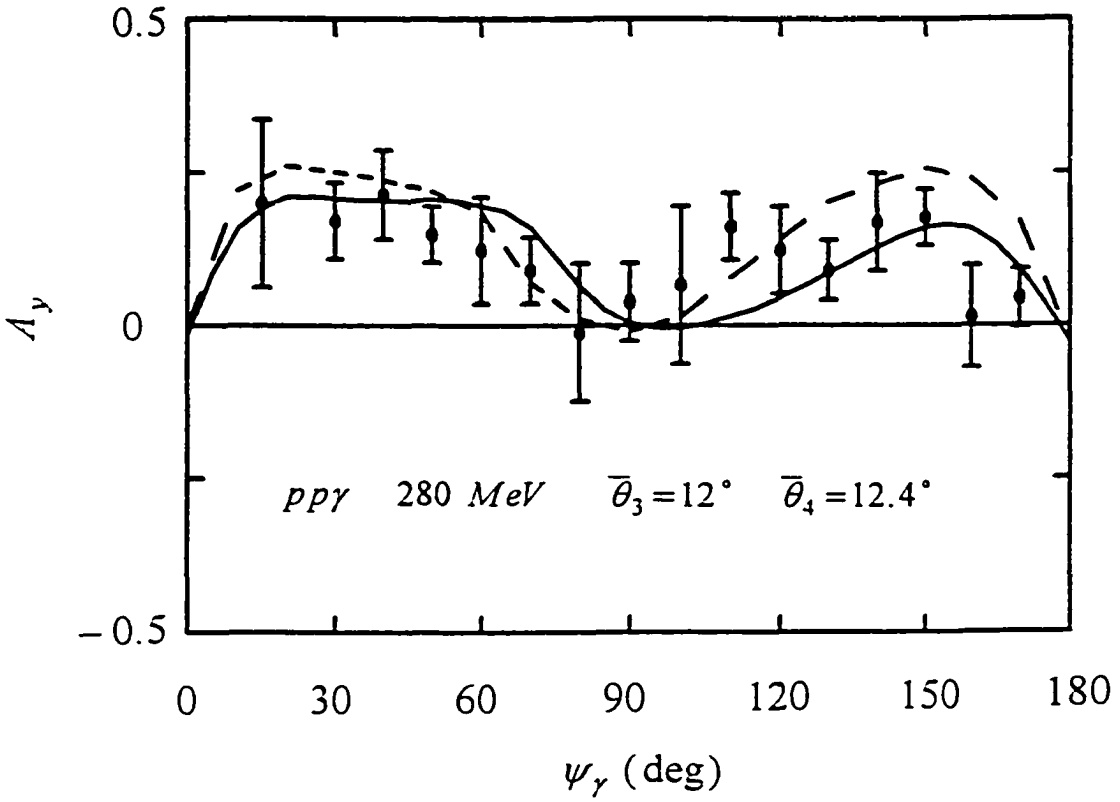

Fig.21. Coplanar $pp\gamma$ analyzing powers A_y as functions of ψ_γ at 280 MeV for $\bar{\theta}_3 = 12°$ and $\bar{\theta}_4 = 12.4°$. Both curves are calculated using the pv coupling and the set I_b parameters (off-shell $p\gamma p$ vertex). The dashed (solid) curve represents calculation with (without) the rescattering contribution. The data are from Ref.[7].

III.7 Conclusion

We have demonstrated that the proton electromagnetic vertex, not the rescattering term, is the major cause of the large discrepancy between the measured analyzing powers and the calculated ones using the on-shell $p\gamma p$ vertex. Thus our hypothesis that the off-shell $p\gamma p$ vertex must be used to calculate $pp\gamma$ analyzing powers is essentially correct. However, the contribution from the rescattering term is important. It enhances cross sections in the forward and backward regions. Furthermore, the calculated analyzing powers are in better agreement with the data, as is particularly seen in the enhancement of the second peak of the spectrum. Finally, the determination of the parameters of the off-shell $p\gamma p$ vertex by including the rescattering term is probably a worthwhile endeavor, though this would require a great deal of additional effort which has heretofore not been done.

Chapter IV

NEUTRON-PROTON BREMSSTRAHLUNG

The previous chapters involved an extensive investigation of the $pp\gamma$ process. In this chapter, we will study another fundamental radiative nucleon-nucleon interaction, the $np\gamma$ process.

An important finding obtained from the nonrelativistic potential model calculations is that meson-exchange currents are the dominant source of high energy photons. More precisely, Brown and Franklin [29] have calculated the $np\gamma$ cross sections using the electromagnetic Hamiltonian which includes the coupling of the electromagnetic field to the nucleon currents V_{em}^{1} and the coupling of the electromagnetic field to the exchange currents V_{em}^{2}. As a result, large exchange effects from V_{em}^{2} were predicted. The inclusion of the V_{em}^{2} term has been found to increase the $np\gamma$ cross section by about a factor of 2. This finding has been confirmed by Nakayama [11]. These exchange effects can also be observed, even more directly, from our OBE approach. This is because the exchange effects have been explicitly taken into account in our calculations. Another important advantage of using the OBE model is that the constructed $np\gamma$ amplitudes are both Lorentz invariant and gauge invariant.

IV.1 Elastic np Amplitude

We consider photon emission accompanying the np scattering:

$$p(p_1^{\mu}) + n(p_2^{\mu}) \rightarrow p(p_3^{\mu}) + n(p_4^{\mu}) + \gamma(K^{\mu}) \ . \qquad \text{(IV-1)}$$

As K tends to zero, the $np\gamma$ process reduces to the corresponding np elastic process,

$$p(p_1^\mu) + n(p_2^\mu) \rightarrow p(\bar{p}_3^\mu) + n(\bar{p}_4^\mu) \ , \qquad \text{(IV-2)}$$

where $\bar{p}_3^\mu$ and $\bar{p}_4^\mu$ are defined by Eq. (II-4b). The Feynman diagrams for the np elastic process in the OBE model are shown in Fig. 22. The corresponding np elastic amplitude

For β = 1 , 2

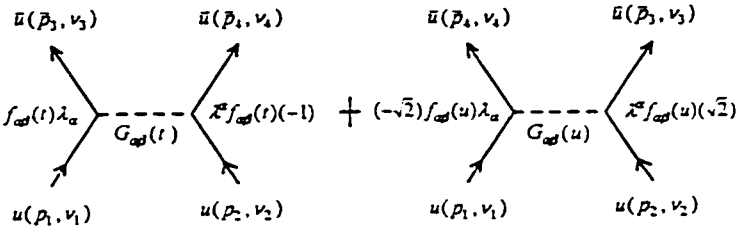

For β = 3 , 4

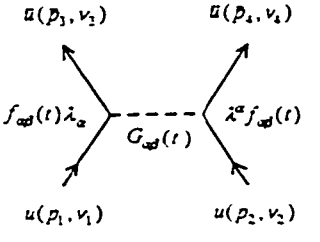

Fig.22. Feynman diagrams for the np elastic scattering process in the OBE model.

$$M_{np}(u,t) = \sum_{\alpha=1}^{5} \Bigg\{ - \sum_{\beta=1}^{2} \Big[G_{\alpha\beta}(t) f_{\alpha\beta}^2(t)\, \bar{u}(\bar{p}_3,\nu_3)\lambda_\alpha u(p_1,\nu_1)\, \bar{u}(\bar{p}_4,\nu_4)\lambda^\alpha u(p_2,\nu_2)$$
$$+ 2\, G_{\alpha\beta}(u) f_{\alpha\beta}^2(u)\, \bar{u}(\bar{p}_4,\nu_4)\lambda_\alpha u(p_1,\nu_1)\, \bar{u}(\bar{p}_3,\nu_3)\lambda^\alpha u(p_2,\nu_2) \Big] \ , \qquad \text{(IV-3)}$$
$$+ \sum_{\beta=3}^{4} G_{\alpha\beta}(t) f_{\alpha\beta}^2(t)\, \bar{u}(\bar{p}_3,\nu_3)\lambda_\alpha u(p_1,\nu_1)\, \bar{u}(\bar{p}_4,\nu_4)\lambda^\alpha u(p_2,\nu_2) \Bigg\}$$

where u, t, $f_{\alpha\beta}$ and $G_{\alpha\beta}$ are defined by Eqs. (II-6), (II-8c), and (II-8d). This amplitude

is valid for both ps and pv couplings.

IV.2 $np\gamma$ Amplitude

The np elastic diagrams exhibited in Fig. 22 are used to generate $np\gamma$ diagrams shown in Fig. 23. Since $np\gamma$ analyzing powers are not available, the unknown off-shell neutron electromagnetic form factor, $F_2^-(\omega^2)$ cannot be determined. Therefore we can only use the on-shell neutron electromagnetic vertex for our calculations. For the proton electromagnetic vertex, we can use either the on-shell $p\gamma p$ vertex or the off-shell $p\gamma p$ vertex. However, because the exchange effects (the internal contribution) dominate the $np\gamma$ cross section, the difference between the results obtained from the on-shell $p\gamma p$ vertex and the off-shell $p\gamma p$ vertex turns out to be small. For consistency, we have also used the on-shell $p\gamma p$ vertex for all $np\gamma$ calculations.

For ps coupling, the $np\gamma$ amplitude corresponding to Fig. 23 has the form

$$
\begin{aligned}
M^{ps}_{np\gamma,\mu} = i\sum_{\alpha=1}^{5}\Bigg\{ & -\sum_{\beta=1}^{2}\Big[G_{\alpha\beta}(t_{24}) f^2_{\alpha\beta}(t_{24})\bar{u}(p_3,\nu_3) X_{\alpha\mu} u(p_1,\nu_1)\bar{u}(p_4,\nu_4)\lambda^{\alpha} u(p_2,\nu_2) \\
& + G_{\alpha\beta}(t_{13}) f^2_{\alpha\beta}(t_{13})\bar{u}(p_3,\nu_3)\lambda_{\alpha} u(p_1,\nu_1)\bar{u}(p_4,\nu_4)\tilde{Y}^{\alpha}_{\mu} u(p_2,\nu_2) \\
& + 2\, G_{\alpha\beta}(u_{14}) f^2_{\alpha\beta}(u_{14})\bar{u}(p_4,\nu_4)\lambda_{\alpha} u(p_1,\nu_1)\bar{u}(p_3,\nu_3)\tilde{Z}^{\alpha}_{\mu} u(p_2,\nu_2) \\
& + 2\, G_{\alpha\beta}(u_{23}) f^2_{\alpha\beta}(u_{23})\bar{u}(p_4,\nu_4)\tilde{T}_{\alpha\mu} u(p_1,\nu_1)\bar{u}(p_3,\nu_3)\lambda^{\alpha} u(p_2,\nu_2) \\
& + 2\, G_{\alpha\beta}(u_{14}) f_{\alpha\beta}(u_{14}) f_{\alpha\beta}(u_{23}) \left[1 + \frac{u_{14}-m^2_{\alpha\beta}}{u_{23}-\Lambda^2_{\alpha\beta}} + \frac{u_{23}-m^2_{\alpha\beta}}{u_{14}-\Lambda^2_{\alpha\beta}} \right] \\
& \frac{(p_1+p_3-p_2-p_4)_{\mu}}{u_{23}-m^2_{\alpha\beta}+i\epsilon_{\alpha\beta}}\, \bar{u}(p_4,\nu_4)\lambda_{\alpha} u(p_1,\nu_1)\bar{u}(p_3,\nu_3)\lambda^{\alpha} u(p_2,\nu_2) \Big]
\end{aligned}
$$

For β = 1 , 2

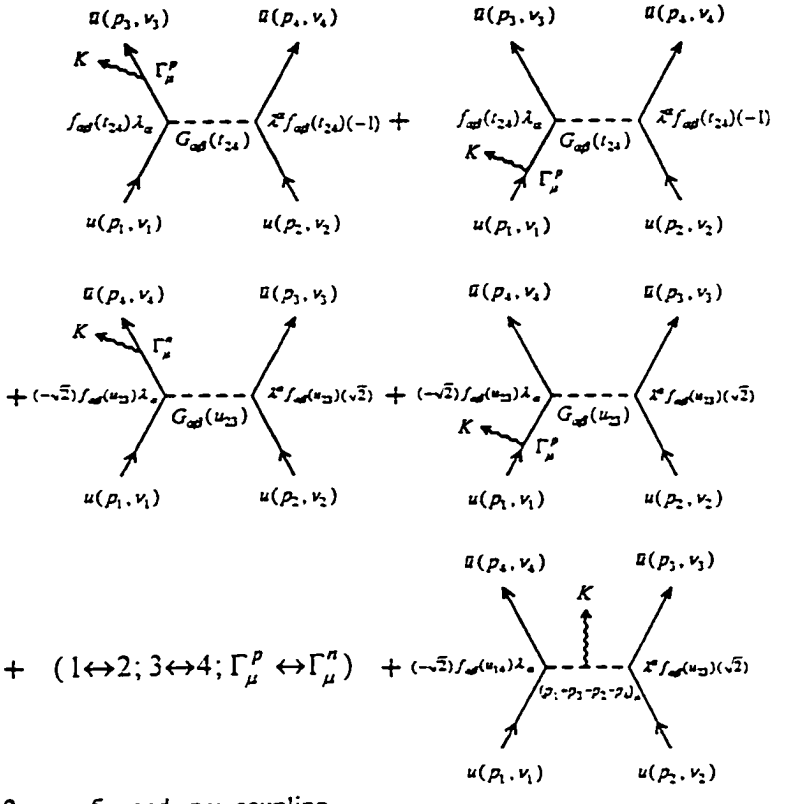

For β = 1 , 2 , α = 5 , and pv coupling

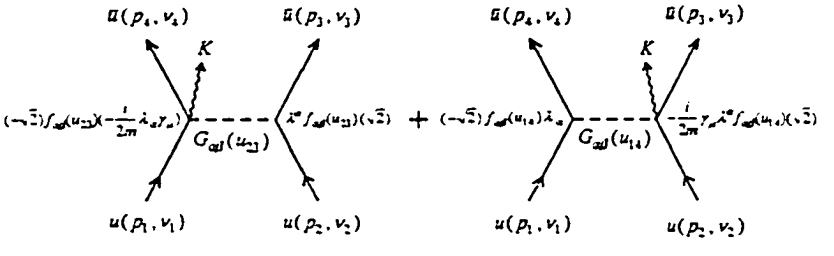

For β = 3 , 4

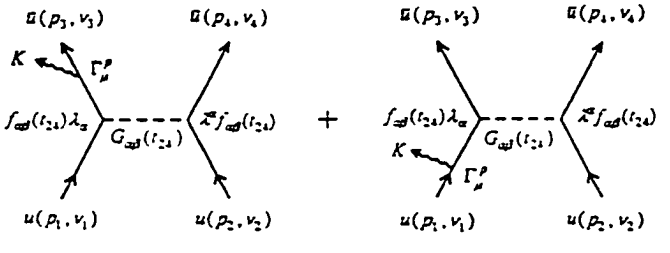

Fig.23. Feynman diagrams for the npγ process in the OBE model. These diagrams are generated from the source graphs, Fig.22.

$$+\sum_{\beta=3}^{4}\Big[G_{\alpha\beta}(t_{24})f^2_{\alpha\beta}(t_{24})\bar{u}(p_3,\nu_3)X_{\alpha\mu}u(p_1,\nu_1)\bar{u}(p_4,\nu_4)\lambda^{\alpha}u(p_2,\nu_2)$$
$$+\ G_{\alpha\beta}(t_{13})f^2_{\alpha\beta}(t_{13})\bar{u}(p_3,\nu_3)\lambda_{\alpha}u(p_1,\nu_1)\bar{u}(p_4,\nu_4)\tilde{Y}^{\alpha}_{\mu}u(p_2,\nu_2)\Big]\Big\} \tag{IV-4}$$

where

$$X_{\alpha\mu}=\lambda_{\alpha}\frac{1}{\not p_1-\not K-m+i\epsilon}\Gamma^p_{\mu}+\Gamma^p_{\mu}\frac{1}{\not p_3+\not K-m+i\epsilon}\lambda_{\alpha}\,,$$
$$\tilde{Y}^{\alpha}_{\mu}=\lambda^{\alpha}\frac{1}{\not p_2-\not K-m+i\epsilon}\Gamma^n_{\mu}+\Gamma^n_{\mu}\frac{1}{\not p_4+\not K-m+i\epsilon}\lambda^{\alpha}\,, \tag{IV-5a}$$

$$\tilde{Z}^{\alpha}_{\mu}=\lambda^{\alpha}\frac{1}{\not p_2-\not K-m+i\epsilon}\Gamma^n_{\mu}+\Gamma^p_{\mu}\frac{1}{\not p_3+\not K-m+i\epsilon}\lambda^{\alpha}\,,$$
$$\tilde{T}_{\alpha\mu}=\lambda_{\alpha}\frac{1}{\not p_1-\not K-m+i\epsilon}\Gamma^p_{\mu}+\Gamma^n_{\mu}\frac{1}{\not p_4+\not K-m+i\epsilon}\lambda_{\alpha}\,, \tag{IV-5b}$$

The on-shell nucleon electromagnetic vertices to be used are expressed as

$$\Gamma^p_{\mu}=\gamma_{\mu}-\frac{i\kappa_p}{2m}\sigma_{\mu\nu}K^{\nu}\quad,\qquad \kappa_p=1.79\ , \tag{II-13}$$

$$\Gamma^n_{\mu}=-i\frac{\kappa_n}{2m}\sigma_{\mu\nu}K^{\nu}\quad,\qquad \kappa_n=-1.91\ . \tag{IV-6}$$

Those terms involving the factors [49]

$$f_{\alpha\beta}(u_{14})\,f_{\alpha\beta}(u_{23})\left[1+\frac{u_{14}-m^2_{\alpha\beta}}{u_{23}-\Lambda^2_{\alpha\beta}}+\frac{u_{23}-m^2_{\alpha\beta}}{u_{14}-\Lambda^2_{\alpha\beta}}\right] \tag{IV-7}$$

in Eq. (IV-4) belong to the internal amplitude. This internal amplitude can be obtained from the external amplitude by imposing the gauge invariance condition. The extra terms which depend on u_{14} and u_{23} in Eq. (IV-7) are needed for current conservation. These terms arise from the fact that the phenomenological form factors given in Eq. (II-8c) have been introduced in Horowitz's model.

For pv coupling, the expression for the $np\gamma$ amplitude is

$$
\begin{aligned}
M^{pv}_{np\gamma,\mu} = i\sum_{\alpha=1}^{5}\Bigg\{ & -\sum_{\beta=1}^{2}\Big[G_{\alpha\beta}(t_{24}) f^2_{\alpha\beta}(t_{24})\bar{u}(p_3,\nu_3) X'_{\alpha\mu} u(p_1,\nu_1)\bar{u}(p_4,\nu_4)\lambda^{\alpha} u(p_2,\nu_2) \\
& + G_{\alpha\beta}(t_{13}) f^2_{\alpha\beta}(t_{13})\bar{u}(p_3,\nu_3)\lambda_{\alpha} u(p_1,\nu_1)\bar{u}(p_4,\nu_4)\,\tilde{Y}'^{\,\alpha}_{\mu} u(p_2,\nu_2) \\
& + 2\, G_{\alpha\beta}(u_{14}) f^2_{\alpha\beta}(u_{14})\bar{u}(p_4,\nu_4)\lambda_{\alpha} u(p_1,\nu_1)\bar{u}(p_3,\nu_3)\tilde{Z}'^{\,\alpha}_{\mu} u(p_2,\nu_2) \\
& + 2\, G_{\alpha\beta}(u_{23}) f^2_{\alpha\beta}(u_{23})\bar{u}(p_4,\nu_4)\tilde{T}'_{\alpha\mu} u(p_1,\nu_1)\bar{u}(p_3,\nu_3)\lambda^{\alpha} u(p_2,\nu_2) \\
& + 2\, G_{\alpha\beta}(u_{14}) f_{\alpha\beta}(u_{14}) f_{\alpha\beta}(u_{23})\left[1 + \frac{u_{14}-m^2_{\alpha\beta}}{u_{23}-\Lambda^2_{\alpha\beta}} + \frac{u_{23}-m^2_{\alpha\beta}}{u_{14}-\Lambda^2_{\alpha\beta}} \right] \\
& \frac{(p_1+p_3-p_2-p_4)_{\mu}}{u_{23}-m^2_{\alpha\beta}+i\epsilon_{\alpha\beta}}\,\bar{u}(p_4,\nu_4)\lambda_{\alpha} u(p_1,\nu_1)\,\bar{u}(p_3,\nu_3)\lambda^{\alpha} u(p_2,\nu_2) \\
& - \delta_{5\alpha}\, G_{\alpha\beta}(u_{23}) f^2_{\alpha\beta}(u_{23})\frac{1}{m}\bar{u}(p_4,\nu_4)\lambda_5\gamma_{\mu} u(p_1,\nu_1)\,\bar{u}(p_3,\nu_3)\lambda^5 u(p_2,\nu_2) \\
& - \delta_{5\alpha}\, G_{\alpha\beta}(u_{14}) f^2_{\alpha\beta}(u_{14})\frac{1}{m}\bar{u}(p_4,\nu_4)\lambda_5 u(p_1,\nu_1)\,\bar{u}(p_3,\nu_3)\gamma_{\mu}\lambda^5 u(p_2,\nu_2)\Big] \\
& + \sum_{\beta=3}^{4}\Big[G_{\alpha\beta}(t_{24}) f^2_{\alpha\beta}(t_{24})\bar{u}(p_3,\nu_3) X_{\alpha\mu} u(p_1,\nu_1)\bar{u}(p_4,\nu_4)\lambda^{\alpha} u(p_2,\nu_2) \\
& + G_{\alpha\beta}(t_{13}) f^2_{\alpha\beta}(t_{13})\bar{u}(p_3,\nu_3)\lambda_{\alpha} u(p_1,\nu_1)\bar{u}(p_4,\nu_4)\,\tilde{Y}^{\alpha}_{\mu} u(p_2,\nu_2)\Big]\Bigg\}
\end{aligned}
\tag{IV-8}
$$

$$= M^{ps}_{n p\gamma,\mu} - \sum_{\beta=1}^{2} \Big[G_{5\beta}(t_{24}) f^2_{5\beta}(t_{24}) \bar{u}(p_3,\nu_3)\left(X'_{5\mu} - X_{5\mu}\right) u(p_1,\nu_1)\bar{u}(p_4,\nu_4)\lambda^5 u(p_2,\nu_2)$$

$$+ G_{5\beta}(t_{13}) f^2_{5\beta}(t_{13}) \bar{u}(p_3,\nu_3)\lambda_5 u(p_1,\nu_1)\bar{u}(p_4,\nu_4)\left(\tilde{Y}'^5_{\mu} - \tilde{Y}^5_{\mu}\right) u(p_2,\nu_2)$$

$$+ 2\, G_{5\beta}(u_{14}) f^2_{5\beta}(u_{14}) \bar{u}(p_4,\nu_4)\lambda_5 u(p_1,\nu_1)\bar{u}(p_3,\nu_3)\left(\tilde{Z}'^5_{\mu} - \tilde{Z}^5_{\mu}\right) u(p_2,\nu_2)$$

$$+ 2\, G_{5\beta}(u_{23}) f^2_{5\beta}(u_{23}) \bar{u}(p_4,\nu_4)\left(\tilde{T}'^5_{\mu} - \tilde{T}^5_{\mu}\right) u(p_1,\nu_1)\bar{u}(p_3,\nu_3)\lambda^5 u(p_2,\nu_2)$$

$$- G_{5\beta}(u_{23}) f^2_{5\beta}(u_{23}) \frac{1}{m} \bar{u}(p_4,\nu_4)\lambda_5\gamma_\mu u(p_1,\nu_1)\bar{u}(p_3,\nu 3)\lambda^5 u(p_2,\nu_2)$$

$$- G_{5\beta}(u_1 u) f^2_{5\beta}(u_{14}) \frac{1}{m} \bar{u}(p_4,\nu_4)\lambda_5 u(p_1,\nu_1)\bar{u}(p_3,\nu_3)\gamma_\mu\lambda_5 u(p_2,\nu_2)\Big]$$

(IV-9)

where

$$X'_{5\mu} = (\lambda_5 \frac{\not p_1 - \not p_3 - \not K}{2m}) \frac{1}{\not p_1 - \not K - m + i\epsilon} \Gamma^p_\mu + \Gamma^p_\mu \frac{1}{\not p_3 + \not K - m + i\epsilon} (\lambda_5 \frac{\not p_1 - \not p_3 - \not K}{2m}),$$

$$\tilde{Y}'^5_{\mu} = (\lambda_5 \frac{\not p_2 - \not p_4 - \not K}{2m}) \frac{1}{\not p_2 - \not K - m + i\epsilon} \Gamma^n_\mu + \Gamma^n_\mu \frac{1}{\not p_4 + \not K - m + i\epsilon} (\lambda_5 \frac{\not p_2 - \not p_4 - \not K}{2m}),$$

$$\tilde{Z}'^5_{\mu} = (\lambda_5 \frac{\not p_2 - \not p_3 - \not K}{2m}) \frac{1}{\not p_2 - \not K - m + i\epsilon} \Gamma^n_\mu + \Gamma^p_\mu \frac{1}{\not p_3 + \not K - m + i\epsilon} (\lambda_5 \frac{\not p_2 - \not p_3 - \not K}{2m}),$$

$$\tilde{T}'_{5\mu} = (\lambda_5 \frac{\not p_1 - \not p_4 - \not K}{2m}) \frac{1}{\not p_1 - \not K - m + i\epsilon} \Gamma^p_\mu + \Gamma^n_\mu \frac{1}{\not p_4 + \not K - m + i\epsilon} (\lambda_5 \frac{\not p_1 - \not p_4 - \not K}{2m}).$$

(IV-10)

Note that the amplitude $M^{pv}_{n p\gamma,\mu}$ takes into account the photon emission from πN

vertices.

Clearly, the two amplitudes $M^{ps}_{npγ,\mu}$ and $M^{pv}_{npγ,\mu}$ depend only upon relativistic invariants and are fully gauge invariant. They have been used to calculate the noncoplanar differential cross sections $\sigma^{ps}_{npγ}$ ($\equiv d^3\sigma^{ps}_{npγ}/d\Omega_3 d\Omega_4 d\psi_\gamma$) and $\sigma^{pv}_{npγ}$ ($\equiv d^3\sigma^{pv}_{npγ}/d\Omega_3 d\Omega_4 d\psi_\gamma$), as a function of the photon angle ψ_γ and the noncoplanarity angle $\bar{\phi}$ ($\bar{\phi}=0$ gives the coplanar cross section). We have also integrated differential cross sections over ψ_γ to obtain the integrated cross sections as a function of $\bar{\phi}$,

$$d^2\sigma^{ps(pv)}_{npγ}/d\Omega_3 d\Omega_4 = \int \left(d^3\sigma^{ps(pv)}_{npγ}/d\Omega_3 d\Omega_4 d\psi_\gamma \right) d\psi_\gamma \ .$$

These integrated cross sections can be used to investigate the noncoplanarity effects in $npγ$.

IV.3 Results

Some important results are shown in Figs. 24-27. In some of these figures, the cross sections calculated using the ps coupling are compared with those calculated using the pv coupling. Our results are also compared with the experimental data and/or the results calculated using other approaches.

In Fig. 24, we present the integrated cross section $d^2\sigma^{ps(pv)}_{npγ}/d\Omega_3 d\Omega_4$ as a function of the noncoplanarity angle $\bar{\phi}$ at 200 MeV for $\bar{\theta}_3 = \bar{\theta}_4 = 30°$, 35°, and 38°. Two interesting features can be observed [21]. (i) The deviation, $\Delta'_{npγ} \equiv d^2\sigma^{ps}_{npγ}/d\Omega_3 d\Omega_4 - d^2\sigma^{pv}_{npγ}/d\Omega_3 d\Omega_4$, is extremely small for all cases, suggesting that the $npγ$ process with large scattering angles cannot be used to resolve

the ps-pv problem. (ii) The general shape of the $np\gamma$ noncoplanar curves shown in this figure is quite different from that of the $pp\gamma$ curve shown in Fig. 6. A similar feature has been obtained by other authors [50,51]. These curves indicate that the experimentally detected bremsstrahlung events must be corrected in order to determine the true coplanar cross sections, and the correction factor for the $np\gamma$ case should be quite different from that for the $pp\gamma$ case. This noncoplanarity effect may explain the large discrepancy between all theoretical predictions and the experimental data at 200 MeV for $\bar{\theta}_3 = \bar{\theta}_4 = 38°$ [52].

In Fig. 25, we show the coplanar $np\gamma$ cross sections $\sigma^{pv}_{np\gamma}$ as functions of ψ_γ at 200 MeV for $\bar{\theta}_3 = \bar{\theta}_4 = 30°, 35°$, and $38°$. The cross sections $\sigma^{ps}_{np\gamma}$ are not shown in this figure because they are very close to the cross section $\sigma^{pv}_{np\gamma}$. From this figure, it is easy to see that the integrated cross section (or the cross section $\sigma^{pv}_{np\gamma}$ for $90° \leq \psi_\gamma \leq 360°$) increases as the symmetric scattering angle $\bar{\theta}_3 = \bar{\theta}_4$ increases.

The comparison with other predictions is shown in Figs. 26 and 27. In Fig. 26a, our coplanar cross sections $\sigma^{ps(pv)}_{np\gamma}$ (at 200 MeV for $\bar{\theta}_3 = \bar{\theta}_4 = 30°$) are compared with the potential-model predictions obtained by Brown and Franklin [29]. Both approaches predict very similar shapes for photon angular distributions, except that one of our double peaks is about 20-30% smaller than that of Brown and Franklin. In Fig. 26b, our coplanar cross sections $\sigma^{ps(pv)}_{np\gamma}$ (at 200 MeV for $\bar{\theta}_3 = 30°$ and $\bar{\theta}_4 = 45°$) are compared with the potential-model results of Herrmann et al. [12]. Agreement between the results calculated using these two different approaches is excellent in this case.

In Fig. 27a, we present integrated $np\gamma$ cross sections $d^2\sigma^{pv}_{np\gamma}/d\Omega_3 d\Omega_4$ as

functions of $\bar{\theta}_4$ at 130 MeV for a fixed angle $\bar{\theta}_3 = 20°$. Our result (solid curve) is compared with the experimental measurements [53] and the potential-model prediction of Brown and Franklin (dashed curve) [29]. In Fig. 27b, we show integrated $np\gamma$ cross sections at 200 MeV for several symmetric scattering angles, $\bar{\theta}_3 = \bar{\theta}_4 = 30°$, 35°, and 38°. Our result (solid curve) is compared with the experimental data and three other calculations, i.e. by Brown and Franklin (dashed curve) [29], by Herrmann et al. (dotted curve) [12], and by Schäfer et al. (dash-dotted curve) [14]. Our result is in very close agreement with that of Herrmann et al..

Finally, the noncoplanarity effects in $np\gamma$ have been systematically investigated. In Fig. 28, we present noncoplanar $np\gamma$ cross sections $\sigma^{pv}_{np\gamma}$ as functions of ψ_γ at 200 MeV for several noncoplanarity angle $\bar{\phi}$. These results demonstrate that the noncoplanarity effects (the dependence of $\sigma^{pv}_{np\gamma}$ upon $\bar{\phi}$) differ markedly as functions of ψ_γ. Because of this significant angular dependence of the noncoplanarity, the noncoplanar cross section as a function of $\bar{\phi}$ for a given ψ_γ, rather than the integrated cross section as a function of $\bar{\phi}$, should be used by the experimentalists for converting the experimental (noncoplanar) cross sections into a coplanar result.

In conclusion, using the on-shell nucleon electromagnetic vertex, we have found that the exchange effects (the internal contribution) dominate the $np\gamma$ cross section, in agreement with what has been found in the potential-model approach. We have also observed very significant noncoplanarity effects in the $np\gamma$ process. These effects might be responsible for some discrepancies between theory and experiment. Unfortunately, the $np\gamma$ cross sections cannot be used to resolve the ps-pv ambiguity because

predictions calculated using either ps or pv coupling produce extremely close results. We note that the off-shell neutron electromagnetic vertex cannot be investigated without $np\gamma$ analyzing power data, which are presently unavailable.

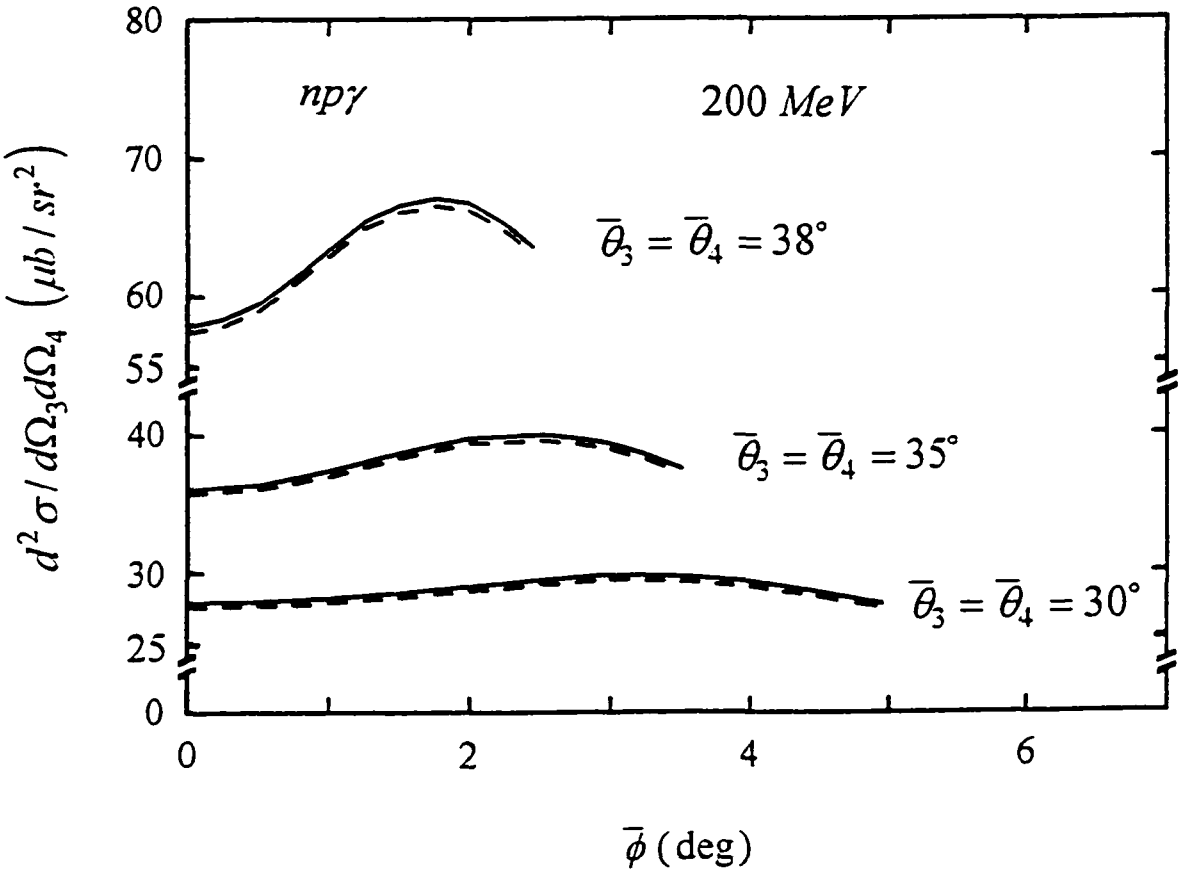

Fig.24. Integrated $np\gamma$ cross section $d^2\sigma^{ps(pv)}/d\Omega_3 d\Omega_4$ as a function of $\bar{\phi}$ at 200 MeV for $\bar{\theta}_3 = \bar{\theta}_4 = 30°, 35°$, and $38°$. The solid and dashed curves represent the results for the ps and pv couplings, respectively.

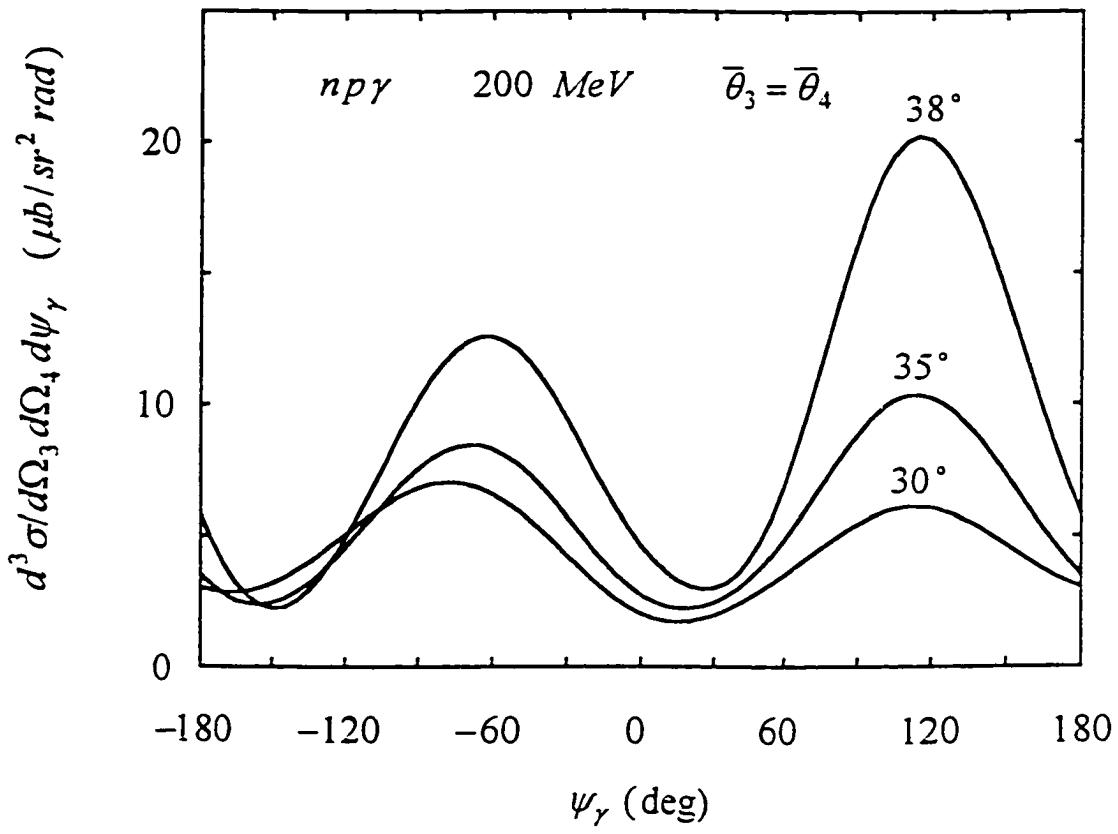

Fig.25. Coplanar $np\gamma$ cross sections $\sigma^{pv}_{np\gamma}$ as functions of ψ_γ at 200 MeV for $\bar{\theta}_3 = \bar{\theta}_4 = 30°, 35°$, and $38°$. The cross sections $\sigma^{ps}_{np\gamma}$ are not shown in this figure mainly because it is very close to the cross section $\sigma^{pv}_{np\gamma}$.

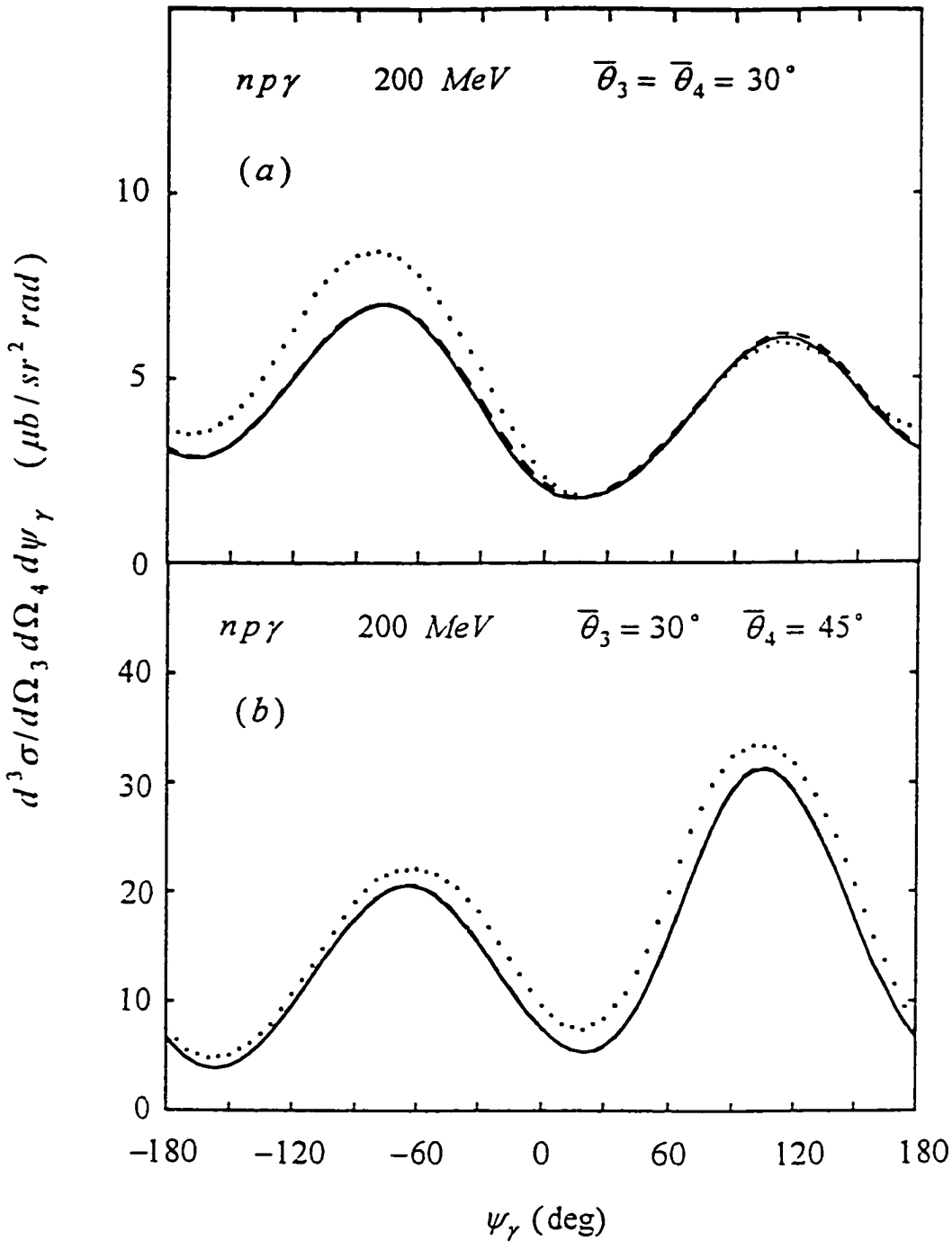

Fig.26. (a) Coplanar $np\gamma$ cross sections as functions of ψ_γ at 200 MeV for $\bar{\theta}_3 = \bar{\theta}_4 = 30°$. Our cross sections, $\sigma^{pv}_{np\gamma}$ (solid curve) and $\sigma^{ps}_{np\gamma}$ (dashed curve), are compared with the potential-model predictions (dotted curve) obtained by Brown and Franklin [29]. (b) Coplanar $np\gamma$ cross sections as functions of ψ_γ at 200 MeV for $\bar{\theta}_3 = 30°$ and $\bar{\theta}_4 = 45°$. Our cross sections, $\sigma^{pv}_{np\gamma}$ (solid curve) and $\sigma^{ps}_{np\gamma}$ (dashed curve), are compared with the potential-model predictions (dotted curve) obtained by Herrmann et al.[12].

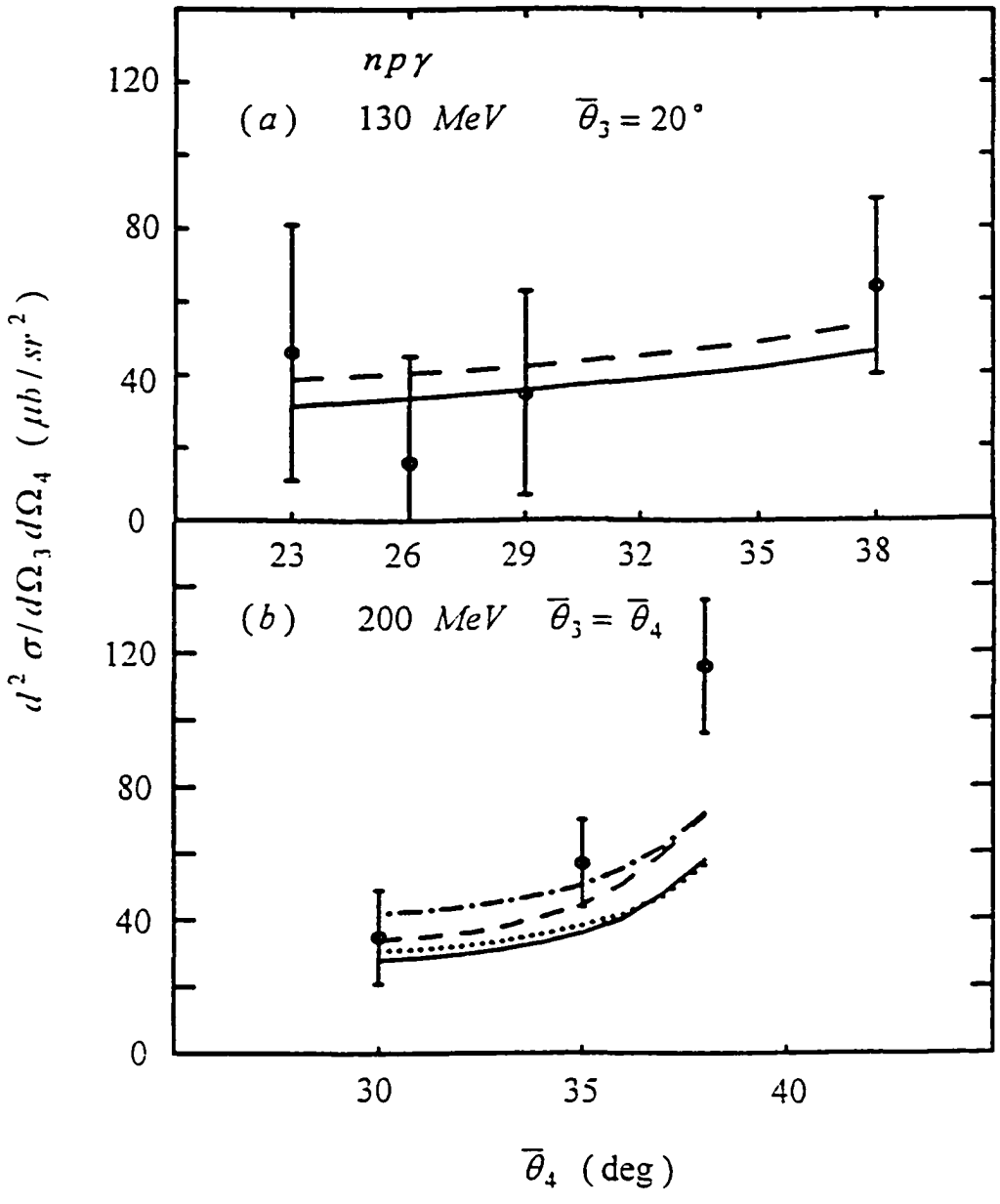

Fig.27. (a) Integrated $np\gamma$ cross sections as functions of $\bar{\theta}_4$ at 130 MeV for $\bar{\theta}_3 = 20°$. Our calculation $d^2\sigma^{pv}_{np\gamma}/d\Omega_3 d\Omega_4$ (solid curve) is compared with the potential model result (dashed curve) obtained by Brown and Franklin [29]. The data are from Ref.[53]. (b) Integrated $np\gamma$ cross sections as functions of symmetric scattering angle ($\bar{\theta}_3 = \bar{\theta}_4$) at 200 MeV. Our result $d^2\sigma^{pv}_{np\gamma}/d\Omega_3 d\Omega_4$ (solid curve) is compared with the results obtained by Brown and Franklin (dashed curve) [29], by Herrmann et al.(dotted curve) [12], and by Schäfer et al. (dash-dotted curve) [14]. The data are from Ref.[52].

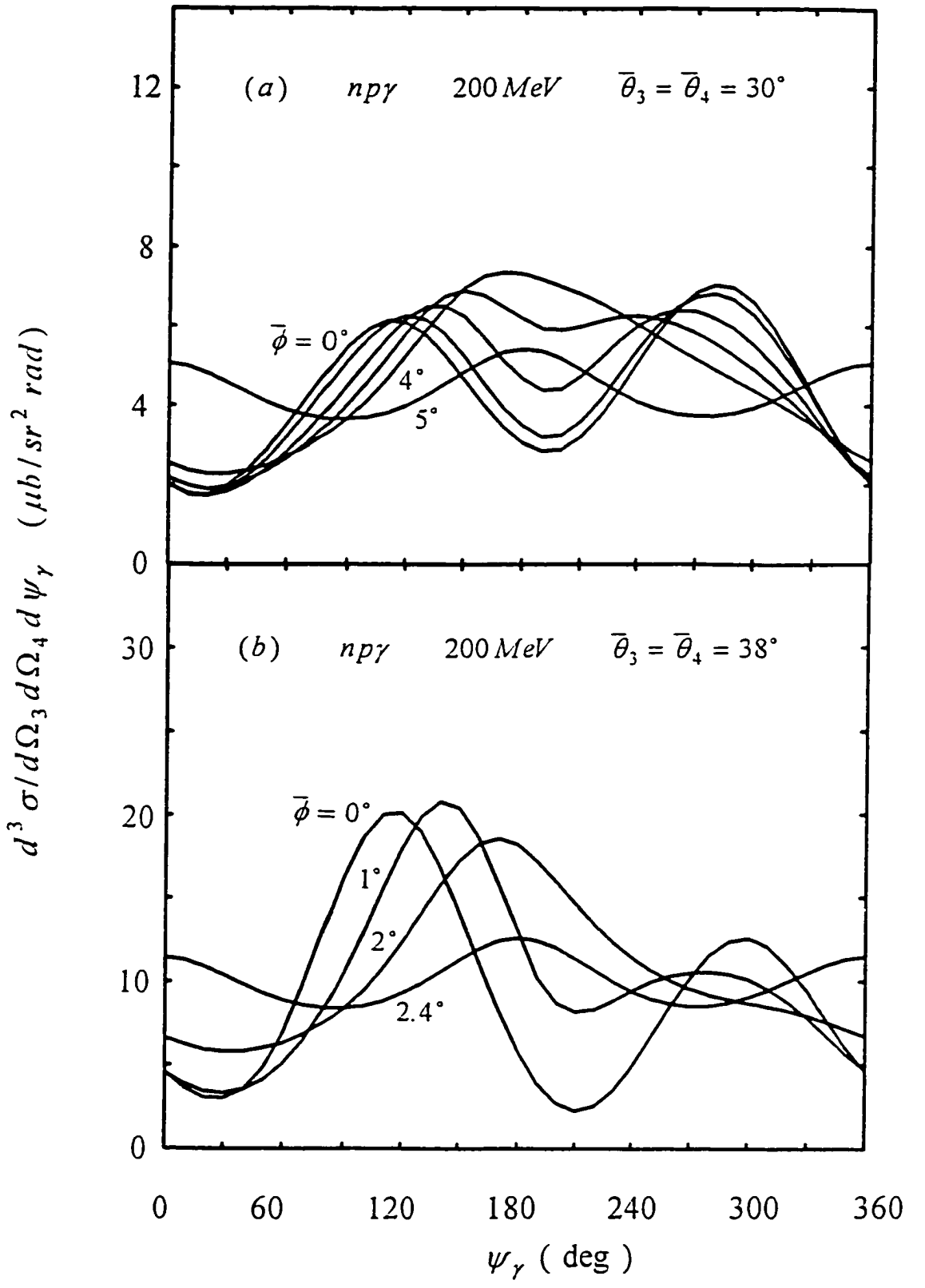

Fig.28. Noncoplanar cross secctions $\sigma^{pv}_{np\gamma}$ as functions of ψ_γ at 200 MeV for several noncoplanarity angles $\bar{\phi}$: (a) $\bar{\theta}_3 = \bar{\theta}_4 = 30°$ and (b) $\bar{\theta}_3 = \bar{\theta}_4 = 38°$.

Appendix

Horowitz's parameters

The complex coupling constants $g^2_{\alpha\beta}$, cut-off parameters $\Lambda_{\alpha\beta}$, and meson masses $m_{\alpha\beta}$ are defined as follows:

$$(g^2_{\alpha\beta}) = \left[\frac{m + 0.5T}{m}\right] \cdot \begin{bmatrix} g^2_\delta & -i\bar{g}^2_\delta & g^2_\sigma & -i\bar{g}^2_\sigma \\ g^2_{t1} & -i\bar{g}^2_{t1} & g^2_{to} & -i\bar{g}^2_{to} \\ g^2_{a1} & -i\bar{g}^2_{a1} & g^2_{ao} & -ig^2_{ao} \\ g^2_\rho & -i\bar{g}^2_\rho & g^2_\omega & -i\bar{g}^2_\omega \\ g^2_\pi & -i\bar{g}^2_\pi & g^2_\eta & -i\bar{g}^2_\eta \end{bmatrix}, \quad \text{(A1)}$$

$$(\Lambda_{\alpha\beta}) = \begin{bmatrix} \Lambda_\delta & \bar{\Lambda}_\delta & \Lambda_\sigma & \bar{\Lambda}_\sigma \\ \Lambda_{t1} & \bar{\Lambda}_{t1} & \Lambda_{to} & \bar{\Lambda}_{to} \\ \Lambda_{a1} & \bar{\Lambda}_{a1} & \Lambda_{ao} & \bar{\Lambda}_{ao} \\ \Lambda_\rho & \bar{\Lambda}_\rho & \Lambda_\omega & \bar{\Lambda}_\omega \\ \Lambda_\pi & \bar{\Lambda}_\pi & \Lambda_\eta & \bar{\Lambda}_\eta \end{bmatrix}, \quad \text{(A2)}$$

$$(m_{\alpha\beta}) = \begin{bmatrix} m_\delta & \bar{m}_\delta & m_\sigma & \bar{m}_\sigma \\ m_{t1} & \bar{m}_{t1} & m_{to} & \bar{m}_{to} \\ m_{a1} & \bar{m}_{a1} & m_{ao} & \bar{m}_{ao} \\ m_\rho & \bar{m}_\rho & m_\omega & \bar{m}_\omega \\ m_\pi & \bar{m}_\pi & m_\eta & \bar{m}_\eta \end{bmatrix}, \quad \text{(A3)}$$

where g^2_i, $\bar{g}^2_i$, Λ_i, $\bar{\Lambda}_i$, m_i and $\bar{m}_i$ ($i = \delta, \sigma, t_1, t_o, a_1, a_o, \rho, \omega, \pi, \eta$) are Horowitz's parameters given in Ref. [25]. The extra factor in (A1), which depends on the incident nucleon energy T, comes from different definition of the spinor $u(p,v)$ used by us.

References

(1) An extensive list of references can be obtained from the following article: M. K. Liou, D. Lin, and B. F. Gibson, Phys. Rev. **C47**, 973 (1993).

(2) Dahang Lin, M. K. Liou, and Z. M. Ding, Phys. Rev. **C44**, 1819 (1991), and references therein.

(3) B. M. K. Nefkens et al., Phys. Rev. **D18**, 3911 (1978).

(4) D. Yan, P. M. S. Lesser, M. K. Liou, and C. C. Trail, Phys. Rev. **C45**, 331 (1992), and references therein.

(5) J. G. Rogers et al., Phys. Rev. **C22**, 2512 (1980).

(6) P. Kitching et al., Nucl. Phys. **A463**, 87c (1987).

(7) K. Michaelian et al., Phys. Rev. **D41**, 2689 (1990).

(8) B. V. Przewoski et al., Phys. Rev. **C45**, 2001 (1992).

(9) N. Kalantar-Nayestanaki et al., Few Body Systems Suppl. **8**, 145(1995); Nucl. Phys. **A631**, 242c(1998).

(10) R. L. Workman and H. W. Fearing, Phys. Rev. **C34**, 780 (1986); H. W. Fearing, Nucl. Phys. **A463**, 95 (1987).

(11) K. Nakayama, Phys. Rev. **C39**, 1475 (1989).

(12) V. Herrmann, J. Speth, and K. Nakayama, Phys. Rev. **C43**, 394 (1991); V. Herrmann and K. Nakayama, Phys. Rev. **C45**, 1450 (1992).

(13) V. R. Brown, P. L. Anthony, and J. Franklin, Phys. Rev. **C44**, 1296 (1991).

(14) M. Schäfer, T. S. Biro, W. Cassing, U. Mosel, H. Nifenecker, and J. A. Pinston, Z. Phys. **A339**, 391 (1991).

(15) M. Jetter, H. Freitag, and H. V. von Geramb, Phys. Scr. **48**, 229 (1993);
M. Jetter and H. V. von Geramb, Phys. Rev. **C49**, 1832 (1994).

(16) A. Katsogiannis and K. Amos, Phys. Rev. **C47**, 1376 (1993).

(17) J. A. Eden, D. Plümper, M. F. Gari, and H. Heback, Z. Phys. **A347**, 145 (1993);
J. A. Eden and M. F. Gari, Phys. Lett. **B347**, 187 (1995).

(18) F. de. Jong, K. Nakayama, V. Herrmann, and O. Scholten, Phys. Lett. **B333**, 1 (1994).

(19) M. K. Liou, R. Timmermans, and B. F. Gibson, Phys. Lett. **B345**, 372 (1995); Erratum, Phys. Lett. **B355**, 606 (1995).

(20) M. Jetter and H. W. Fearing, Phys. Rev. **C51**, 1666 (1995).

(21) M. K. Liou, Yi Li, W. M. Schreiber, and R. W. Brown, Phys. Rev. **C52**, R2346 (1995).

(22) A. I. Titov, B. Kämpfer, B. L. Reznik, and V. Shklyar, Phys. Lett. **B372**, 15 (1996).

(23) J. A. Eden and M. F. Gari, Phys. Rev. **C53**, 1102 (1996).

(24) F. de. Jong and Nakayama, Phys. Lett. **B385**, 33(1996);
Phys. Rev. **C52**, 2377(1995).

(25) M. K. Liou, R. Timmermans, and B. F. Gibson, Phys. Rev. **C54**, 1574(1996).

(26) G. H. Martinus, O. Scholton, and J. A. Tjon, Phys. Rev. **C56**, 2945(1997); Phys. Lett. **B402**, 7(1997).

(27) Yi Li, M. K. Liou, and W. M. Schreiber, Phys. Rev. **C57**, 507(1998).

(28) H. Nifenecher and J. A. Pinston, Annu. Rev. Nucl. Part. Sci. **40**, 113 (1990), and references therein.

(29) V. R. Brown and J. Franklin, Phys. Rev. **C8**, 1706 (1973).

(30) Yi Li, M. K. Liou, R. Timmermans, and B. F. Gibson, Phys. Rev. C (to be published).

(31) F. E. Low, Phys. Rev. **110**, 974(1958).

(32) S. L. Adler and Y. Dothan, Phys. Rev. **151**, 1267(1966);
T. H. Burnett and N. M. Kroll, Phys. Rev. Lett. **20**, 86(1968);
J. S. Bell and R. Van Royen, Nuovo Cimento **60A**, 62(1969).

(33) M. K. Liou and Z. M. Ding, Phys. Rev. C **35**, 651(1987).

(34) Z. M. Ding, Dahang Lin, and M. K. Liou, Phys. Rev. C **40**, 1291(1989).

(35) C. J. Horowitz, Phys. Rev. **C31**, 1340 (1985).

(36) E. M. Nyman, Nucl. Phys. **A154**, 97 (1970); **A160**, 517 (1971).

(37) B. Gottschalk, W. J. Schlaer, and K. H. Wang, Nucl. Phys. **A94**, 491 (1967).

(38) J. L. Mathews, Slide Report of the " Workshop on Nucleon-Nucleon Bremsstrahlung ", Groningen, July 21, 1997.

(39) M. L. Goldberger, M. T. Grisaru, S. W. MacDowell, and D. Y. Wang, Phys. Rev. **120**, 2250(1960).

(40) M. K. Liou and M. I. Sobel, Ann. Phys. (N. Y.) **72**, 323 (1972).

(41) J. A. Tjon and S. J. Wallace, Phys. Rev. **C32**, 267(1985).

(42) A. M. Bincer, Phys. Rev. **118**, 855 (1960).

(43) S. D. Drell and H. R. Pagels, Phys. Rev. **140**, B397(1965).

(44) H. W. L. Naus and J. H. Koch, Phys. Rev. **C39**, 1907(1989).

(45) P. C. Tiemeijer and J. A. Tjon, Phys. Rev. **C42**, 599(1990).

(46) V. Herrmann, K. Nakayama, O. Scholten, and H. Arellano, Nucl. Phys. **A 582**, 568(1995).

(47) P. C. Tiemeijer and J. A. Tjon, Phys. Rev. **C42**, 599(1990).

(48) F. Gross, J. W. Van Orden, and K. Holinde, Phys. Rev. **C45**, 2094(1992).

(49) I. S. Towner, Phys. Rep. **155**, 263(1987).

(50) R. Baier, H. Kühnelt, and P. Urban, Nucl. Phys. **B11**, 675(1969).

(51) L. S. Celenza, B. F. Gibson, M. K. Liou, and M. I. Sobel, Phys. Lett. **41B**, 283(1972).

(52) F. P. Brady and J. C. Yonug, Phys. Rev. **C2**, 1579(1970).

(53) J. A. Edgington et al., Nucl. Phys. **A218**, 151(1974).

IMAGE EVALUATION
TEST TARGET (QA-3)

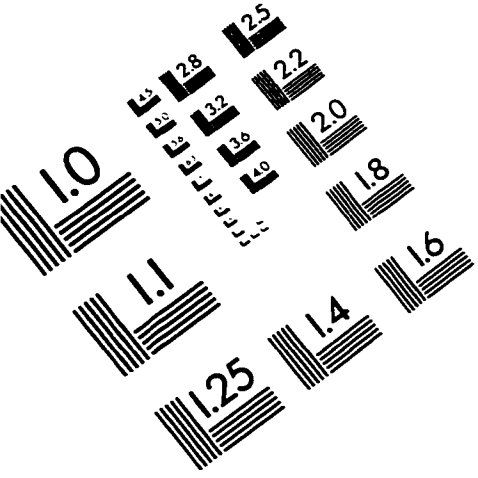

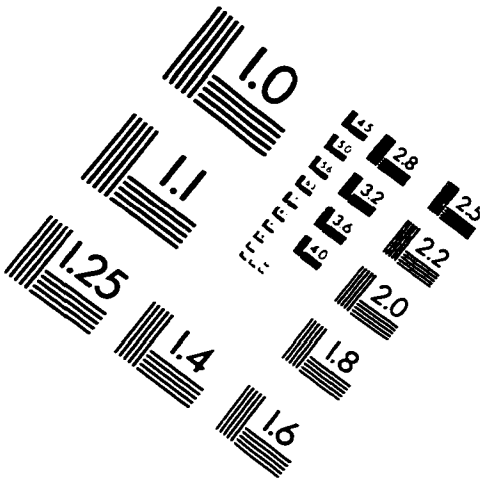

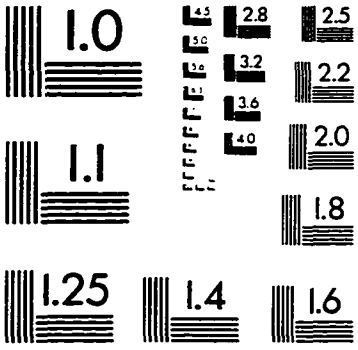

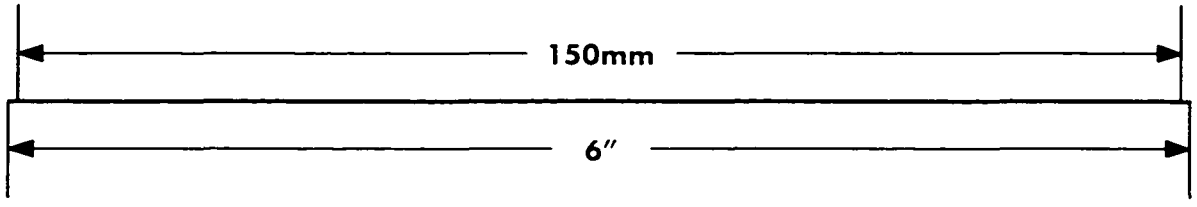

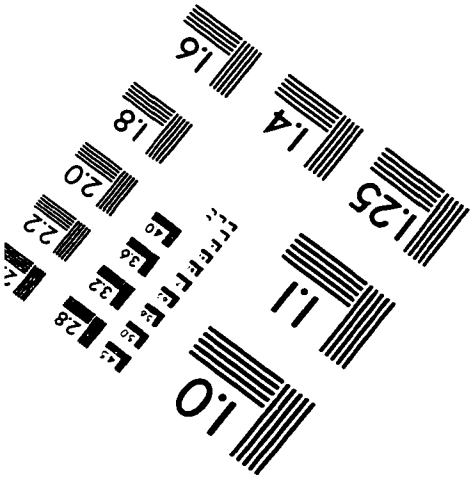

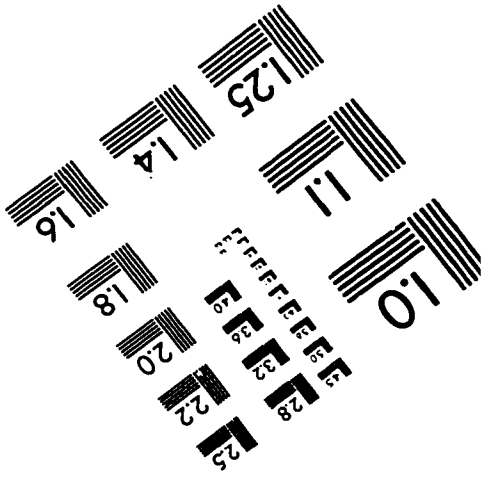

APPLIED IMAGE, Inc
1653 East Main Street
Rochester, NY 14609 USA
Phone: 716/482-0300
Fax: 716/288-5989